Design of Solarimeter

by

Uthman Abdullatif Fattah

A Thesis Presented to the

FACULTY OF THE COLLEGE OF GRADUATE STUDIES

KING FAHD UNIVERSITY OF PETROLEUM & MINERALS

DHAHRAN, SAUDI ARABIA

In Partial Fulfillment of the
Requirements for the Degree of

MASTER OF SCIENCE

In

ELECTRICAL ENGIEERING

February, 1982

Order Number 1355741

Design of solarimeter

Fattah, Uthman Abdullatif, M.S.

King Fahd University of Petroleum and Minerals (Saudi Arabia), 1982

U·M·I
300 N. Zeeb Rd.
Ann Arbor, MI 48106

DESIGN OF SOLARIMETER

BY

UTHMAN ABDULLATIF FATTAH

THESIS

PRESENTED TO THE FACULTY OF THE COLLEGE OF GRADUATE STUDIES

UNIVERSITY OF PETROLEUM & MINERALS

DHAHRAN, SAUDI ARABIA

IN PARTIAL FULFILLMENT OF THE
REQUIREMENTS FOR THE DEGREE OF

MASTER OF SCIENCE IN ELECTRICAL ENGINEERING

FEBRUARY 1982

UNIVERSITY OF PETROLEUM & MINERALS

DHAHRAN, SAUDI ARABIA

This thesis, written by

Mr. Uthman Abdullatif Fattah

under the direction of his Thesis Committee, and approved by all its members, has been presented to and accepted by the Dean, College of Graduate Studies, in partial fulfillment of the requirements for the degree of

MASTER OF SCIENCE IN ELECTRICAL ENGINEERING

Dean, College of Graduate Studies

Date 1/12/82

Department Chairman Jan 12 1982

THESIS COMMITTEE

Chairman Jan. 12, 1982

Member

Member

This thesis is dedicated to my wife

ACKNOWLEDGEMENTS

Acknowledgement is due to the University of Petroleum and Minerals for supporting this research.

I am in great debt, and faithfully thankful to a number of persons who helped me directly or indirectly in keeping up, until the final touches have been successfully reached, especially my advisor Dr. M. Ali Kettani who brought up the idea into my mind and helped me with the basic principles of the design. I also thank the two members of the committee supervising my work, Dr. Khaja F. Subhani and Dr. Samir S. Rofail, Assistant Professors in the Department of Electrical Engineering.

I wish to express my gratitude to Dr. Fareed M. Zedan, Chairman of the Electrical Engineering Department for his continuous cooperation and encouragement.

Finally, thanks are due to all lab. technicians and secretaries for their help and cooperation.

TABLE OF CONTENTS

LIST OF TABLES

LIST OF GRAPHS AND ILLUSTRATIONS

ABSTRACT

First a survey of principles used in designing the principal types of solar radiation-measuring instruments is described together with a brief description of the various factors affecting their calibration and limiting their lifetimes. Then a theoretical analysis of thermal effect in transistors is developed, with the aim of designing an electronic apparatus for measuring total and possibly direct solar radiation. Finally a laboratory set-up of such "transheliometer" is reported along with the pertinent calculations and experimental observations.

The major objective in this work is to assess the suitability of the bipolar junction transistor (BJT) as a radiation sensing device in order to meet the requirement of designing simple, effective and economic radiation-measuring instrument.

INTRODUCTION

Reliable, quantitative meteorological and climatological as well as solar data are essential parameters for designing solar systems, and for prediction of environmental hazards. Development of simple, rugged, and inexpensive instruments for measuring solar radiation, is of great importance, particularly for countries with limited manpower resources. Several instruments are in use for this purpose operating on different principles. These instruments convert solar radiation into some other form of energy, and provide a measure of the energy flux produced by the incident radiation. Some of these instruments are based on the detection of the difference between the temperatures of black surfaces and white surfaces by thermopiles, and others are based on the photovoltaic detectors. Sensitivity of calibration, in these instruments, is subject to changes due to surrounding atmosphere and aging.

Technology of solid-state devices allows the development of a temperature-dependent model for the transistor which can be utilized in the design of a modern electronic solarimeter. The new solarimeter

described here has been designed especially to fulfil the increasingly stringent demands for an economic, sensitive, and easy to build heliometer. The operation of this heliometer is based on the increase of the collector current with temperature in a bipolar junction transistor.

1. LITERATURE SURVEY

1.1 SOLAR RADIATION

The sun emits radiant energy at the same average rate in all directions. Since the earth is small compared to the radius of its orbit, it intercepts only a small fraction of the total energy emitted by the sun. The thermal radiation from the surface of the sun is similar to the radiation that a blackbody would emit at a temperature of 6000^{o}K. A blackbody is a hypothetical, ideal object that emits maximum intensity of thermal radiation as a result of its temperature alone.

Solar radiation is one form of electromagnetic radiation. The sun emits strongly in the infrared, visible and ultraviolet portions of the electromagnetic spectrum. However, solar radiation is considerably modified when it passes through the relatively cooler solar corona. It also interacts with the gas molecules in the earth's atmosphere by absorption and scattering. Absorption is a selective process and depends on wavelength. Gas molecules absorb radiant energy and convert is into a different form. Scattering, can occur at any wavelength. It involves the redirection of solar beams so that earth receives light from the sky in addition to the light coming directly from the sun. In the troposphere, where clouds form, part of the incoming solar

radiation is reflected by clouds. The reflection process has a significant effect on solar energy input to the earth's surface.

The appropriate measure for discussing the distribution of radiant energy is the amount of energy that falls on an area of standard size. In meteorology, measurements of solar radiation or insolation are specified in units of energy per unit time per unit area of a horizontal surface.

Solar radiation data are available in several forms. Any form should include the time interval and location of measurements, as well as the type of radiation, whether direct, diffuse, or total. The measuring instruments and their orientation, should also be mentioned.

Direct solar spectral irradiance for any time of the day and any location can be computed from the extra-terrestrial values of the solar spectrum, using atmospheric parameters of scattering and absorption and the air mass. The atmospheric parameters are known to a fair degree of accuracy[14]. Figure 1 shows a standard spectral irradiance curve at the mean-sun-earth distance.

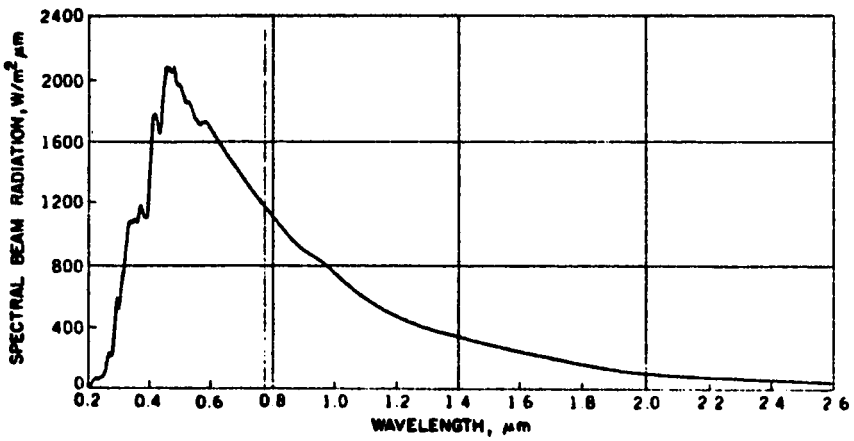

Figure 1. A standard spectral irradiance at the mean-sun-earth distance[11].

1.2 TERMINOLOGY AND LAWS OF RADIATION

Terms and symbols used for the physical quantities involved in the statement of radiation laws will be followed here.

Radiation energy density or radiant density, U, at a given point in space is the energy per unit volume in the vicinity of that point.

The radiant flux (insolation), ϕ, through a given surface is the radiant energy which crosses a unit area per unit time.

The radiant emittance (flux density), W, of a radiating surface at a given point is the radiant energy emitted per unit area in the vicinity of that point per unit time.

The radiance, N, of a radiating surface at a given point is the radiant energy emitted per unit area, per unit solid angle at that point, per unit time.

Related quantities are radiant reflectance, ρ, transmittance, τ, and absorptance, α, which are the ratios of energy, reflected, transmitted, and absorbed, respectively, to the energy on a given surface.

Emissivity, ε, of a given surface, is the ratio of the radiant emittance of the surface to that of a blackbody surface at the same temperature.

The quantities mentioned previously refer to the energy radiated at all frequencies or in the entire wavelength range. The corresponding spectral quantities are denoted by adding the subscript λ, the wavelength, or ν, for frequency, to the respective symbols.

The spectral radiance ϕ_λ, for example, is related to the radiant flux ϕ by the following equation:

$$\phi = \int_0^\infty \phi_\lambda \, d\lambda \qquad (1\text{-}1)$$

Certain simple relations hold between the quantities ϕ, W, N, and U that is

$W = \pi \, \Omega \, N$, where Ω is in steradians

$U = 4\pi\Omega \, N/C_0$, where C_0 is the velocity of light, and

$W = C_0 U/4$.

Radiation in the region of the electromagnetic spectrum from about 0.2 to about 100 μm is called thermal radiation and is emitted by all substances as a result of their temperature. The spectral distribution of this radiation for a blackbody is given by Planck's law.

$$\phi_\lambda = \frac{2\pi h C_0^2}{\lambda^5 (e^{h C_0/\lambda k T} - 1)}, \qquad (1\text{-}2)$$

where h is Planck's constant (6.6256×10^{-34} J.Sec), k is Boltzmann's constant (1.38054×10^{-23} J/^{o}K), and T is the temperature in degrees Kelvin.

Planck's law is illustrated in Fig. 2, which shows spectral radiation distribution for a blackbody radiating at 400^{o}K, 1000^{o}K, and 6000^{o}K. It is noticed that the distribution shown for 6000^{o}K is an approximation of the distribution of solar radiation outside the earth's atmosphere shown in Fig. 1.

In engineering calculations, the overall energy is often of more interest, so by integrating Planck's law over all wavelengths, the total energy emitted by a blackbody is found to be

$$\phi = \int_0^\infty \phi_\lambda \, d\lambda = \sigma T^4 \qquad (1\text{-}3)$$

where σ is Stefan-Boltzmann constant, it is equal to 5.6697×10^{-8} watt/m^2 ^{o}K^4.

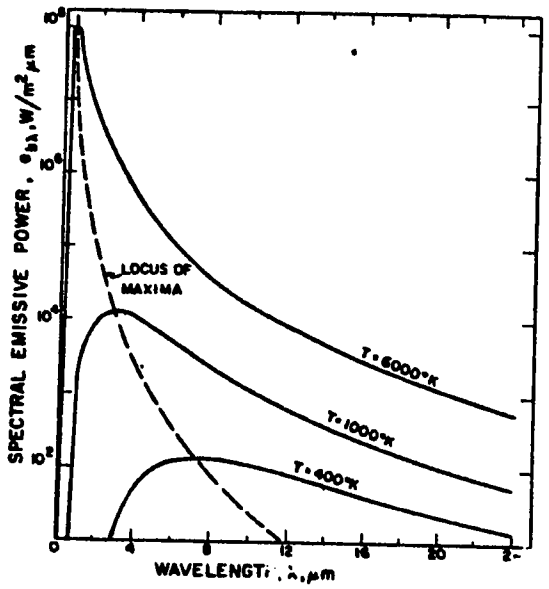

Figure 2. Spectral distribution of blackbody radiation[2].

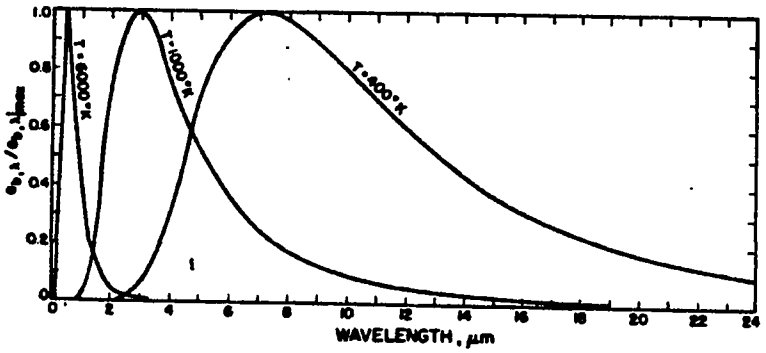

Figure 3. Normalized spectral distribution of blackbody radiation[3].

In order to predict the performance of the radiation sensing surface in a radiometer, it is necessary to evaluate the radiation exchange between the sensing surface and the sky. Considering the sky as a blackbody at some equivalent temperature T_{sky} it is found that the net radiant energy per unit time, q_i radiation to a surface with emittance ε and temperature T, is

$$q_i = \varepsilon s \sigma \, (T_{sky}^4 - T^4) \qquad (1\text{-}4)$$

where s is the surface area of the sensor.

Several relations for clear skies have been proposed to relate T_{sky} to other measurable meteorological variables.

Swinbank[13] [1963] related sky temperature to the local air temperature in the following simple relationship

$$T_{sky} = 0.0552 \, T_{air}^{1.5} ,$$

where both temperatures are in degrees Kelvin. But Whillier[16] [1967] used a simpler expression

$$T_{sky} = T_{air} - 6^{\circ}C$$

1.3 SOLAR RADIATION MEASUREMENTS

Usually solar irradiance measurements, at the earth's surface, are made for the overall amount of radiant energy in all wavelengths. Several instruments have been designed for insolation measurements. Direct radiation is measured by instruments which can only accept radiation from a cone of semi-angle about 5^{o}. Total radiation (direct + diffuse) is measured by instruments which have a view angle of 2π radians. Different principles have been used for designing such instruments.

1.3.1 Thermopile[a] Instruments[8]

In a thermopile, a thin blackened surface is exposed to radiation and difference in temperature, between the surface and some reference points, is measured in terms of an electromotive force generated by several thermo-junctions connected in series.

The rate of heat loss must be independent of the external climatic conditions. By making the instrument case massive and with a polished outer surface, the temperature is kept uniform over the radiation sensor

a) a single compact unit of thermocouples joined in series

and only changes slowly.

Many instruments are based on the principle of thermopiles, like Epply pyranometers, Moll-Gorczynski solarimeter, which are used for measuring total radiation, and Linke-Feussner actinometer for measuring direct solar radiation.

Considering Moll-Gorczynski solarimeter as an illustration for the thermopile principle (Fig. 4), it is noticed in this instrument, the sensor consists of alternate thin strips of manganin[a] and constantan[b] with the reference (cold) junctions are in good thermal contact with the supporting posts. If the temperature at the center of the receiving service is raised, an electromotive force is set up which can be measured with a suitable galvanometer. The receiving surface is covered with two concentric hemispherical glass domes. The glass domes shield the sensitive surface from wind and rain, and reduce the convection losses.

Figure 5 shows a complete diagram for Linke-Fuessner actinometer which operates on the principle of thermopiles. The thermopile is at the base of a cylindrical tube which limits the view angle to the sun

---

a) an alloy principally of copper, manganese, and nickel.

b) an alloy of 55% copper and 45% nickel.

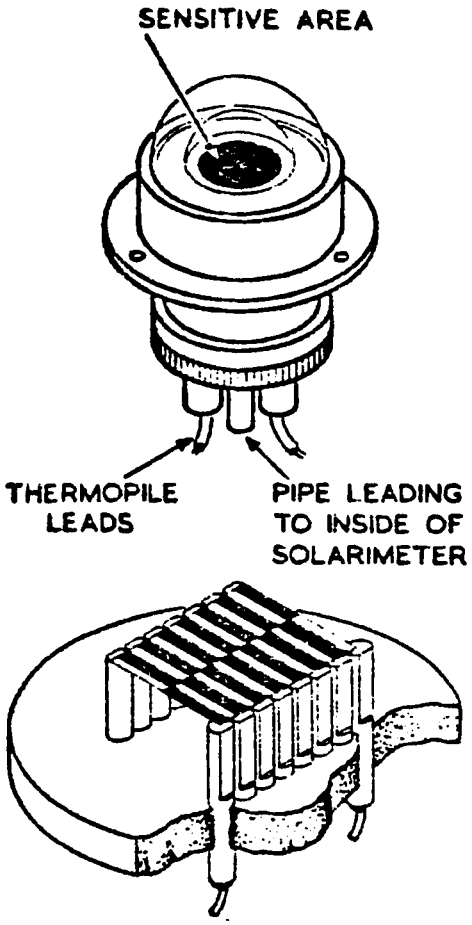

Figure 4. Moll-Gorczynski Solarimeter[8].

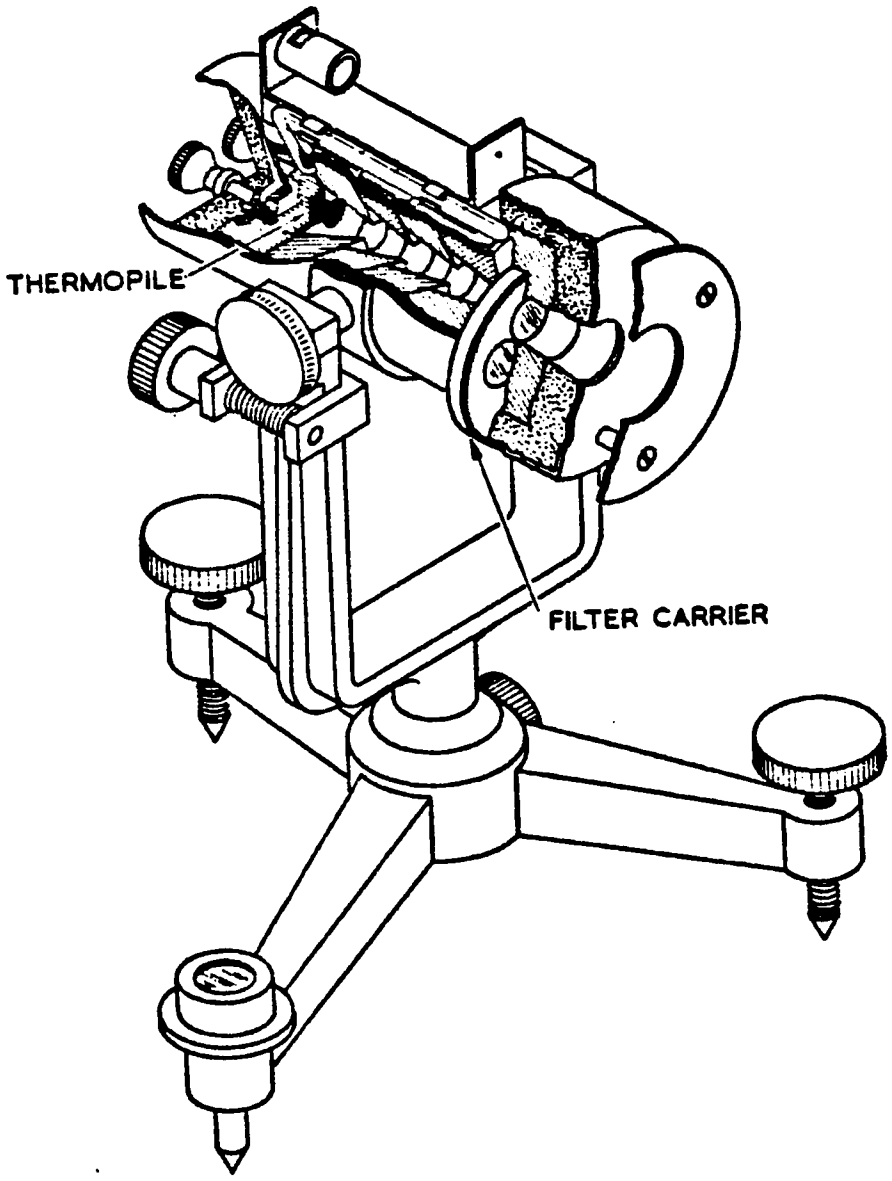

Figure 5. Linke-Fuessner Actinometer[8].

and to about 5^{o} of circumsolar sky.

The Ångström pyrhiometer, shown in Fig. 6, is a standard instrument for the measurements of direct radiation. It has two identical strips of platinum coated black, similarly mounted except that, one strip is exposed to the radiation while the other is shielded from it.

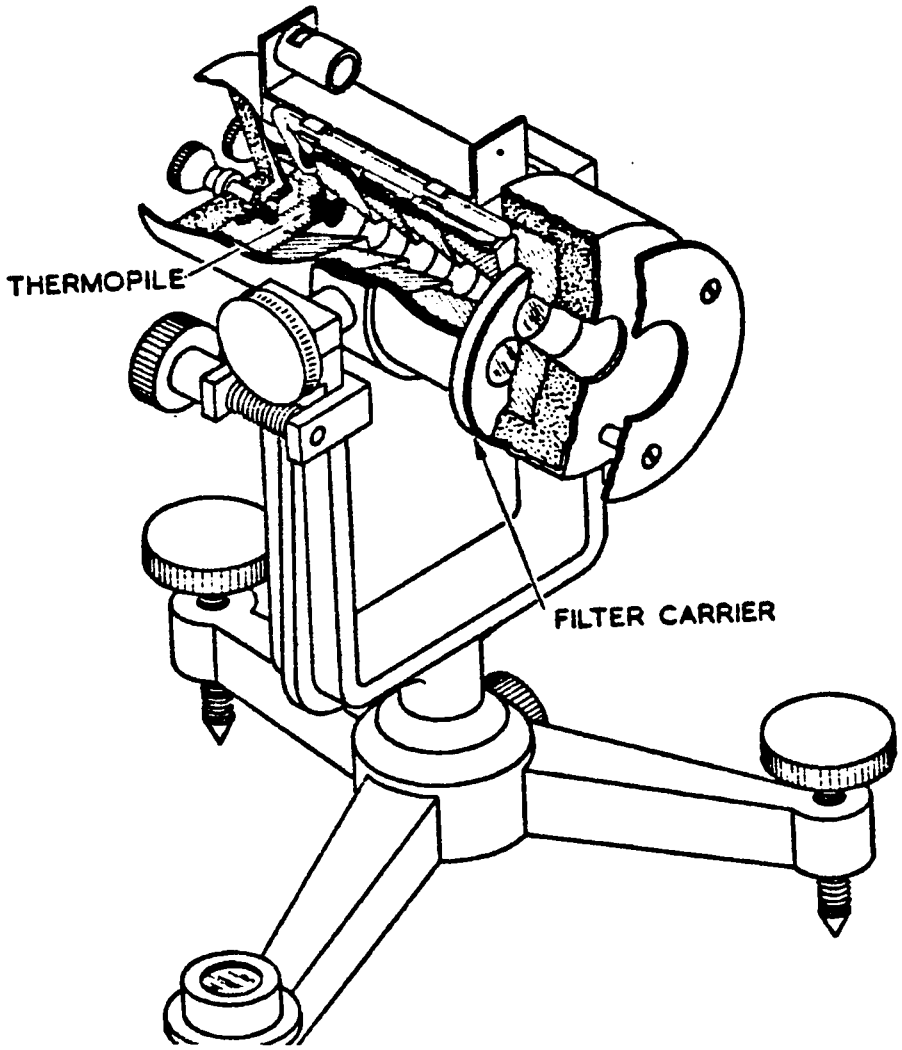

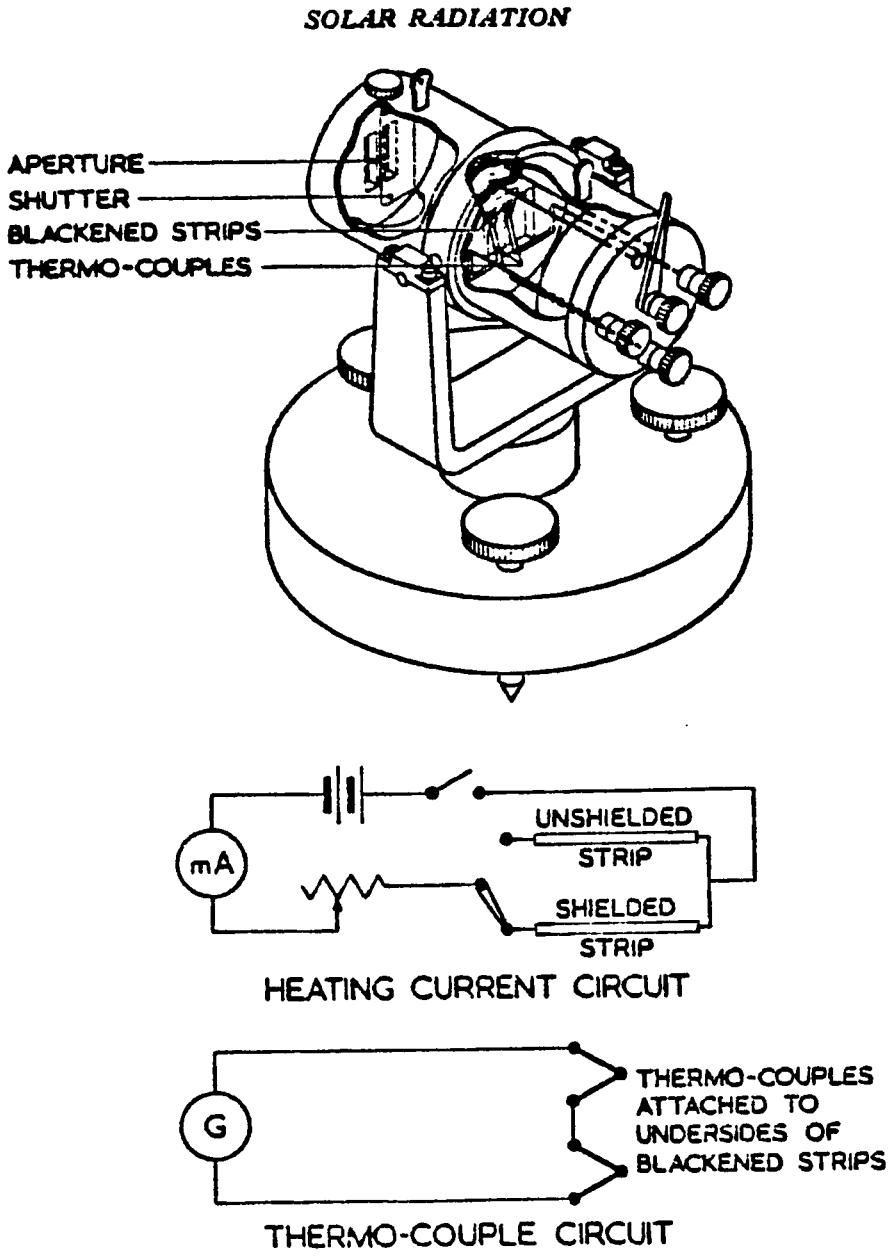

Figure 6. Angstrom Pyrheliometer[8].

properties of the material composing them, which are temperature-dependent quantities. Thus, when thermopile instruments are put into service, gradual and cummulative changes begin to occur altering the characteristics of the thermoelements beyond the allowable tolerance. The causes of these changes are varied and depend upon such factors as the temperatures encountered, the length of time in service, and the atmospheric conditions surrounding the thermopile. The introduced inhomogeneity in composition and physical state of the couple material causes parasitic emf's which add to or subtract from the total couple emf.

Furthermore, the successive expansions and contractions of the thermocouples resulting from the daily fluctuating temperatures, deform the thermocouple by twisting and bending (Fig. 7).

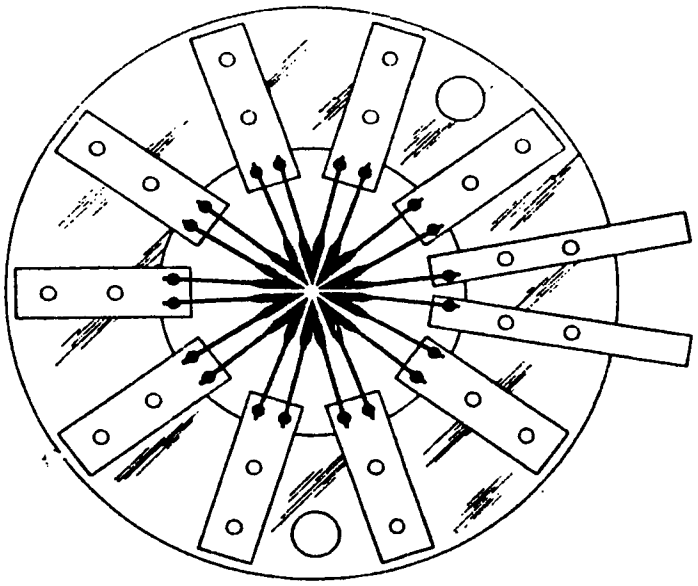

Figure 7. Enlarged view of thermopile showing hot junctions flattened to form, receiver, and terminal strips staked to annular ring of mica [7].

1.3.3 Silver-disc Pyranometer (Fig. 8)

This instrument is used for measuring direct solar radiation. A blackened silver-disc is exposed to the incident radiation. The temperature of the disc is measured by a mercurry thermometer mounted on the case. The initial rate at which the silver disc is heated by radiation is found by measuring the rate of change of the disc temperature. The radiation intensity ϕ is computed by the following expression:

$$\phi = BR\,[1+K(T-30)-K'(T_a-20)] \qquad (1\text{-}5)$$

where T is the disc temperature, T_a is the ambient temperature, and B,R,K, and K' are instrumental correction constants.

This expression is found as an approximate solution of the differential equation which describes the temperature change of the disc.

The procedure, when using this instrument involves five steps. These steps must be followed and repeated many times in order to compute the correction constants. Also the ambient temperature should be measured at the time and place of observation.

1.3.4 Photovoltaic Cells Principle

Photovoltaic, or solar cells, are characterized by the generation of a small voltage upon illumination.

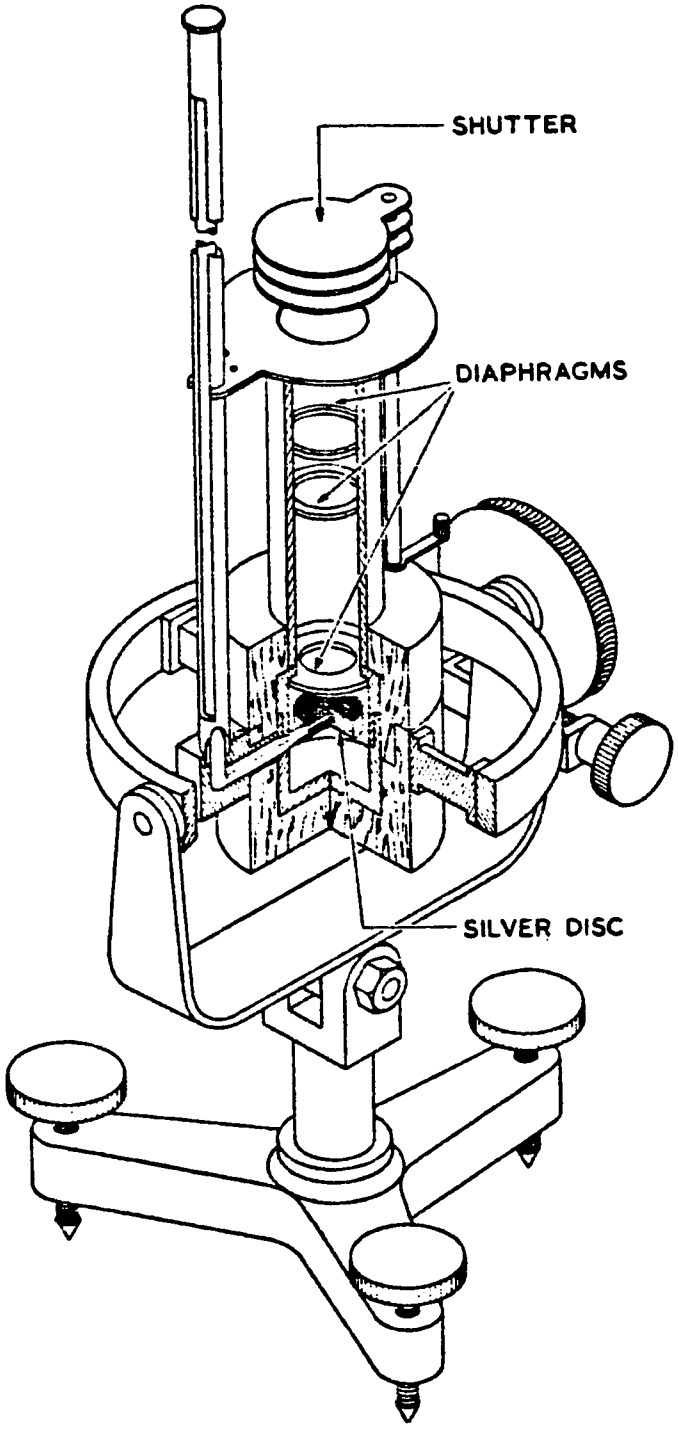

Figure 8. Silver-disc Pyrheliometer[8].

The solar cell contains a pn junction, commonly fabricated from silicon. When the junction is illuminated, charge carriers are liberated. Thus, a terminal voltage is generated as a result of light striking the pn junction of the cell. Fig. 9 shows a silicon solar cell.

As the name "solar cells" might suggest, photovoltaic cells can be used to convert solar energy into electrical energy directly. One of the applications of such cells is their use for measuring solar radiation. The short-circuit current, at normal radiation levels, is almost a linear function of the incident solar radiation in these cells. But solar cells have the disadvantage that their spectral response is not linear and the volt-ampere characteristics is dependent on ambient temperature (Figs. 10 and 11). Thus instrument calibration is a function of the spectral distribution of the incident radiation, and ambient temperature. Also the calibration varies with the angle of incidence of the radiation.

1.4 FURTHER CONSIDERATIONS

In the case of thermopile instruments, it is noticed that the generated electromotive force is very small. It may be measured along with any voltage induced by electromagnetic waves originating from various sources. If the number of the thermocouples

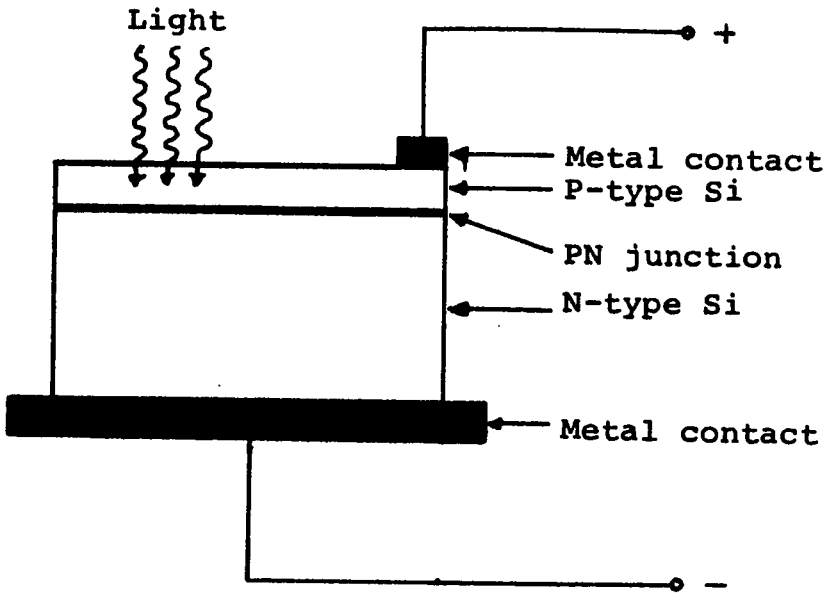

Figure 9. The construction of a silicon solar cell.

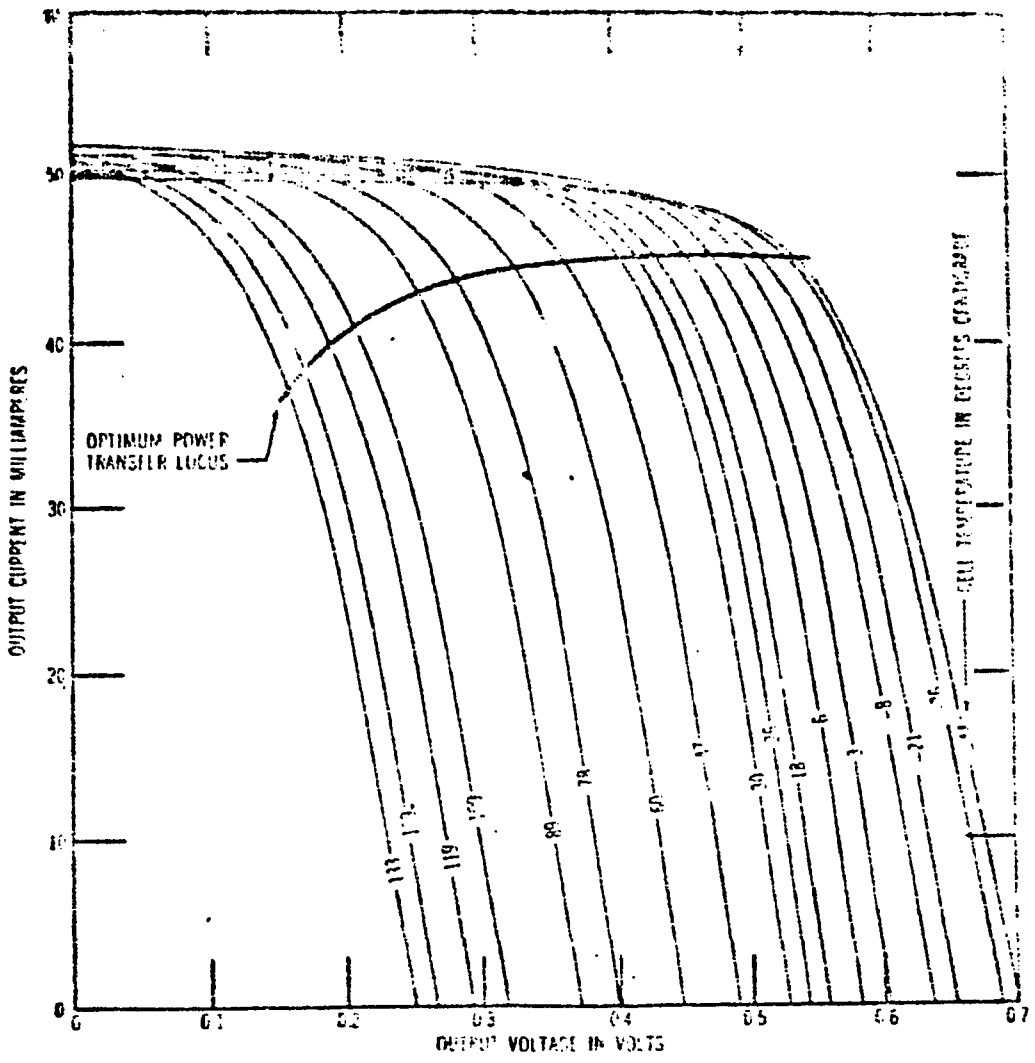

Figure 10. Dependence of the volt-ampere characteristics of a silicon cell (1x2 cm) with 10% conversion efficiency[5].

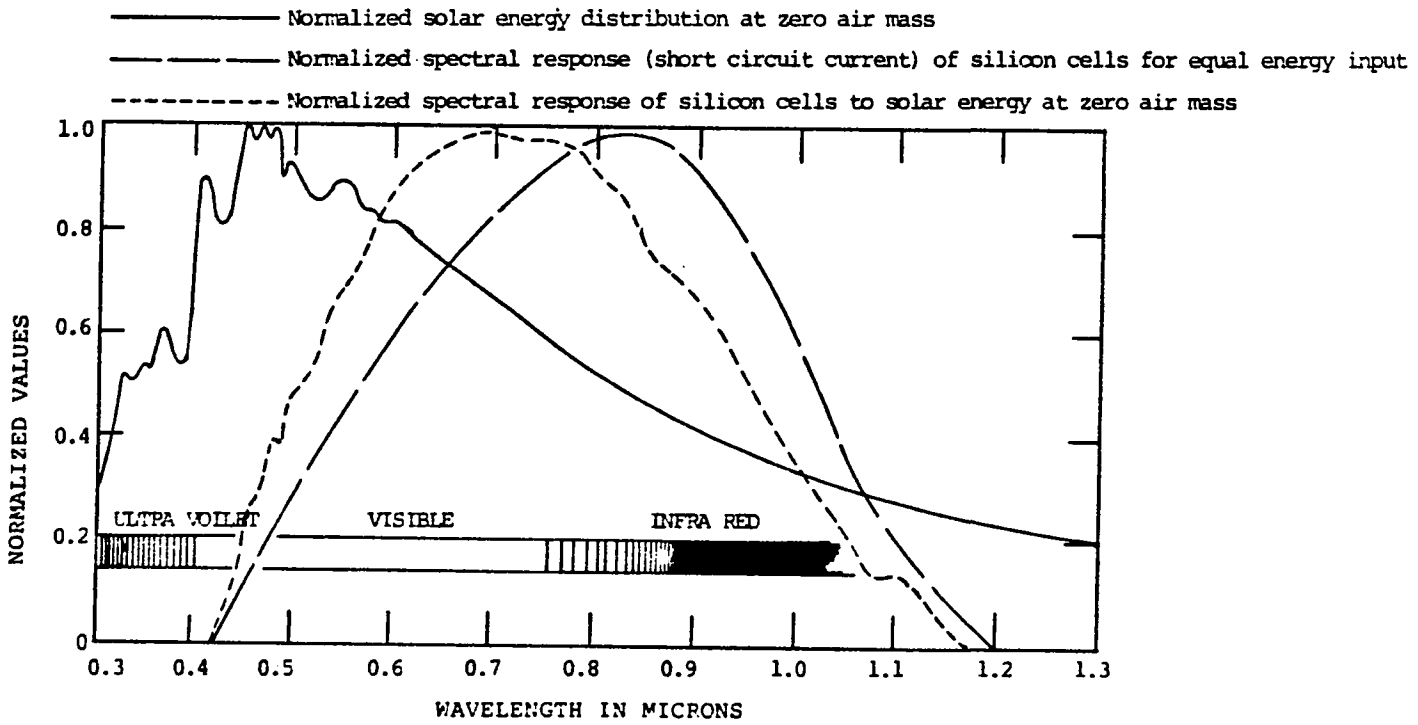

Figure 11. Solar radiation distribution and spectral response of silicon solar cell[5].

is increased to make the thermoelectric emf relatively high so that the effect of induced voltages is minimized, then the thermal junctions become difficult and costly to construct. On the other hand, for a given thermo-electric effect, the sensitivity limit is soon reached because of the difficulty of crowding more and more junctions into a specified space.

Furthermore, the radiation sensing surfaces in these instruments, should essentially be flat so that they receive the irradiance at normal incidence for maximum absorption of the radiant energy. But these surfaces are not suitable because of the diurnal course of the sun's path across the sky, which varies from day to day. Some pyrheliometers are provided with a clock mechanism which automatically maintains the receiving surface normal to the sun's rays. The clock must be set at the beginning of each day. Therefore, these instruments are costly, and require especially trained personnel for their operation and maintenance.

From the economical point of view, the most comprehensive radiation-measuring networks exist within countries where solar energy competes with abundant alternative cheap energy sources. At the same time, only limited solar-radiation records are available in countries where solar energy could be effectively and economically utilized to improve the standard of living of the people.

The major objective in this work is to assess the suitability of the transistor as a radiation sensitive element to meet the requirement of designing simple, effective, and economical radiation measuring devices.

1.5 TRANSISTORS AS RADIATION SENSORS

Is the transistor suitable for measuring solar radiation ? An examination of the previously discussed instruments, and a study of transistors as radiation sensing devices will answer this question.

The transistor collector current increases almost exponentially with increasing temperature. A modern radiation-measuring instrument can be designed, using a transistor based on the temperature effect, and calibrated at thermal equilibrium with the help of Eqn. (1-2). This method of calibration eliminates completely the errors due to temperature changes. Also the transistor current gain increases the power-handling capability making the measured voltage independent of externally induced emf's. Furthermore, choosing a transistor, sealed in a spherical case, normal incidence is ensured, and the same cross sectional area, $2\pi r^2$ will be exposed to sun rays for all positions of the sun. The whole network needed can be fabricated as a small integrated circuit with transistor as a plug-in device for replacement if it is necessary. Such networks are known for their long-term reliability; they are also inexpensive compared to thermopiles or solar cells.

2. THEORETICAL FUNDAMENTALS

2.1 INTRODUCTION

A transistor is a three-terminal device made of silicon or germanium, used also in the fabrication of other solid-state devices. By doping the intrinsic semiconductor the transistor takes on several properties which make it useful in designing many electronic circuits, such as, amplifiers, oscillators, multivibrators, and logic circuits.

All practical solid-state devices are temperature-sensitive to some extent. Therefore, it is necessary to follow some prescribed constraints, throughout the design of any electronic circuit, to minimize thermal effects and thus establish stabilized operating points.

As a new utilization of transistors, the thermally generated leakage current will be used here to design a solarimeter based on heating the transistor with the thermal energy produced by solar radiation.

In order to arrive at an optimum realization of the desired circuit, a brief study of thermal effect in semiconductor materials, and in pn junctions will follow.

2.2 SEMICONDUCTOR MATERIAL

The name semiconductor is given to a group of materials whose resistivities lie between those of insulators and good (i.e. metallic) conductors.

The most striking difference between the physical behavior of semiconductors and metals is that the resistivity of semiconductors decreases with increasing temperature instead of increasing in the manner of all metals.

Physical constants such as resistivity and thermal conductivity, depend strongly on temperature according to laws of the general form.

$$\rho = \rho_0 \, e^{eV/kT} \qquad (2\text{-}1)$$

where, by way of example, ρ and ρ_0 are the resistivities at $T\,^0K$ and $0\,^0K$ respectively, eV is a so-called activation energy, characteristic of the semiconducting material.

2.2.1 Temperature Dependence of Energy Gap and Charge Carriers

The energy band structure of semiconductor materials is shown in Fig. 12. This structure has a full valence band separated by a large energy gap E_g (in eV) from the empty conductor band.

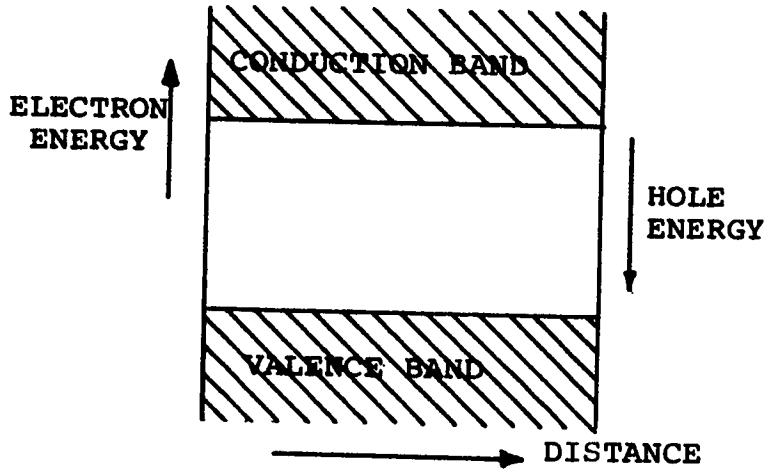

Figure 12. Simplified band diagram.

When the temperature is raised, some electrons in the valence band will have enough energy to be excited into conduction band state. Also experimental results show that the band gaps of most semiconductors decrease with increasing temperature. The detailed variations of band gaps as a function of temperature for Ge, Si, and GaAs are shown in Fig. 13.

The temperature-dependence of the band gaps can be expressed by a universal function

$$E_g(T) = E_g(0) - \frac{\alpha T^2}{T+\beta} \qquad (2\text{-}2)$$

where $E_g(0)$, α, and β are given in Fig. 13, and T represents the temperature in degrees Kelvin.

For intrinsic semiconductors at finite temperature there is continuous thermal agitation that results in the creation of electrons and holes in pairs, therefore the conduction band electron density, n (electron per cm^3), is equal to the density of holes, p (holes per cm^3), in the valence band. Each of these intrinsic carrier densities is commonly referred to as n_i. Thus for intrinsic semiconductor,

$$n = p = n_i$$

which means that at a given temperature there is a certain density of electron-hole pairs n_i.

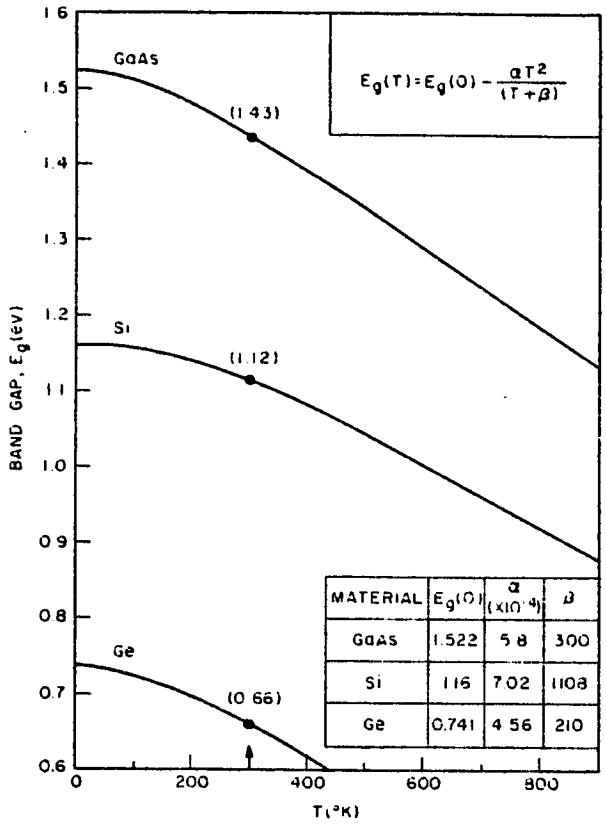

MATERIAL	$E_g(0)$	α ($\times 10^{-4}$)	β
GaAs	1.522	5.8	300
Si	1.16	7.02	1108
Ge	0.741	4.56	210

Figure 13. Energy band gaps of Ge, Si, and GaAs as a function of temperature [15].

The intrinsic carrier density is found to vary with temperature according to the following relation:

$$n_i(T) = 2 \left(\frac{2\pi kT}{h^2}\right)^{3/2} (m_n^* m_p^*)^{3/4} e^{-E_g/kT} \qquad (2\text{-}3)$$

where m_n^*, and m_p^* are the effective masses of electron and hole respectively.

Figure 14 shows the variation of n_i as a function of temperature for Ge, Si and GaAs[9].

2.2.2 Impurity Effect in Semiconductors[12]

The electrical action of silicon or germanium can be modified by the addition of impurities, leading to n- and p-type semiconductors. It will be recalled that the majority charge carriers in these materials are the electrons and holes, respectively.

When impurities are introduced into an otherwise perfect crystal, additional impurity energy levels are created in the energy band structure, usually within the band gap. For example, an impurity donor from column V of the periodic table (P, As, or sb) introduces energy level very near the conduction band in Ge or Si. This level is filled with electrons at $0^{o}K$, and very little thermal energy is required to excite these electrons to the conduction band Fig. 15.

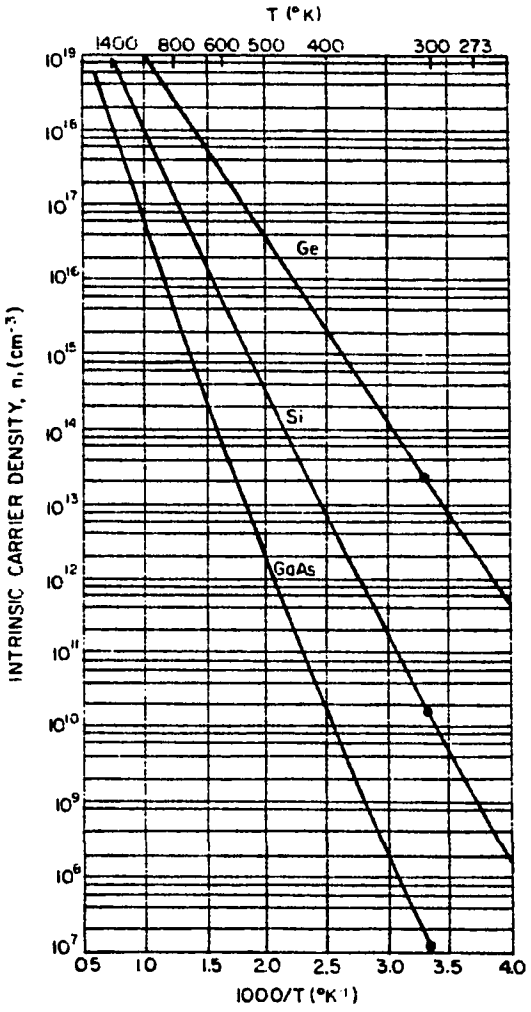

Figure 14. Intrinsic carrier densities of Ge, Si and GaAs as a function of the reciprocal temperature[9].

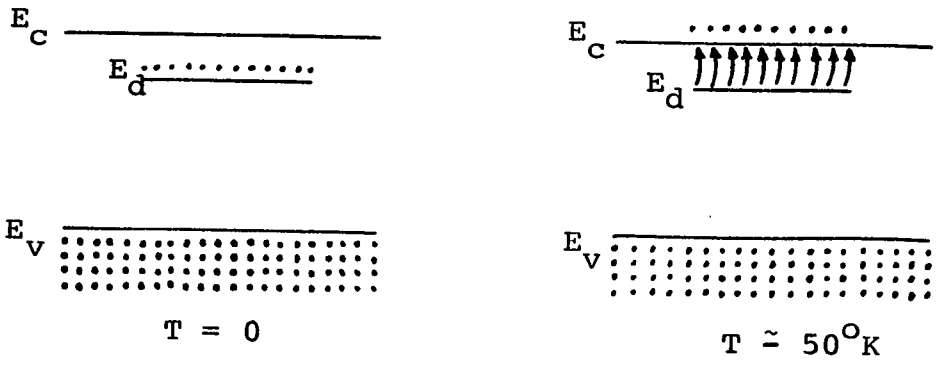

Figure 15. Donation of electrons from a donor level to the conduction band.

Similarly impurity acceptors from column III (B, Al, or Ga) introduce impurity levels in Ge or Si near the valence band. These levels are empty of electrons at $0^{o}K$ (Fig. 16). At low temperatures, enough thermal energy is available to excite electrons from the valence band into the impurity level, leaving behind holes in the valence band.

2.2.3 Temperature-Dependence of Majority Carriers

The np product in intrinsic or extrinsic material, at thermal equilibrium is given by

$$np = n_i^2 \qquad (2\text{-}4)$$

However the temperature dependence of the majority carrier density in extrinsic material will differ from that shown in Fig. 14. A typical example is shown in Fig. 17, where n is plotted as a function of the reciprocal temperature. In this example Si is doped n-type with a donor density of 10^{15} cm^{-3}.

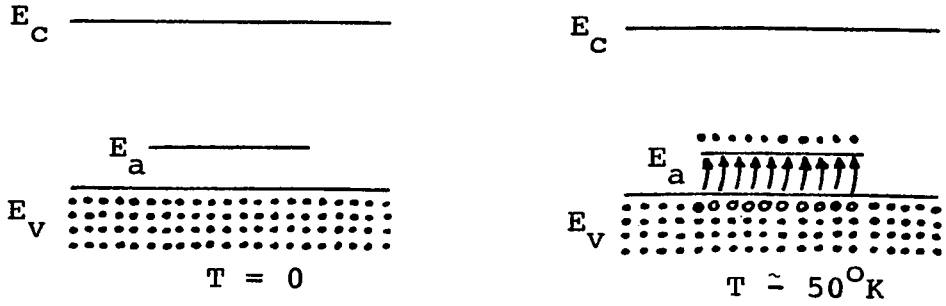

Figure 16. Acceptance of valence band electrons by an acceptor level, and the resulting creation of holes.

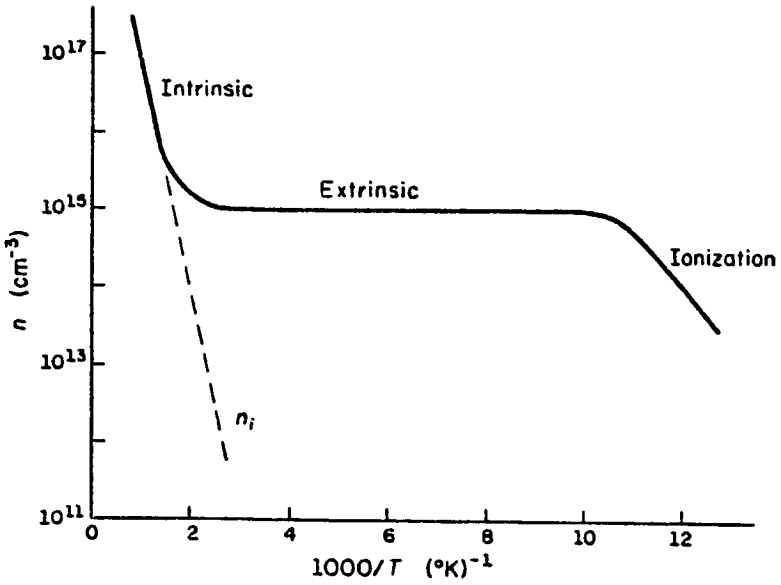

Figure 17. Carrier concentration vs. inverse temperature for Si^{12} with 10^{15} donor/cm^3.

2.3 pn JUNCTION

The pn junction is the heart of all semiconductor diodes and transistors, therefore attention is focussed initially on the pn junction characteristics under forward and reverse biasing.

A pn junction consists of p- and n-type semiconductors material joined together to form an unbroken structure. Electrons from the n-side diffuse across the junction into the p-side, and holes from the p-side diffuse into the n-side, as shown in Fig. 18a.

Figure 18b shows the saturation taking place after equilibrium is reached. The region on either side of the junction, where diffused carriers appear, is called the depletion region. An electric field is set up across the width of the depletion region resulting in a potential difference between the n and p regions. This difference in potential is usually called the contact potential and is the equilibrium potential difference across the pn junction. The symbol representing the junction as an element (diode) in electrical networks is shown in Fig.19a.

When the positive terminal of a battery is connected to the p-side and the negative terminal to the n-side, the depletion region is reduced (Fig. 19b) and a fairly high current is observed. This current is called the forward biased. If the terminals of the battery,

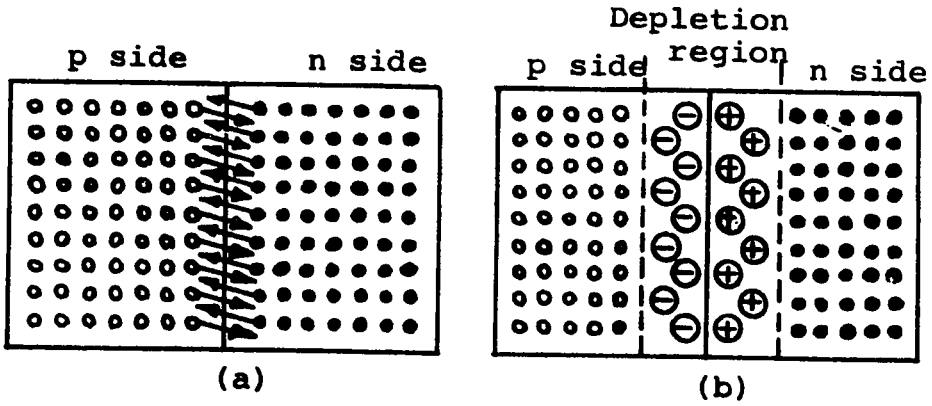

Figure 18. Formation of depletion region (a) carriers diffuse across the junction until (b) equilibrium is reached.

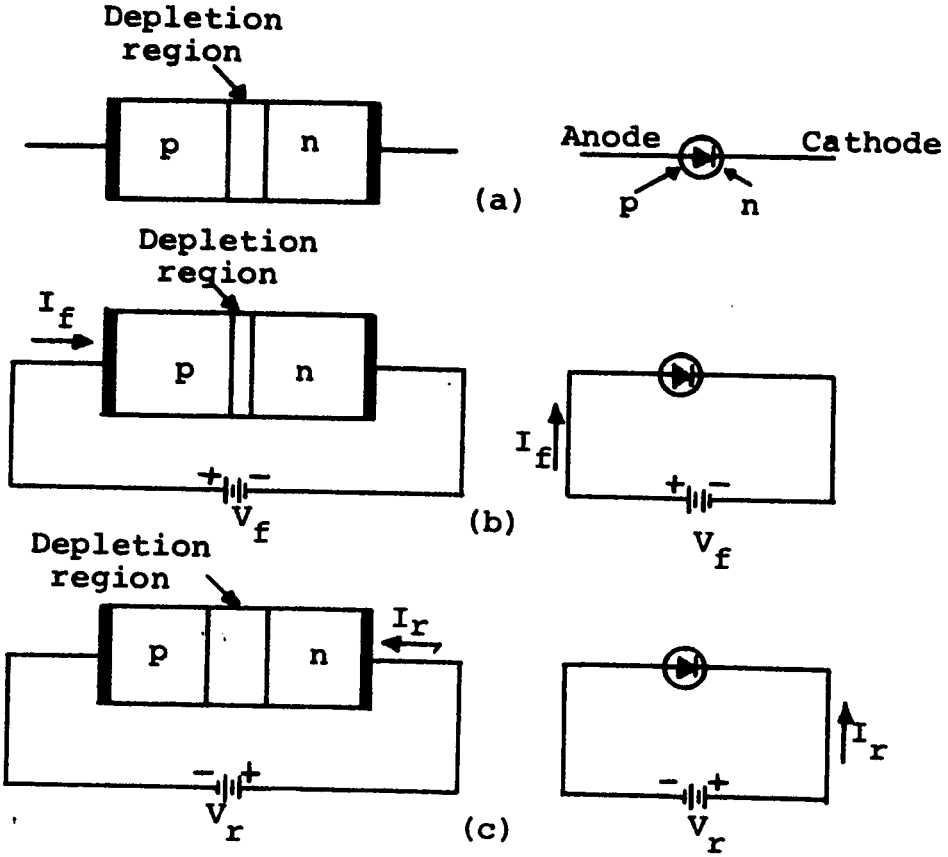

Figure 19. pn-junction diode (a) no bias. (b) forward biased (c) reverse biased.

in the previous connection, are interchanged the depletion region increases (Fig. 19c) and a minute current is observed. The current is called the reverse current, and the junction is said to be reverse biased.

2.3.1 pn junction Characteristics

The measured volt-ampere characteristics of a typical germanium junction diode at room temperature are shown in Fig. 20a. Figure 20b shows an expanded scale for reverse biasing.

The V-I relationship of a pn junction diode is given by

$$I = I_s \, (e^{qV/kT} - 1) \qquad (2\text{-}5)$$

where I and V denote the current and volrage of the diode and I_s denotes the saturation current.

2.3.2 The Temperature-Dependence of the V-I Characteristics

The v-i relationship Eqn.(2-6) contains the temperature explicitly in the exponent $\frac{qV}{kT}$, as well as implicitly in the saturation current I_s. This current is strongly dependent on temperature according to the following equation

$$I_s = AT^{(3+\gamma/2)} e^{-E_g/kT} \qquad (2\text{-}6)$$

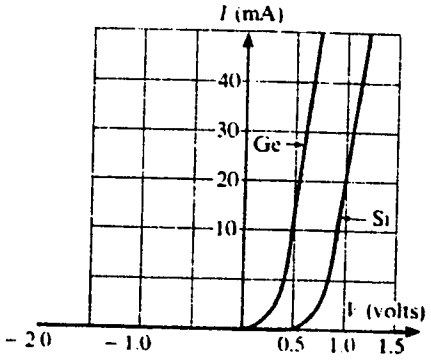

(a)

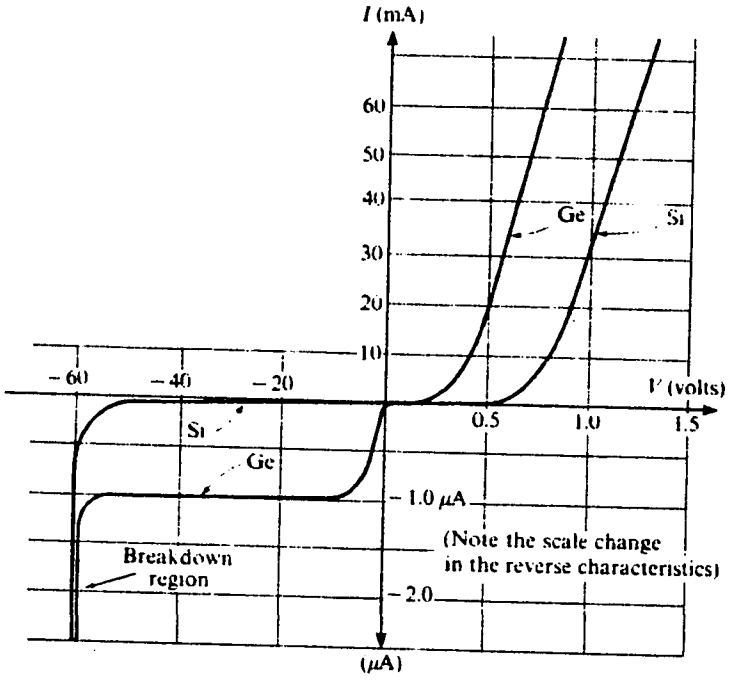

(b)

Figure 20: (a) v-i characteristics of typical junction diodes

(b) v-i characteristics on expanded scale[6].

where A and γ are constants.

The overall temperature effect is clearly seen in Fig. 21 which shows v-i characteristics at two different temperatures T_1 and T_2 where $T_2 > T_1$.

The previous discussion concerning the temperature effect will be given a close attention in conjunction with the operation of transistors in the next section.

2.4 BIPOLAR JUNCTION TRANSISTORS

A bipolar junction transistor consists of a silicon or (germanium) crystal in which a layer (base) of n-type is sandwiched between two layers of p-type silicon. Alternatively, a transistor may consist of a layer of p-type sandwiched between two layers of n-type material. In the former case the transistor is referred to as a pnp-type, and in the later case, as an npn-type. The semiconductor sandwich is extremely small, and is hermetically sealed against moisture inside a metal or plastic case.

The two types of transistors are represented in Fig. 22a. The symbols employed when transistors are used as circuit elements are shown in Fig. 22b. The three portions of a transistor are known as emitter, base, and collector. The arrow on the emitter lead

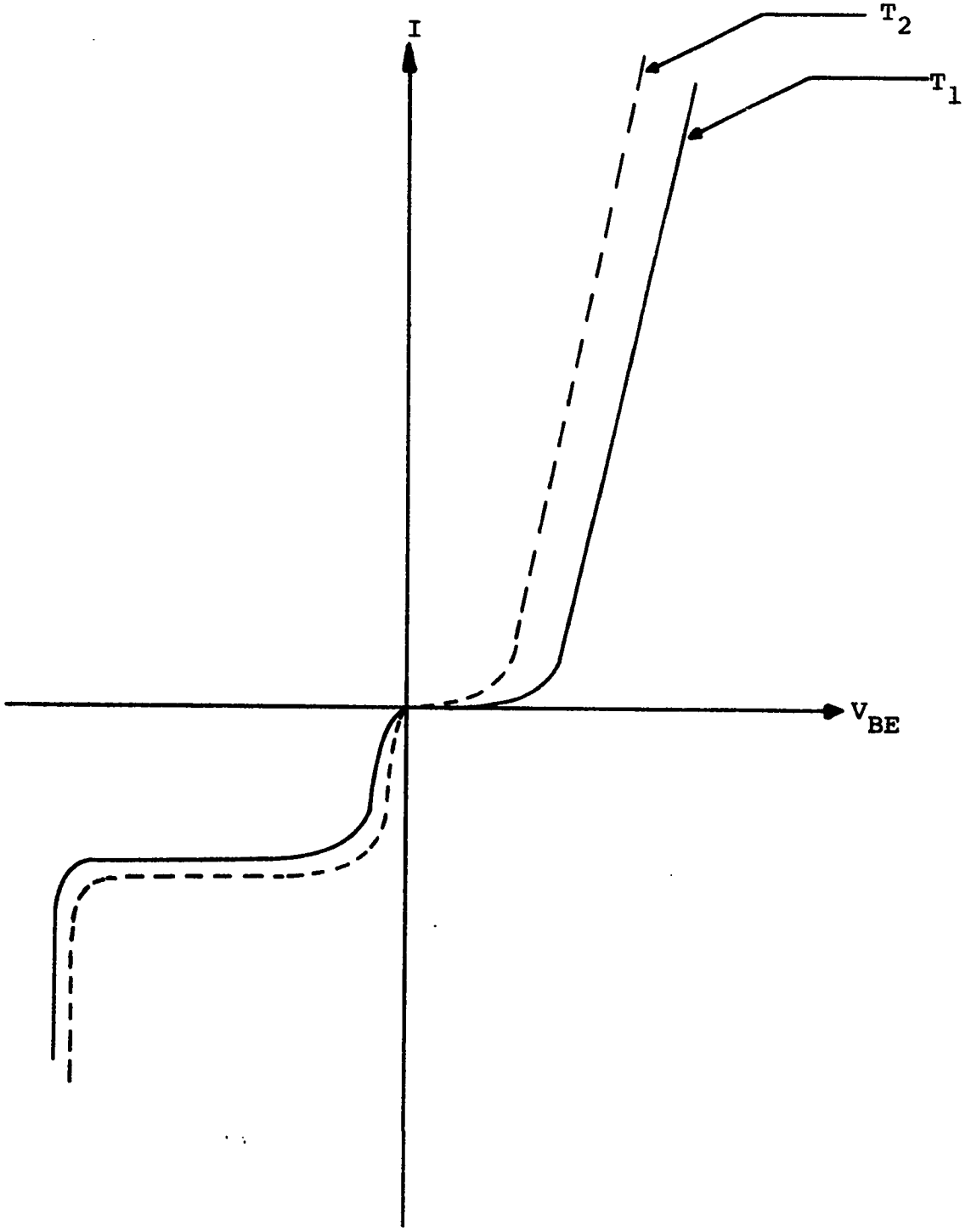

Figure 21. Junction diode characteristic at two different temperatures, T_1, and T_2 ($T_2 > T_1$).

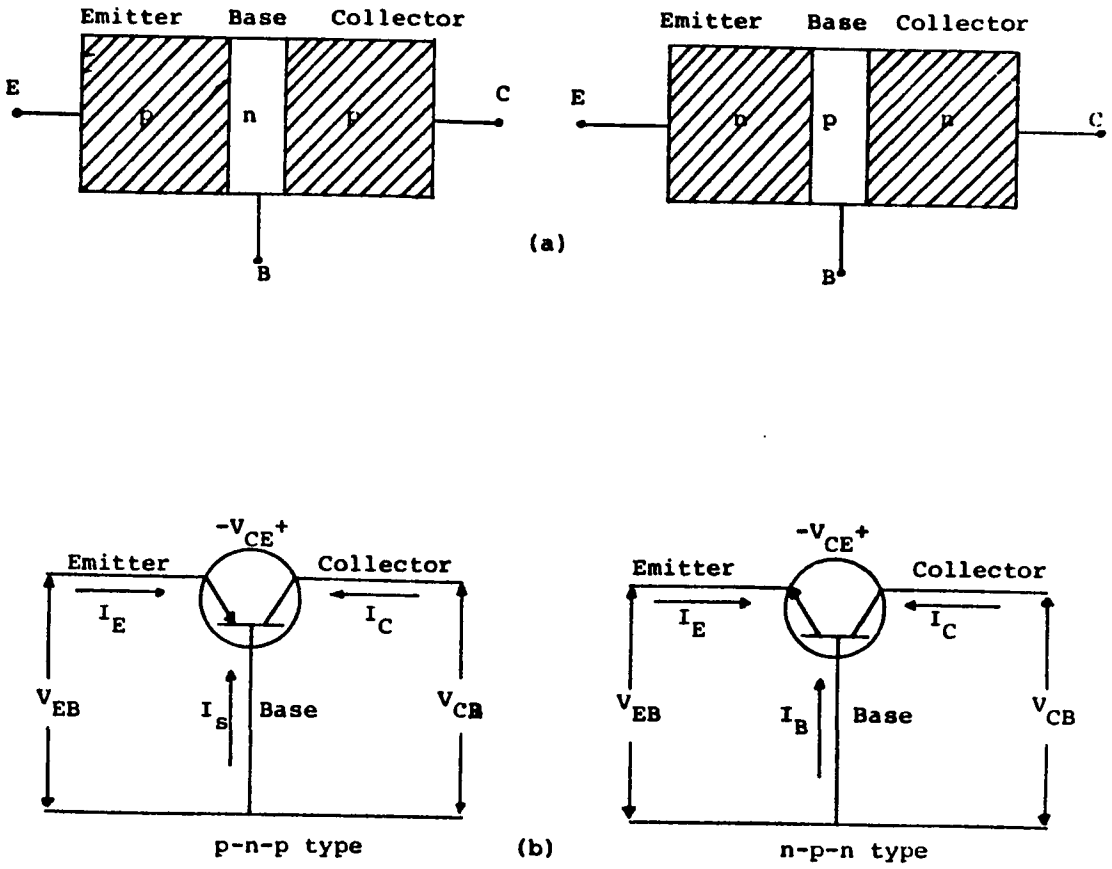

Figure 22. (a) pnp and npn transistors. The emitter (collector) junction is $J_E(J_c)$.

(b) Circuit symbols of the two transistor types.

specifies the direction of current flow under normal operating conditions, i.e. forward-biased emitter junction and reverse-biased collector junction. In both cases, however, the emitter, base, and collector currents, I_E, I_B, and I_C, respectively, are assumed positive when the currents flow into the transistor. The symbols V_{EB}, V_{CB}, and V_{CE} are the emitter-base, collector-base, and collector-emitter voltages, respectively.

2.4.1 Static Characteristic of Transistors

A transistor can be connected in three circuit configurations depending on which lead is common to the input and output circuits. Figure 23 shows the common-base, common-emitter, and common collector configurations for a pnp transistor. The current and voltage connections are given for normal operations. All the signs and polarities should be inverted for an npn transistor.

2.4.1.1 The Common-Emitter Characteristics

The discussion will be restricted to the CE configuration because it is capable of both current gain and voltage gain greater than unity. Also its output characteristic curves change markedly with increasing temperature making it suitable for designing the intended solarimeter.

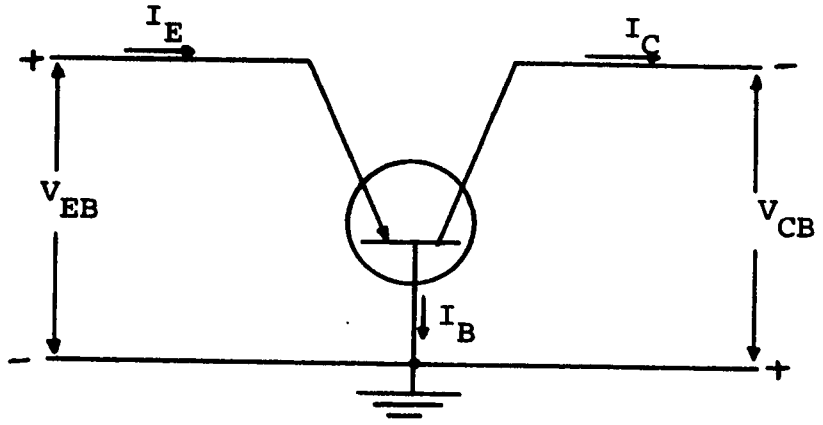

(a) Common-base configuration.

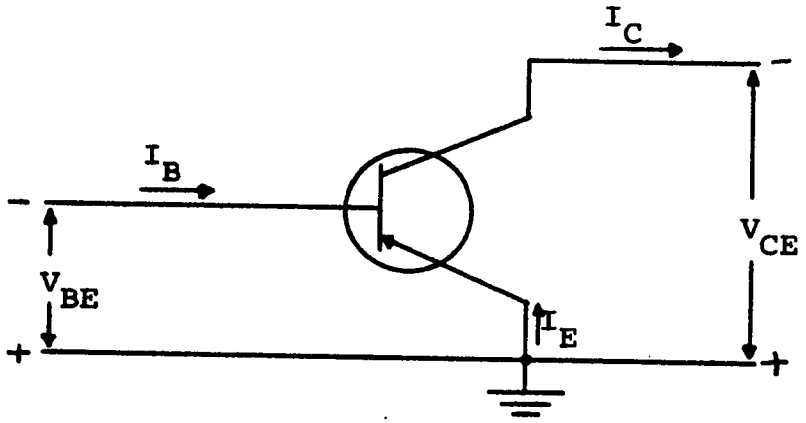

(b) Common-emitter configuration.

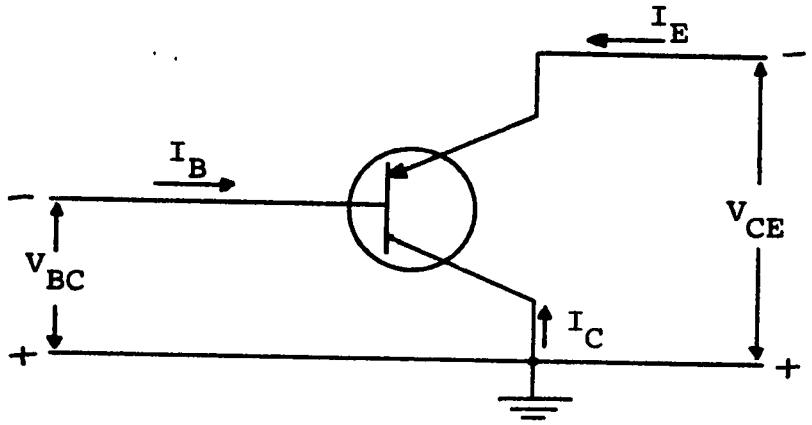

(c) Common-collector configuration.

Figure 23. Three configurations of a pnp transistor.

In this configuration, shown in Fig. 22b, the input current and output voltage are taken as the independent variables, whereas the input voltage and output current are dependent variables. We may write

$$V_{BE} = f_1 (V_{CE}, I_B) \qquad (2\text{-}7a)$$

$$I_C = f_2 (V_{CE}, I_B) \qquad (2\text{-}7b)$$

Eqn.'s (2-7a) and (2-7b) describe the family of input and output characteristic curves, respectively. Figures 24a and 24b show typical curves for a real transistor[4]. Various currents and voltages that exist for different operating conditions can be read from these curves.

Three regions of operation are defined in the output characteristic curves, depending on the state of voltages of the two junctions. Referring to Fig. 24b, the cutoff region is the area near the abcissa where $I_C = I'_{CO}$ (or $I_B = 0$). I'_{CO} is the transistor saturation current. The saturation region is the area defined by the ordinate and the slightly sloping line (saturation line) rising from the point at which $V_{CE} = V_{CEsat}$, where V_{CEsat}, the saturation voltage varies between zero and 0.4 for the values shown. The active region is the area to the right of the saturation line and above $I_C = I'_{CO}$. In this region the transistor output

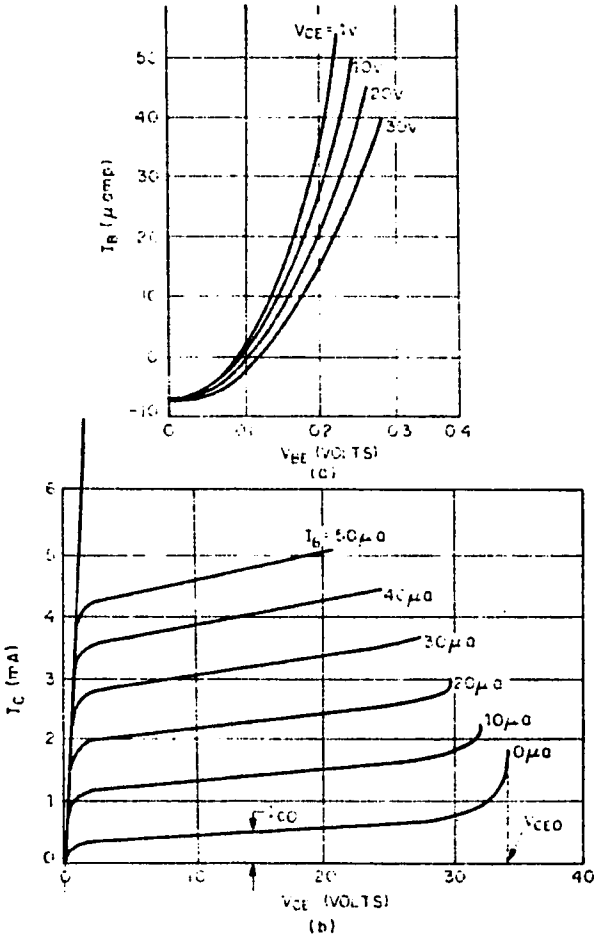

Figure 24. (a) Input characteristic and (b) Output characteristic of a typical pnp transistor in common-emitter configuration[4].

current responds more sensitively to an input signal and temperature variations.

2.4.2 Temperature Effect in Transistors

normal operation is given by

$$I_C = \beta I_B + (\beta + 1)\ I_{CO} \qquad (2\text{-}8)$$

where β is the d.c. current gain at constant V_{CE}.

This equation contains three variables, all dependent on temperature.

The current gain, β, variation with temperature can be approximately expressed as the following[6]

$$\beta(25°C + \Delta T) = \beta(25°C)\ (1 + \Delta T/80°C), \text{ for Si transistor, and}$$

$$\beta(25°C + \Delta T) = \beta(25°C)\ (1 + \Delta T/60°C) \text{ for Ge transistors}$$

If V_{BE} is held constant, I_B increases in the same manner as the diode current depicted in Fig. 21. The leakage current, I_{CO}, is the reverse current of the collector junction. Thus it varies with temperature according to Eqn. (2-6) which is repeated here.

$$I_{CO} = A\ T^{3+\gamma/2}\ e^{-Eg/kT} \qquad (2\text{-}6)$$

The net result of the increase in, β, I_B, and I_{CO} is evident from Eqn. (2-8). I_C will increase shifting the output characteristic curves upwards as shown in Fig. 24.

An important parameter of the transistor is the saturation current, I'_{CO}, which is the collector current with zero base current, is much larger than I_{CO}. This, because from Eqn. (2-8), the collector current for $I_B = 0$, is given by

$$I_C = I'_{CO} = (\beta + 1)\ I_{CO} \qquad (2\text{-}9)$$

2.3.4 Power Dissipation and Temperature

The practical design of a transistor circuit always involves thermal as well as electrical considerations, because the maximum average power that the transistor can dissipate is dependent upon the maximum temperature that the junction can stand and the actual ambient temperature expected in operation.

A reasonable approximation for the power P_C, dissipated at the junction is the product of the collector current and voltage

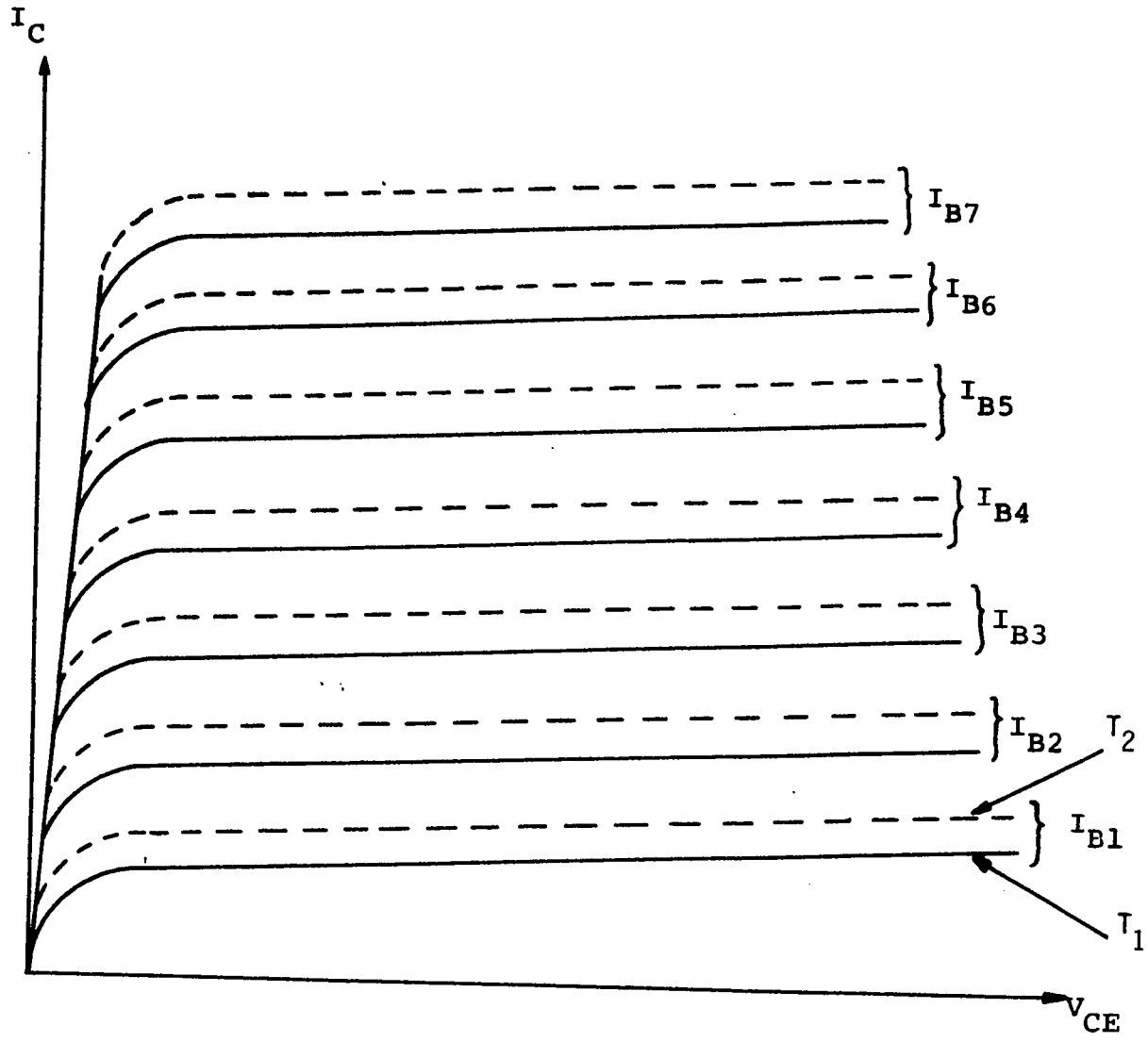

Figure 25. The output characteristic curves of the transistor at two different temperatures T_1 and $T_2 (T_1 < T_2)$.

$$P_C = I_C V_{CE} \qquad (2\text{-}10)$$

This power may vary from a few milliwatts to several hundred watts. The permissible region of operation may be shown graphically on the CE output characteristics. It has distincts boundaries: two are provided by the transistor characteristics, one being the cutoff region and the other is the saturation region, as shown in Fig. 26.

Three other boundaries are provided by the ratings specified by the manufacturer for the collector current, I_{Cmax}, collector-emitter, BV_{CEO}, and the hyperbola defined by

$$P_{Cmax} = I_C V_{CE} \qquad (2\text{-}11)$$

This hyperbola represents the locus of all operating points at which the collector dissipation is exactly P_{Cmax}. With no electrical connection made to the transistor (Fig. 27) the junction temperature, T_j, is the same as the case temperature, T , which is equal to the ambient temperature T_a. That is

$$T_j = T_c = T_a$$

When a signal is applied, power will be dissipated in the transistor, causing the junction temperature to

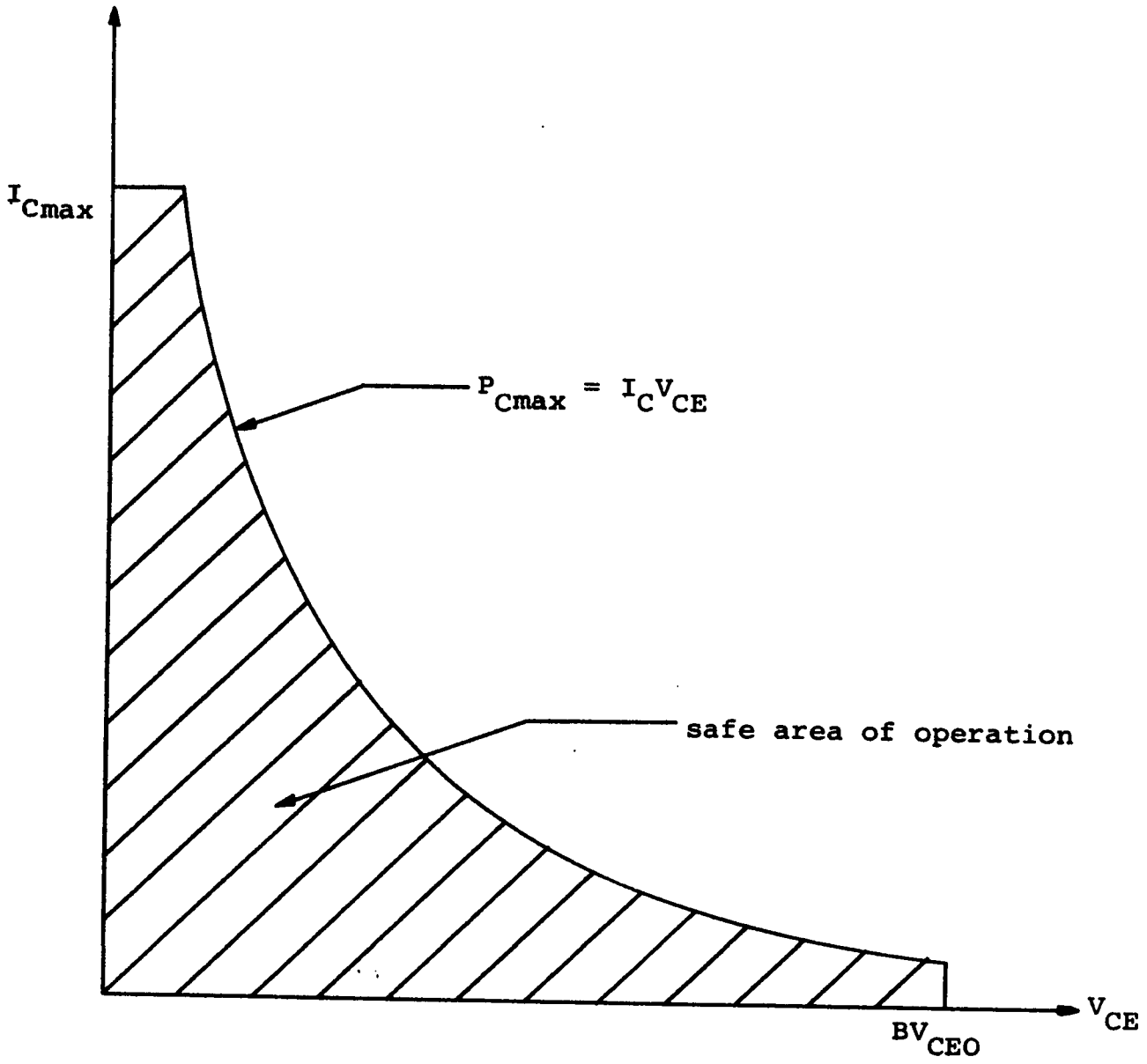

Figure 26. Permissible region of operation for the transistor.

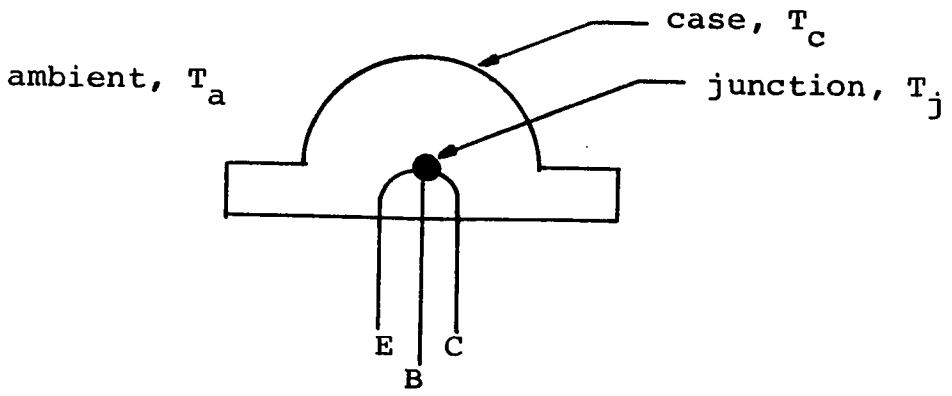

Figure 27. Transistor and temperature.

rise. If the power dissipated at the junction is within the limits of the transistor, then, after a sufficient time, the system will reach thermal equilibrium. Assuming the temperature gradient linear throughout the system, the steady-state temperature rise can be expressed as

$$\Delta T = T_{jmax} - T_{CO} = P_{Cmax} / \theta_{jc} \qquad (2\text{-}12)$$

where θ_{jc} (in w/c) is called thermal resistance of the transistor, its value is dependent on the material of the case, and the manner in which the transistor is mounted.

Therefore, the power rating must be decreased as the case temperature rises, to keep the junction temperature within a safe limit (Fig. 28).

2.4.3.1 Derating Curve

To avoid excessive temperature rise, power rating of a transistor is usually specified for an ambient temprature of 25°C. Also the manufacturer supplies derating curves which can be used to determine the maximum permissible power dissipation for a given case temperature.

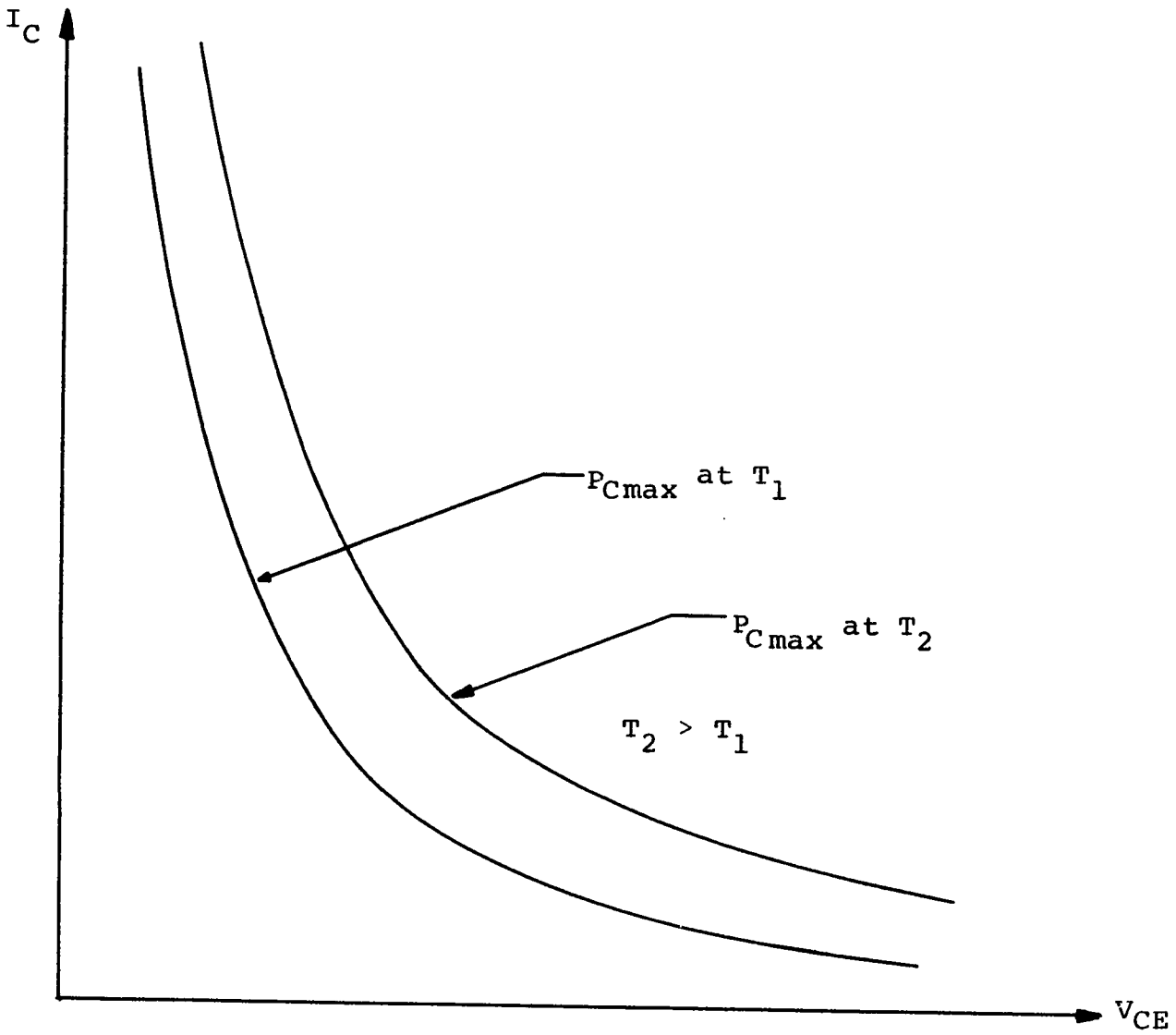

Figure 28. Power rating of transistor at two temperature T_1 and T_2.

A typical derating curve is shown in Fig. 29. At case temperature less than T_{co}, the transistor can dissipate its maximum allowable power. At case temperature exceeding T_{co}, the maximum dissipation is decreased until $T_c = T_{jmax}$, at which the transistor cannot dissipate any power unless T_{jmax} is exceeded. Then thermal runaway takes place and the transistor is damaged.

The rate of decrease of permissible maximum power with increased temperature is shown below to be θ_{jc}

$$\theta_{jc} = \frac{P_{C\,max}}{T_{jmax} - T_{co}}$$

2.4.4 Transistor Model

Because the currents and voltages are changing with temperature the transistor is considered under dynamic operation. Two equations can be used to describe the transistor behavior. One equation is for the emitter-base junction and the other is the characteristic of the collector terminal.

$$I_B = I_{BS}\, e^{qV_{BE}/kT} \qquad (2\text{-}13)$$

$$I_C = \beta I_B + (\beta + 1)\, I_{CO} \qquad (2\text{-}14)$$

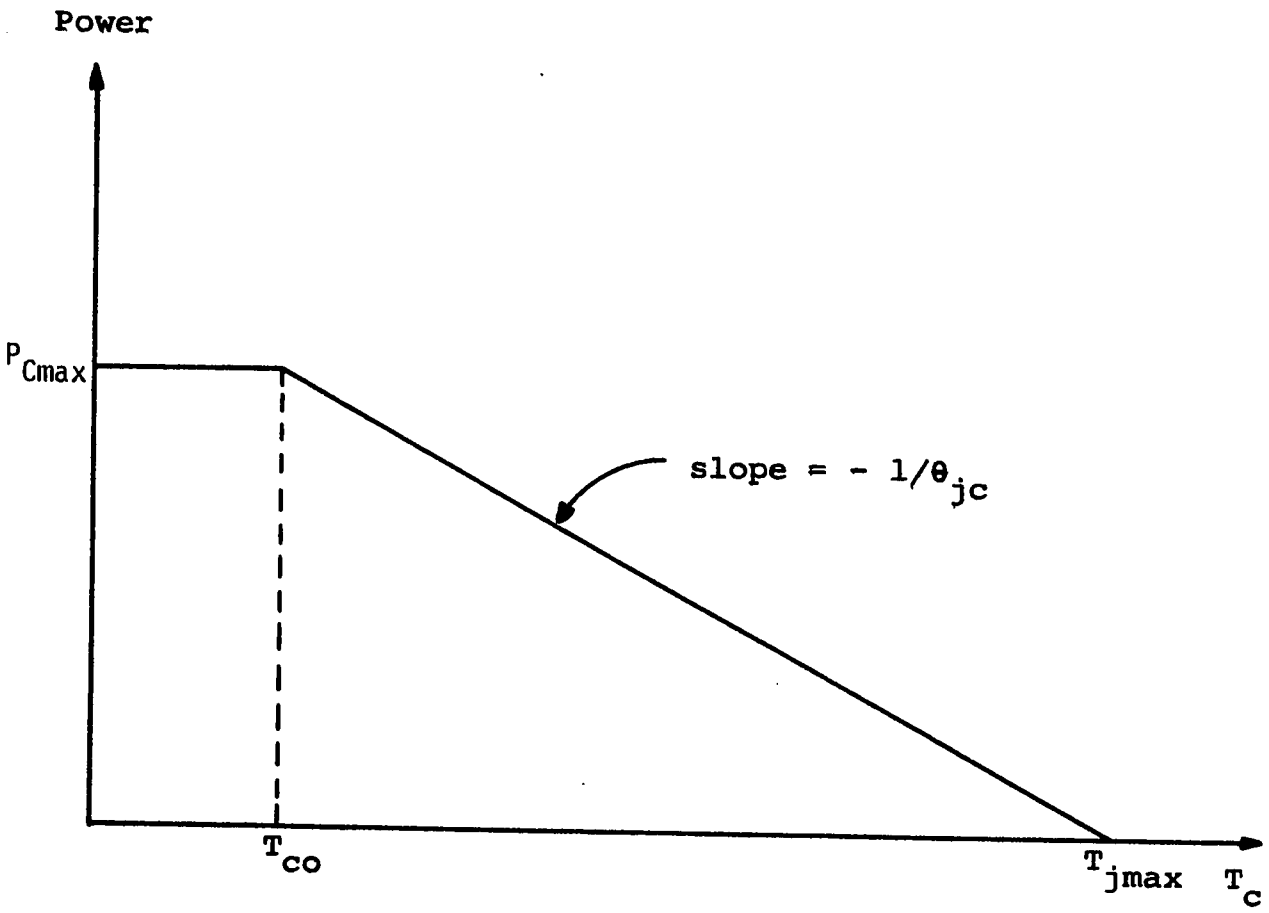

Figure 29. Transistor derating curve.

The dynamic resistance of the emitter-base junction is found by differentiating Eqn. (3-25) with respect to V_{BE}

$$\frac{1}{r} = \frac{\partial I_B}{\partial V_{BE}} = \frac{q}{kT} I_{BS} e^{qV_{BE}/kT}$$

or $$r = \frac{kT}{qI_B} \qquad (2\text{-}15)$$

The circuit of Fig. 30 obeys the same equations as does the transistor. So far as any V-I measurements on the input and the output terminals are concerned, the given circuit could not be distinguished from the actual transistor

There are two dependent current sources, one depends on the input current I_B and the other depends on the saturation current I_{CO}, which increases exponentially with temperature. If the transistor is biased close to the cutoff region, the input current I_B will be very small and can be neglected. Therefore, the model will reduce to the circuit shown in Fig. 31. In this model the resistance, r, is very large.

The reactive effects of the depletion-regions and diffusion will be included later, where it is appropriate.

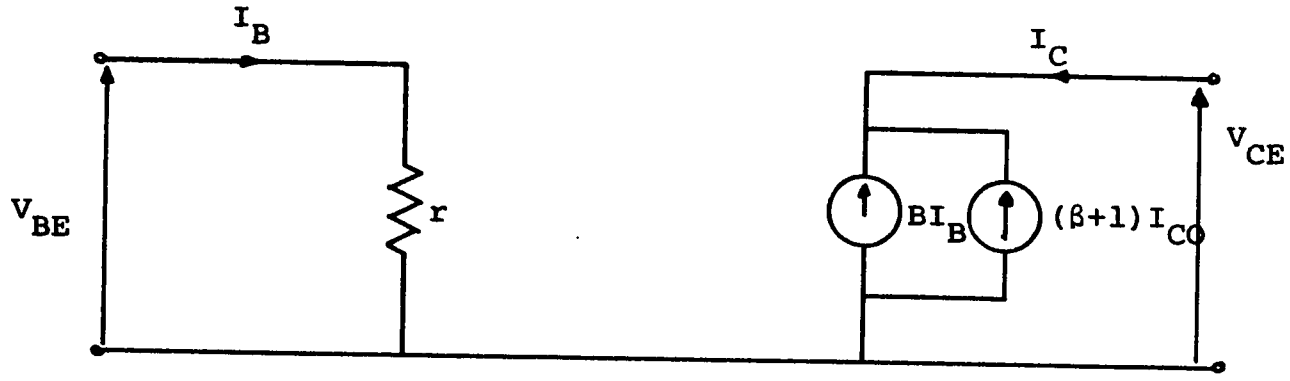

Figure 30. Transistor model in the common-emitter configuration.

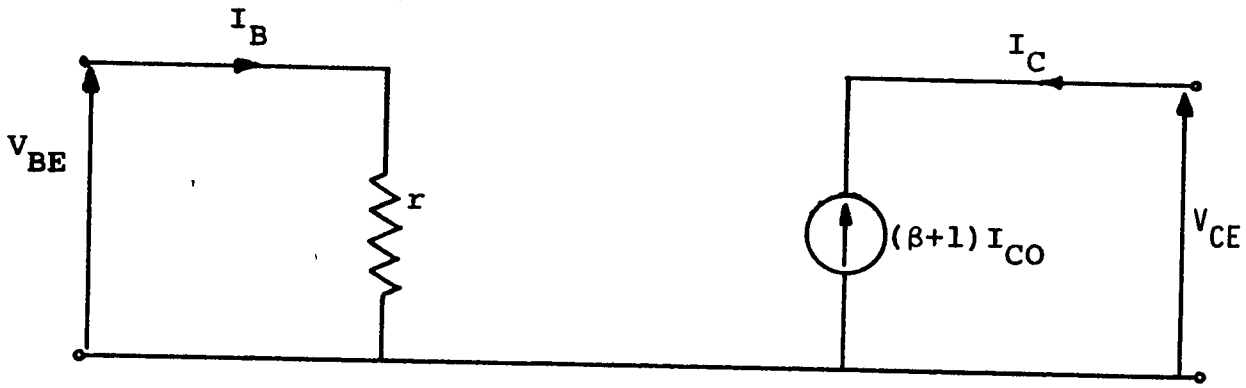

Figure 31. Temperature-dependent model of the transistor.

3. DESIGN OF THE SOLARIMETER

3.1 THEORETICAL ANALYSIS

The prime consideration in this design is to establish an operating point such that it moves along the load line with increasing temperature. The shift of this point will be restricted within the active region for all case temperatures resulting from incident solar radiation. Furthermore, the power dissipation of the transistor will be taken into account to avoid thermal runaway.

To achieve this goal, a study of bias instability will be developed and a criterion for safe power handling capability will be established.

3.1.1 Bias Instability

The sources of instability of I_C are essentially three.[2] These are leakage current I_{CO}, the base-emitter voltage, V_{BE}, and the current gain β. Three stability factors, S_I, S_V, and S_β are defined to give a measure of the operating point stabilization. The larger the values of S_I, S_V and S_β, the more likely the circuit is to exhibit thermal instability. These factors are

$$S_I = \frac{\partial I_C}{\partial I_{CO}}, \qquad (3\text{-}1)$$

$$S_V = \frac{\partial I_C}{\partial V_{BE}}, \quad \text{and} \qquad (3\text{-}2)$$

$$S_\beta = \frac{\partial I_C}{\partial \beta} \qquad (3\text{-}3)$$

To find the total change in collector current over a specified temperature range, this change can be expressed as the sum of the individual changes due to three stability factors. Specifically, by taking the total differential of $I_C = f\ (I_{CO}, V_{BE}, \beta)$ as follows

$$\Delta I_C = \left[\frac{\partial I_C}{\partial I_{CO}} \frac{\Delta I_{CO}}{\Delta T} + \frac{\partial I_C}{\partial V_{BE}} \frac{\Delta V_{BE}}{\Delta T} + \frac{\partial I_C}{\partial \beta} \frac{\Delta \beta}{\Delta T}\right] \Delta T$$

or

$$\Delta I_C = \left[S_I \frac{\Delta I_{CO}}{\Delta T} + S_V \frac{\Delta V_{BE}}{\Delta T} + S_\beta \frac{\Delta \beta}{\Delta T}\right] \Delta T \qquad (3\text{-}4)$$

The values of the factors S_I, S_V and S_β are dependent upon the elements of the biasing circuit, whereas the variations of I_{CO}, V_{BE}, and β with temperature are dependent upon the variations of the energy gap and carrier concentrations. For the purpose of estimating the change of the collector current over atmospheric temperature, empirical formulae are used to calculate the changes in I_{CO}, V_{BE}, and β. These

formulae, for Ge transistor, are [5]

$$I_{CO}\ (T_2) = I_{CO}\ (T_1)\ 2^{\Delta T/10°C} \qquad (3\text{-}5)$$

$$V_{BE}\ (T_2) = 0.2 - 0.002\Delta T, \text{ and} \qquad (3\text{-}6)$$

$$\beta\ (T_2) = \beta(T_1)\ (1+\Delta T/60°C) \qquad (3\text{-}7)$$

where $\Delta T = T_2 - T_1\ °C$

Changes in I_{CO}, V_{BE}, and β are evaluated as follows

$$\frac{\Delta I_{CO}}{\Delta T} = \frac{I_{CO}(T_2) - I_{CO}(T_1)}{T_2 - T_1} = \frac{I_{CO}\ (2^{\Delta T/10} - 1)}{\Delta T} \qquad (3\text{-}8)$$

$$\frac{\Delta V_{BE}}{\Delta T} = \frac{V_{BE}(T_2) - V_{BE}(T_1)}{T_2 - T_1} = -0.002\ V/^{o}C, \text{ and} \qquad (3\text{-}9)$$

$$\frac{\Delta \beta}{\Delta T} = \frac{\beta(T_2) - \beta(T_1)}{T_2 - T_1} = \beta(T_1)/60 \qquad (3\text{-}10)$$

3.1.2 Transistor Bias

The circuit shown in Fig. 32 represents the common-emitter configuration. This circuit is chosen for designing the solarimeter because the collector current changes appreciably with temperature.

Writing the KVL around the base-emitter loop yields the base current

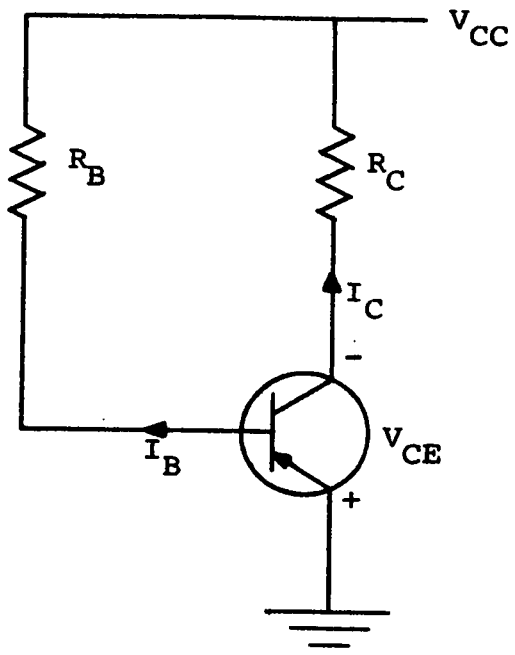

Figure 32. Circuit diagram for the solarimeter.

$$I_B = \frac{V_{CC} - V_{BE}}{R_B} \qquad (3\text{-}11)$$

Substituting for I_B in Eqn. (2-8)

Hence

$$I_C = \left(\frac{V_{CC} - V_{BE}}{R_B}\right)\beta + (\beta + 1)\, I_{CO} \qquad (3\text{-}12)$$

This equation is used to compute the stability factors. That is

$$S_I = \frac{\partial I_C}{\partial I_{CO}} = \beta + 1 \qquad (3\text{-}13)$$

$$S_V = \frac{\partial I_C}{\partial V_{BE}} = -\frac{\beta}{R_B} \qquad (3\text{-}14)$$

$$S_\beta = \frac{\partial I_C}{\partial \beta} = \frac{V_{CC} - V_{BE}}{R_B} + I_{CO}$$

$$S_\beta = I_B + I_{CO} \qquad (3\text{-}15)$$

If the transistor is biased near the cutoff region, which is the case for this design, then I_B is very small compared to I_{CO}

$$I_B << I_{CO}$$

Therefore Eqn. (3-15) becomes

$$S_\beta \cong I_{CO}$$

Substituting in Eqn. (3-4) for all quantities involved, hence

$$\Delta I_C = \left[(\beta(T_1) + 1) \frac{I_{CO}(T_1)(2^{\Delta T/10} - 1)}{\Delta T} + \frac{\beta(T_1)}{R_B} (.002) + \frac{I_{CO}(T_1)\ \beta(T_1)}{60} \right] \Delta T \qquad (3\text{-}16)$$

The dc load line eqution is obtained by using KVL around the collector-emitter loop. Thus

$$I_C = \frac{V_{CC} - V_{CE}}{R_C} \qquad (3\text{-}17)$$

Figure 33 shows the CE characteristics with Eqn. (3-17) plotted showing the load line which represents the locus of the operating point under different conditions.

3.1.3 Selection of R_B and R_C

The quiescent point will shift as a result of the transistor parameters variations with temperature. Thus, one of the first steps in this design, is to choose a permissible range of variation for V_{CE} and I_C. This choice is based on a knowledge of the temperature encountered and the transistor output characteristics. The circuit resistances are then chosen to give the appropriate stability factors which make the change in the collector

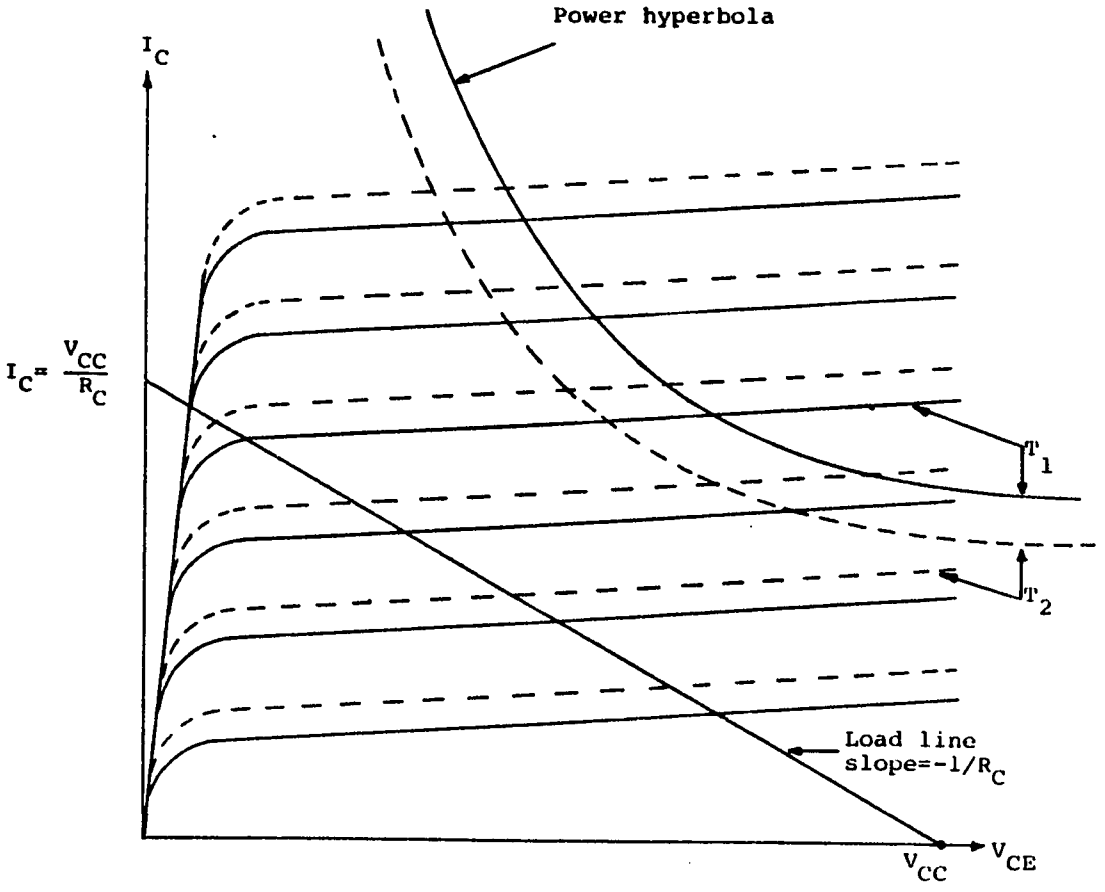

Figure 33. CE characteristics with load line and power hyperbola at two temperatures T_1 and T_2 ($T_1 < T_2$).

current large enough to cover the temperature range.

Figure 34 shows the two extremes for operation. At T_1 the quiescent point is near the cutoff region and at T_2 it is near the saturation region, where $T_1 < T_2$. Therefore, the base current is chosen to be very small. Knowing I_B, V_{CC} and V_{BE}, then R_B is computed from Eqn. (3-11)

$$R_B = \frac{V_{CC} - V_{BE}}{I_B} \tag{3-18}$$

The value of R_B will be very large. Also to prevent operation in the saturation region it is required that

$$|V_{CE2}| > |V_{CEsat}| \tag{3-19}$$

where V_{CE2} is the collector-to-emitter voltage at temperature T_2.

The collector current I_{C2} at temperature T_2 is obtained from the following expression

$$I_{C2} = I_{C1} + \Delta I_C \tag{3-20}$$

where ΔI_C is estimated using Eqn. (3-16).

At T_2, Eqn. (3-17) becomes

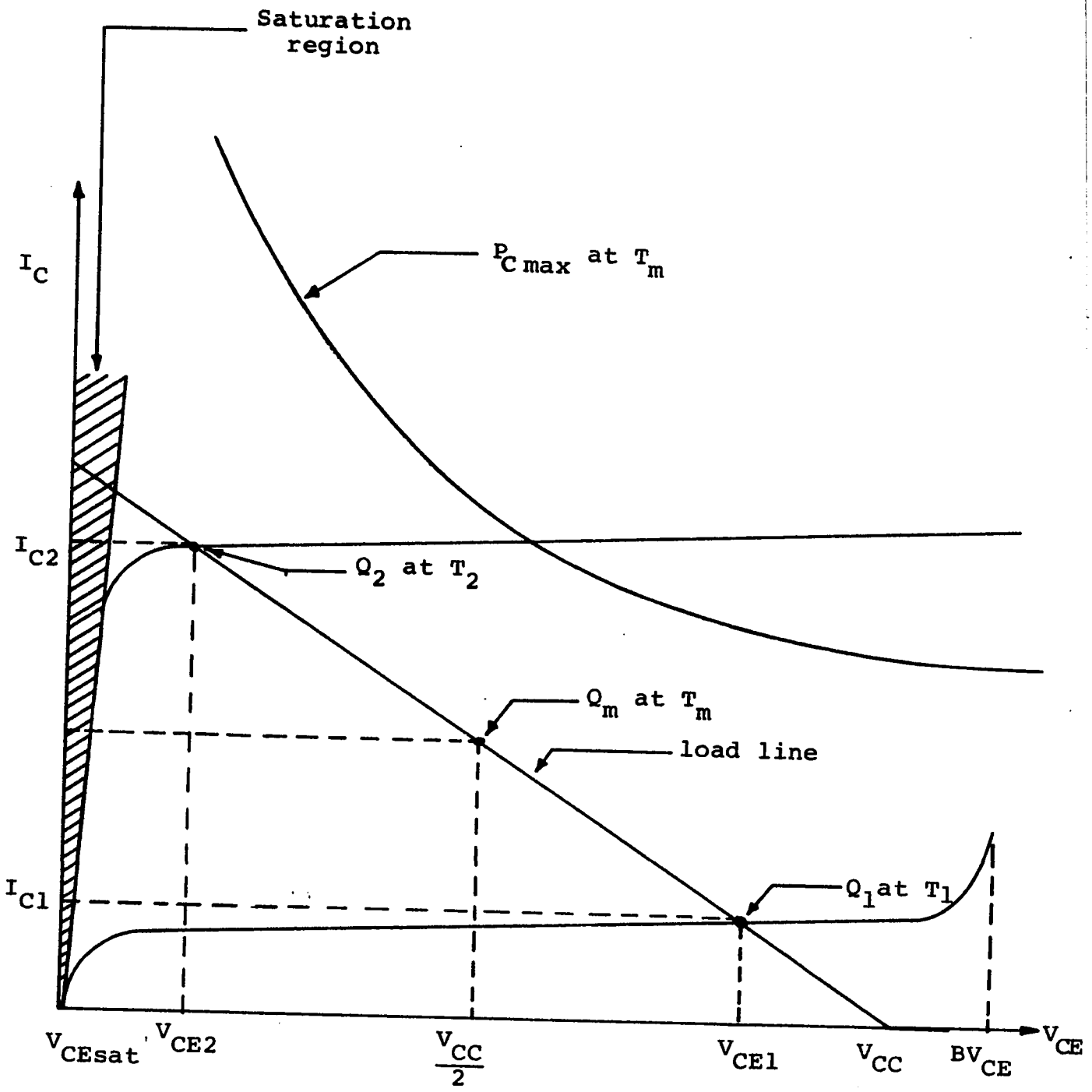

Figure 34 . The two limits of the operating point.

$$I_{C2} = \frac{V_{CC} - V_{CE2}}{R_C}$$

Solving for V_{CE2}, and substituting in relation (3-19) Hence

$$\left|V_{CE2}\right| = \left|V_{CC} - I_{C2}R_C\right| > \left|V_{CEsat}\right|$$

or $$R_C < \frac{V_{CC} - V_{CEsat}}{I_{C2}} \qquad (3\text{-}21)$$

And this establishes an upper bound for R_C. Also a lower bound can be established by considering power dissipation.

3.1.4 Safe Power-Handling Criterion

It has been stated that thermal runaway occurs if the transistor is operated outside the safe area illustrated in Fig. 26. To take care of this problem, the maximum permissible dissipation in the transistor is found first.

For this case, the power dissipated in the transistor is

$$P_t = V_{CE}I_C$$

But $$I_C = \frac{V_{CC} - V_{CE}}{R_C}$$

Therefore $$P_t = \frac{V_{CE}V_{CC} - V_{CE}^2}{R_C} \qquad (3\text{-}22)$$

Figure 35 shows P_t plotted against V_{CE}.

It is clear from this diagram that when the operating point moves along the load line from Q_1 the dissipation increases until it is maximum at Q_m where $V_{CE}=V_{CC}/2$. Then it decreases as the operating point moves towards Q_2. At the same time the power hyperbola moves towards the origin as the temperature increases shrinking the safe area of operation. Therefore, the operating point is likely to enter into the unsafe area, above the power hyperbola, causing thermal runaway. To prevent this, both the dissipation of the transistor and the solar power input, q_i, should be taken into consideration.

If the sum of the maximum dissipation, P_{tmax}, at Q_m on the load line, and the power delivered by maximum solar radiation, is made less than the permissible maximum dissipation, at T_2, determined from the derating curve, then safe power handling is guaranteed at all temperatures falling in the interval $T_1 \leq T \leq T_2$. That is

$$P_{tmax} + q_i < P_{Cmax} @ T_2 \qquad (3\text{-}23)$$

where from Eqn. (3-22) and Fig. 35

$$P_{tmax} = \frac{V_{CC}^2}{4R_C} \quad , \quad \text{and}$$

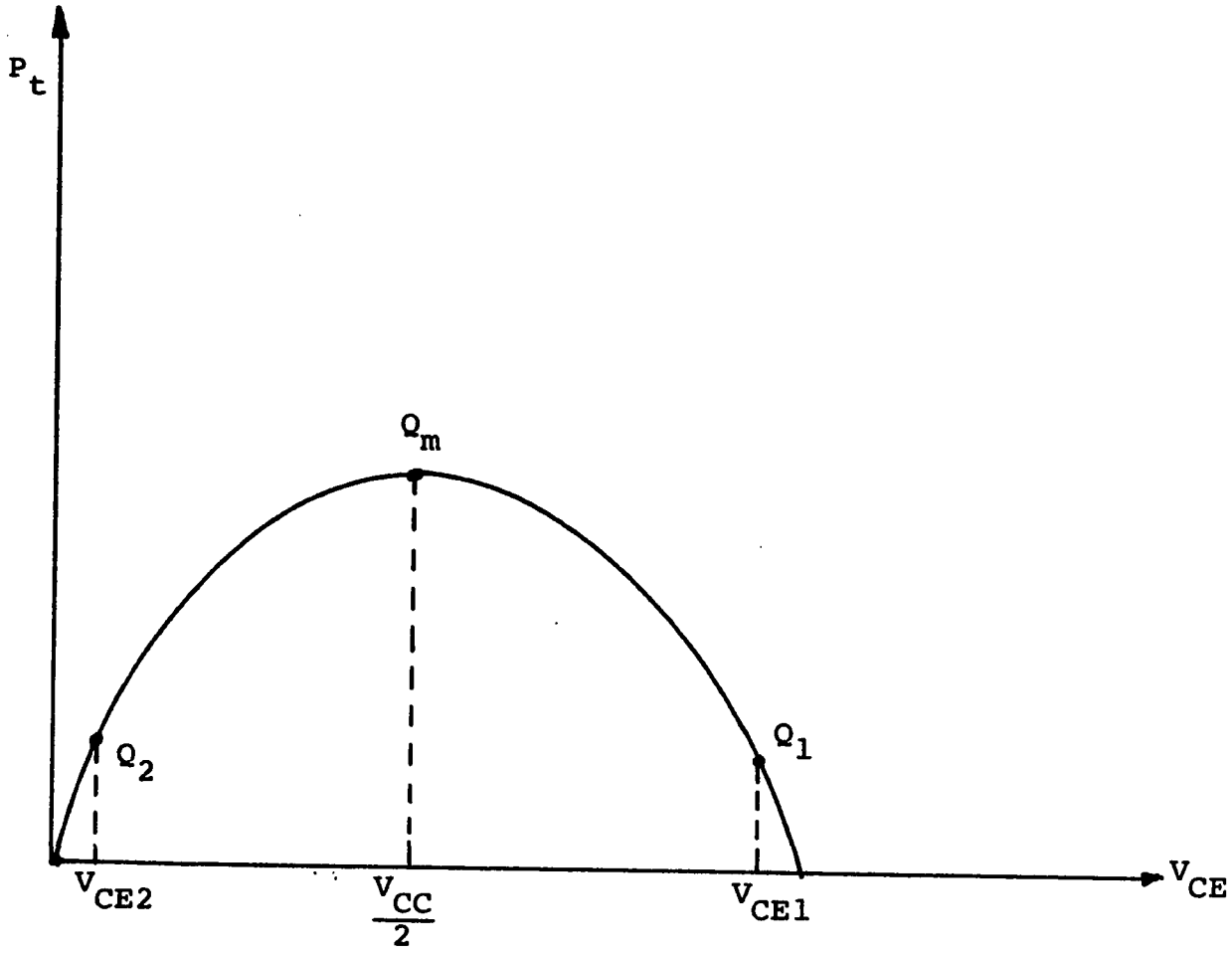

Figure 35. Maximum dissipation in transistor.

$$q_i = S \, \phi_{max}$$

where S is the case area exposed to solar radiation, and ϕ_{max} is the maximum insolation on the earth's surface.

Substituting for P_{tmax} and q_i in relation (3-23),

$$\frac{V_{CC}^2}{4R_C} + S \, \phi_{max} < P_{cmax} @ T_2$$

Solving for R_C, then

$$R_C > \frac{V_{CC}^2}{4(P_{Cmax} @ T_2 - S \, \phi_{max})} \qquad (3\text{-}24)$$

From inequalities (3-21) and (3-24), R_C must satisfy the following

$$\frac{V_{CC}^2}{4(P_{Cmax} @ T_2 - S \, \phi_{max})} < R_C < \frac{V_{CC} - V_{CEsat}}{I_{C2}}$$

3.2 EXPERIMENT AND DISCUSSION

3.2.1 Part (a) Objective: To investigate the relation between the intensity of solar radiation and the collector current in the circuit shown in Fig. 32.

Equipments:

1 - AC132 germanium PNP transistor

2- 110V/1000 watts lamp

3- 1500W light dimmer

4- 3 digital multimeters model 8020A

5- Temperature probe model 80T-150,

6- Epply pyranometer

7- H.P. d.c. power supply

8- Transistor-curve tracer 575

9- Gould Brush 220 Recorder, zero with respect to time $\pm$ 0.1 div. for 8 hours.

10- 1N661 silicon diode

The transistor AC 132 has the following specifications:

1- Maximum collector dissipation at 25^{o} in free air, P_{Cmax} = 500 mW.

2- Derating factor in free air, θ_{jc} = 3.3 mW/^{o}C. Derating starts at 45^{o}C.

3- Maximum junction temperature, T_{max} = 100^{o}C

4- Absolute maximum ratings at 25^{o}C

a) Breakdown voltage, collector-to-base, emitter open-circuit, V_{cbo} = 32V.

b) Breakdown voltage, emitter-to-base, collector open-circuit, V_{ebo} = 10V

c) Breakdown voltage, collector-to-emitter, base open-circuit, V_{ceo} = 32 V

d) Maximum collector current I_{emax} = 200 mA.

e) Forward current transfer ratio, common emitter, β = 115

f) Output capacitance, C_{ob} = 40 pF

3.2.1.1 Theoretical Calculations

Three characteristics are taken for the transistor. These characteristics are the input forward curves (Fig. 36), the output curves (Fig. 37), and the reverse curves (Fig. 38).

Several important parameters are read from these curves. They are

V_{CEsat} = -0.05 Volt

$I_{CO} \tilde{}$ - 0.088 mA

$I'_{CO} \tilde{}$ - 7.5 mA

$V_{BE} \tilde{}$ 0.18 Volt

All values are taken at 25°C.

Biasing the transistor with input current I_B = 20μA at 25°C and V_{CC} = -9.0 volts, then from Eqn. (3-18)

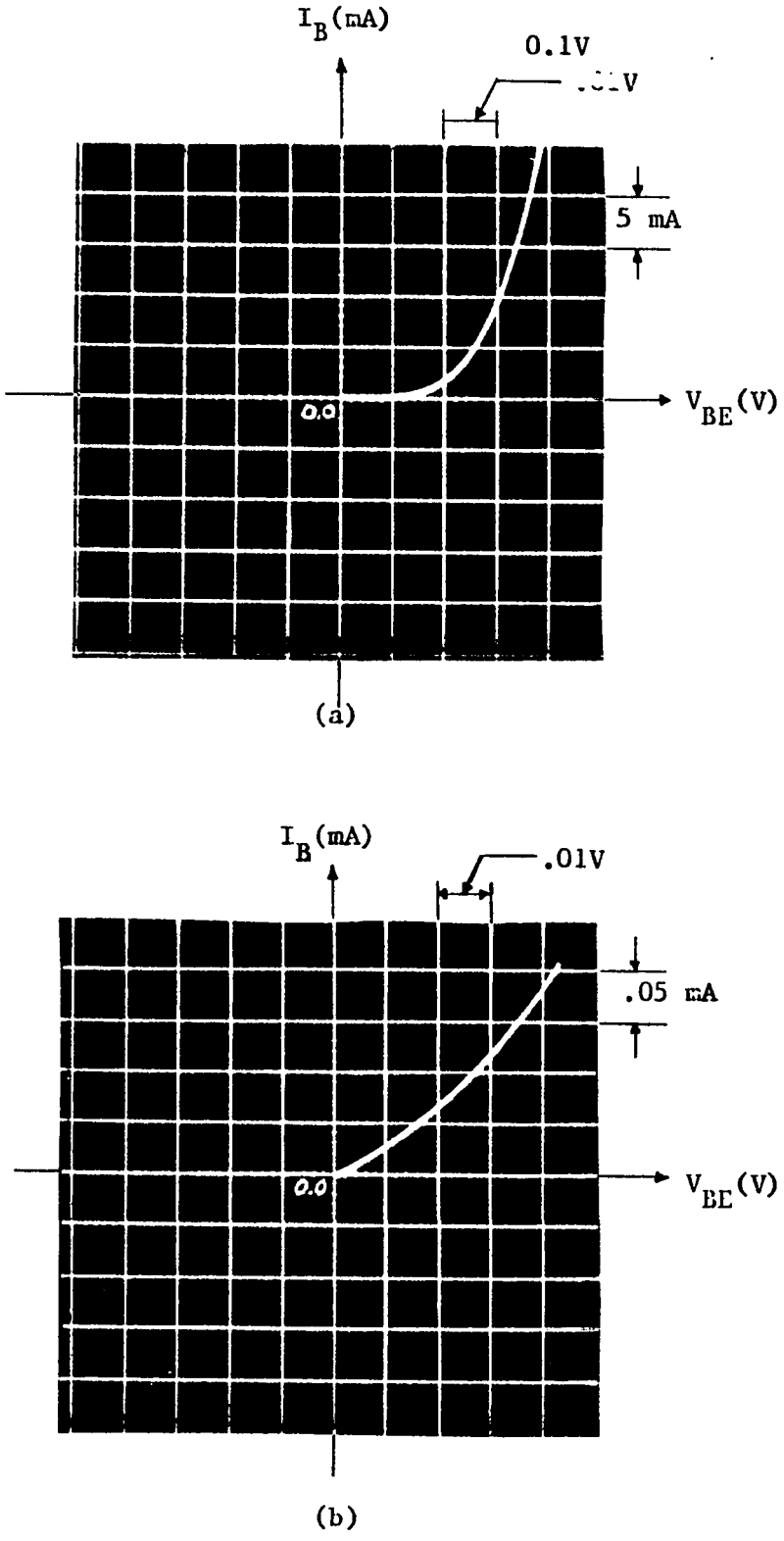

Figure 36. The input characteristic curve at (a) 25°C and (b) 60°C.

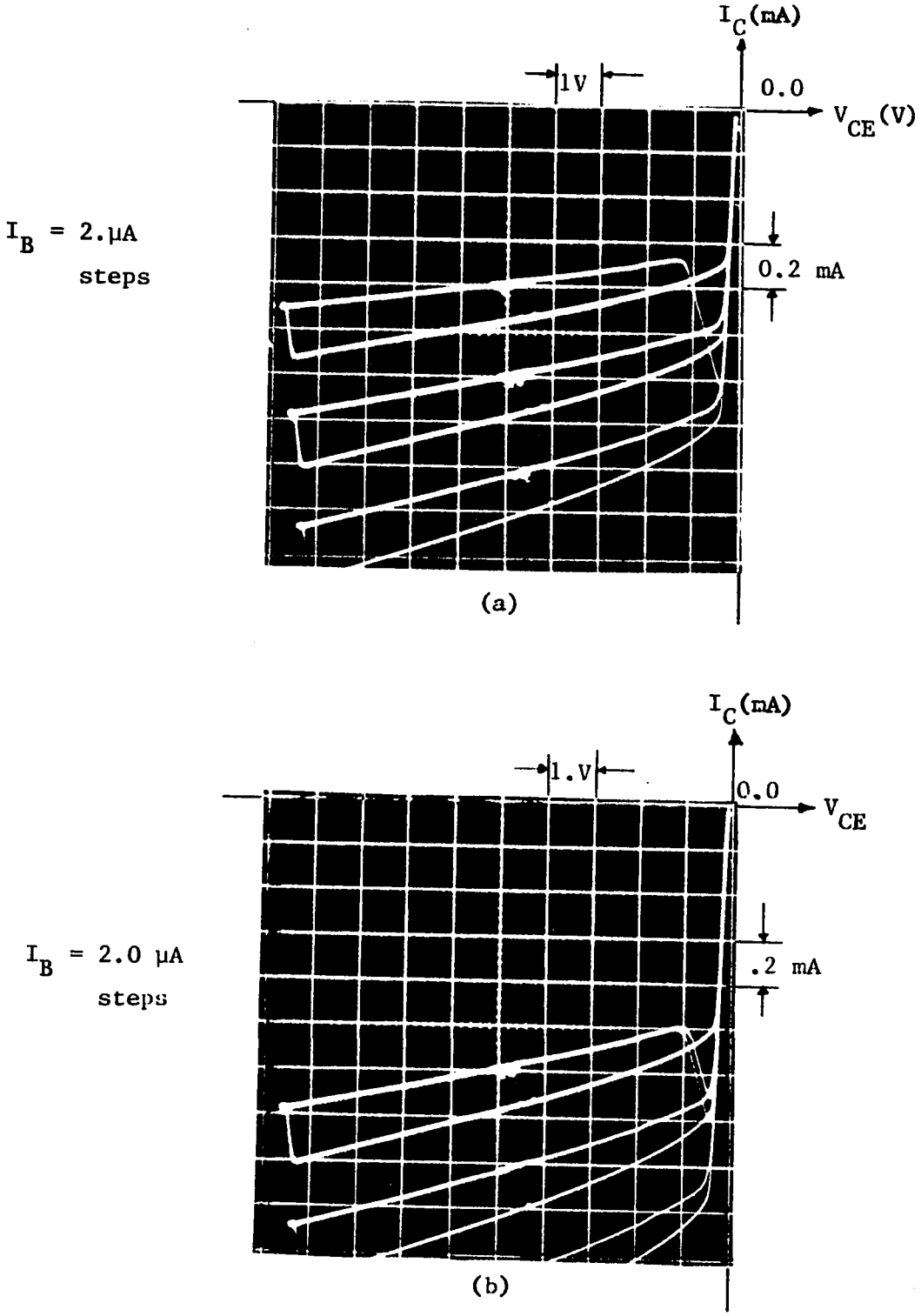

Figure 37. The output characteristic curves at (a) 25°C and (b) 30°C, with I_B = 2.0 μA steps.

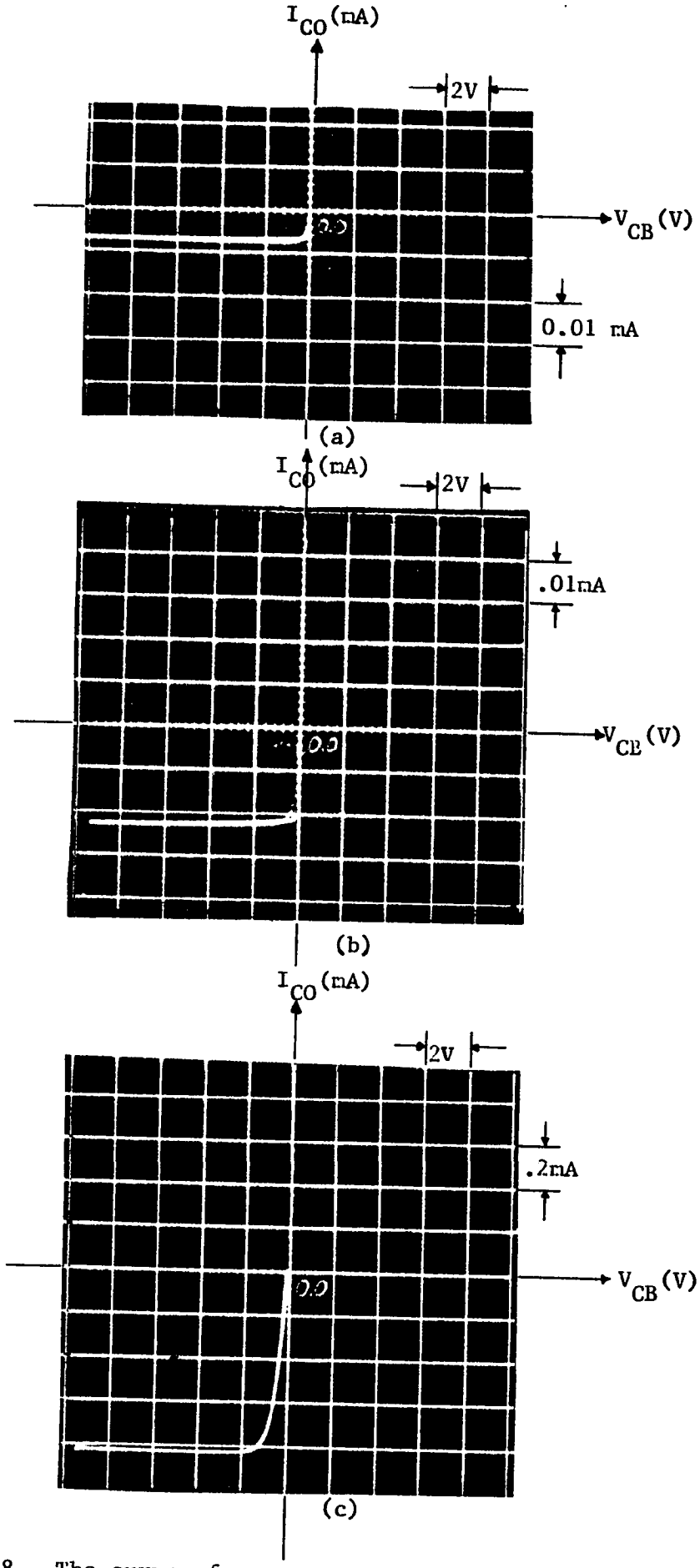

Figure 38. The curve of reverse current in the base-collector junction at (a) 25°C, (b) 45°C, (c) 60°C.

$$R_B = 441\ k\Omega$$

The temperature of the transistor case, due to solar radiation, varies between T_{min} and T_{max} which assume the values 25^oC and 60^o respectively and, $\Delta T = 35^oC$. Using Eqn. (3-16)

$$\Delta I_C = 10.1\ mA.$$

To follow the same consistency of the current directions in a pnp transistor, ΔI_C must be negative. I_{C2} is computed from Eqn. (3-20), where I_{C1}, in this case, is approximately equal to I'_{CO}, therefore

$$I_{C2} = -11\ mA.$$

The upper bound of R_C, from inequality (3-21), is

$$R_C = 813.3\ \Omega$$

In order to compute the lower bound, the maximum permissible dissipation at 60^oC and the power delivered by maximum insulation are calculated first. From Eqn. (2-12), and the manufacturer's specifications $T_j = 196.5^oC$.

And therefore the dissipation decreases according to

$$P_{C\,max} = 3.3\ (196.5 - T_{co})$$

T_j is greater than the maximum temperature specified which is 80^oC, indicating that the transistor is damaged before its dissipation becomes zero at 196.5^oC.

Now at 60^oC

$$P_{Cmax} = 450 \text{ mW}$$

Dimensions of the transistor case are given in Fig. 39 from which the area is

$$S = \pi r^2 + 2\pi r\ell = 2 \text{ cm}^2$$

ϕ_{max} is taken to be the solar constant, 1.353 KW/m^2. Therefore, the lower bound of R_C from inequality (3-24) is 45Ω.

Therefore

$$45 < R_C < 813$$

3.2.1.2 Procedure

(1) The values of R_B and R_C are chosen as shown in Fig. 40.

(2) The collector current and collector-emitter voltage are measured at different temperatures in the range $25 \leq T \leq 60^oC$, where the temperature is varied by exposing

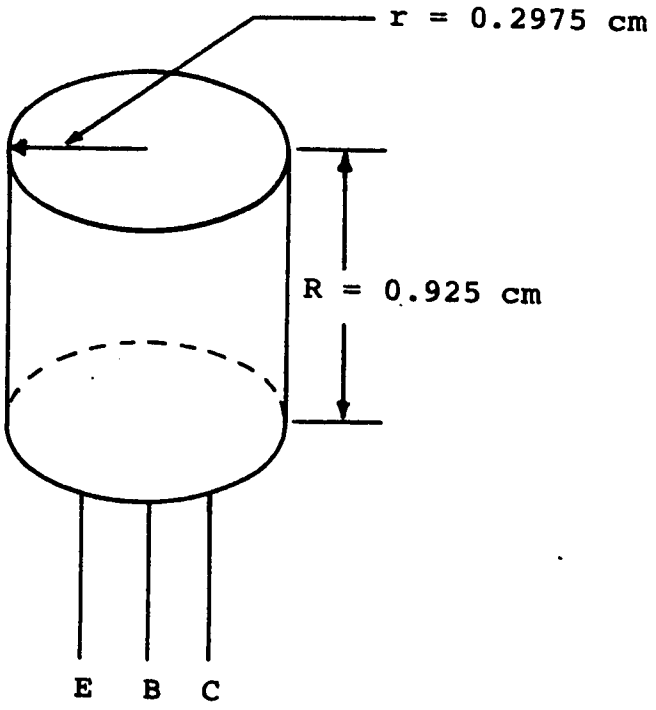

Figure 39. Dimensions of the transistor case.

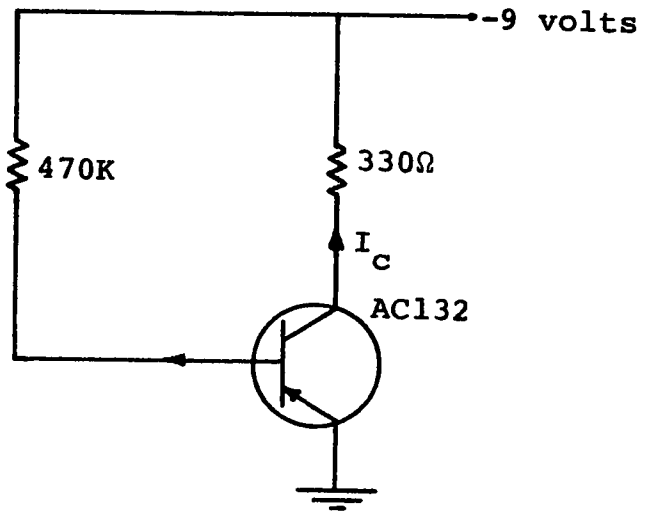

Figure 40. Solarimeter circuit.

the transistor to light coming from a lamp and a dimmer is used to control the light intensity which is proportional to the fourth power of the temperature. At the same time a probe is used to measure the case temperature.

Figure 41 shows the set-up used for taking the measurements.

(3) Also the temperature of the transistor case is measured at different intervals by exposing the transistor to solar radiation which is read using an Epply pyranometer. All values taken are tabulated in Table I and Table II.

3.2.1.3 Discussion of the Results

As shown in Fig. 42 the increase in the collector current is exponential as expected from theory. This increase covers the specified temperature range before the transistor saturates. The measured collector current at $60^{o}C$ is -20.6 mA, whereas the calculated one is I_{C2} = -11 mA. But there is no discrepancy because the resistance, R_C, chosen is different from the upper bound which is established using I_{C2} = -11 mA.

The graph in Fig. 42 demonstrates that the case temperature increases with insolation. The insolation-temperature curve does not follow the theoretical blackbody relation

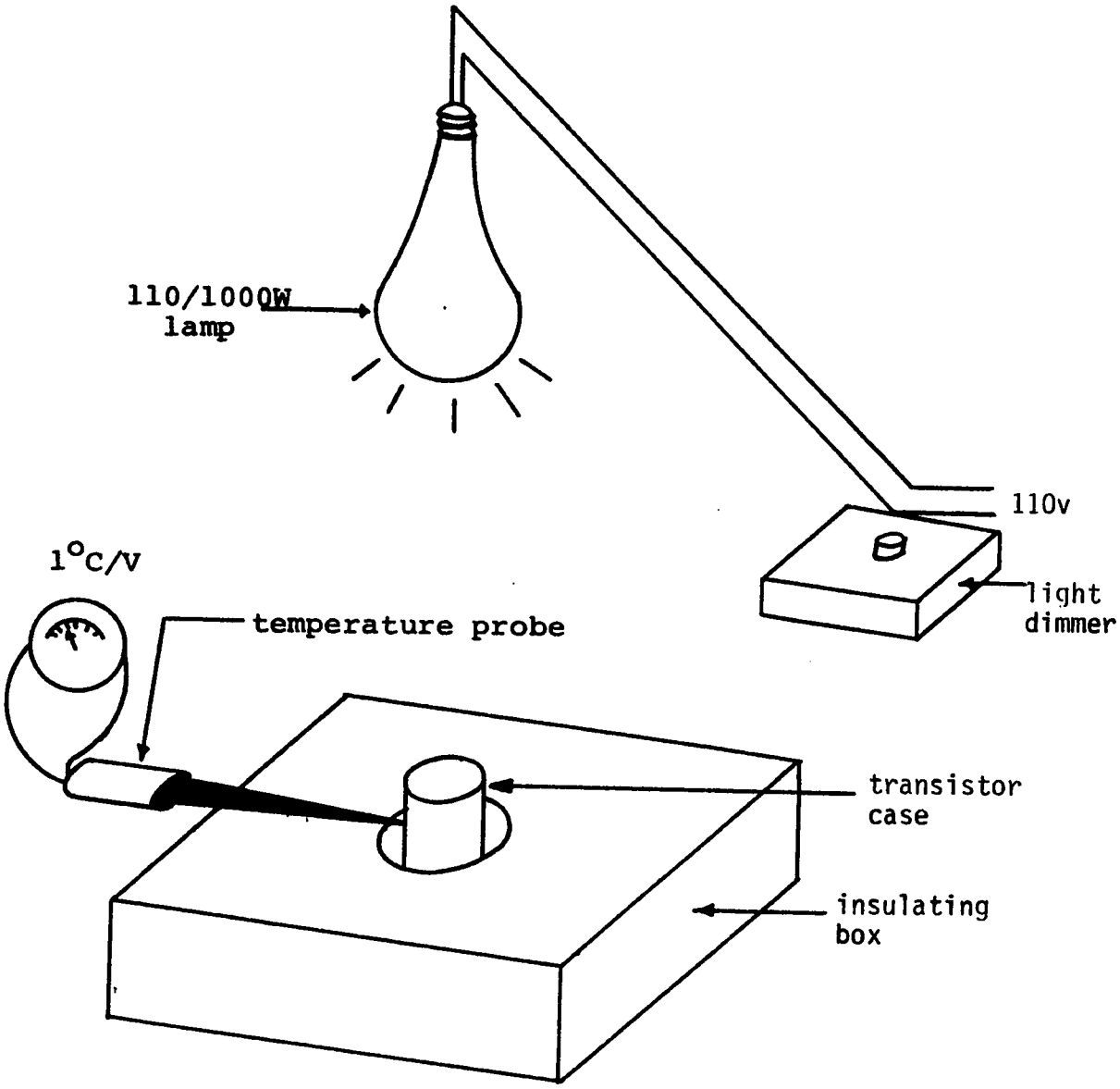

Figure 41. Schematic diagram of the experiment set-up.

TABLE I. These Readings Were Taken at a Room Temperature of 25°C, where T is the Temperature of the Transistor Case and $\Delta T = T - 25$.

$\Delta T^{\circ}C$	I_C(mA)
0.0	- 4.12
2.0	- 4.27
4.2	- 4.68
6.1	- 5.06
8.3	- 5.66
10.0	- 6.10
12.1	- 6.85
14.3	- 7.78
16.0	- 8.52
17.1	- 9.11
18.3	- 9.9
20.0	-10.79
22.0	-11.81
24.0	-13.12
26.9	-14.75
29.1	-16.45
32.0	-18.39
35.0	-20.6

TABLE II. Solar Radiation Intensity and the Transistor Temperature*.

$T^{o}C$	Solar radiation (Watts/m^2)
31.8	74.8
33.4	147.55
35.0	277.78
36.7	363.25
37.7	470.09
40.2	600.03
41.7	755.5
43.1	850.31
44.7	1014.95

*Ambient temperature = $31^{o}C$.

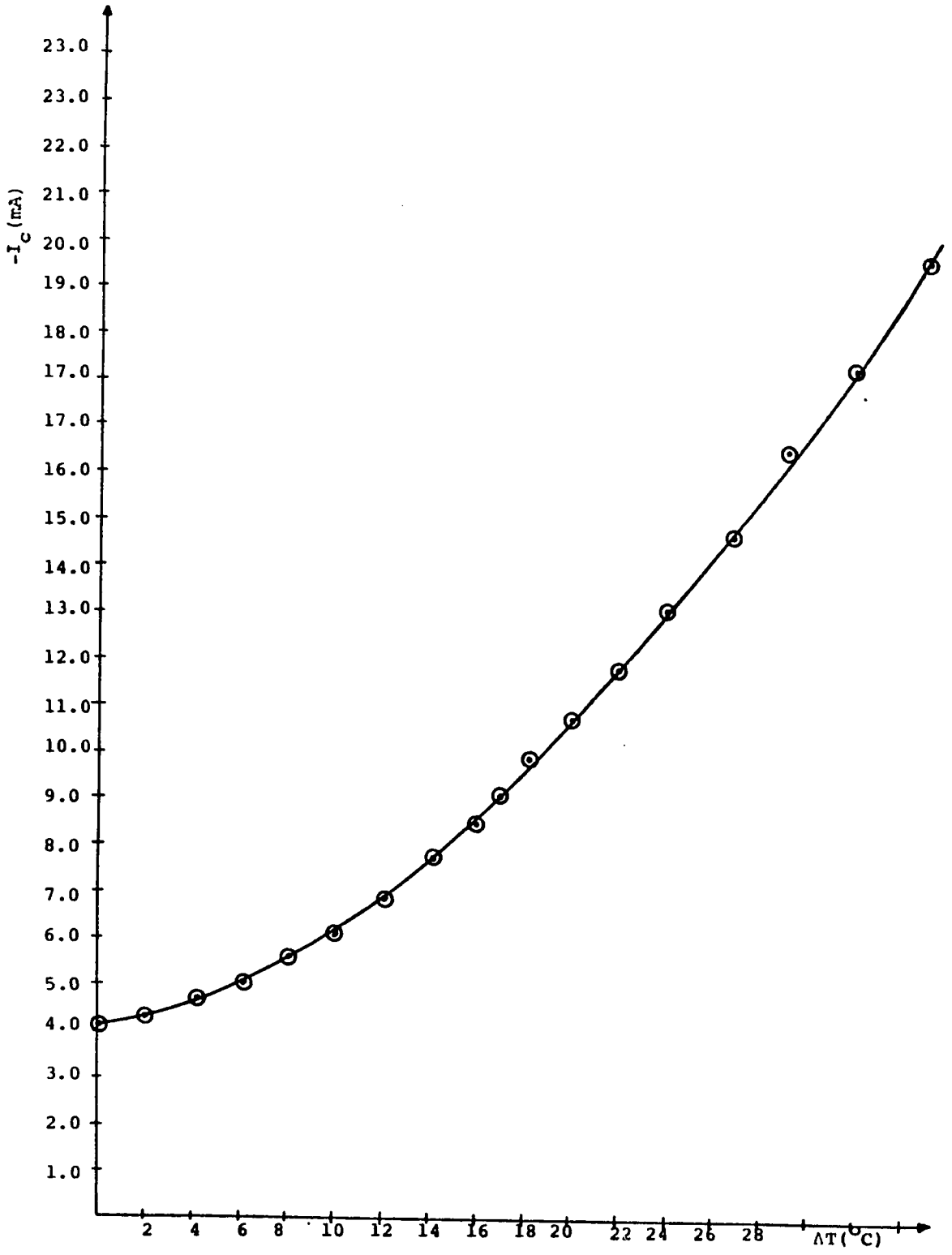

Figure 42. Collector current versus temperature change of the transistor case, $\Delta T = T - 25^{o}C$, (Part a).

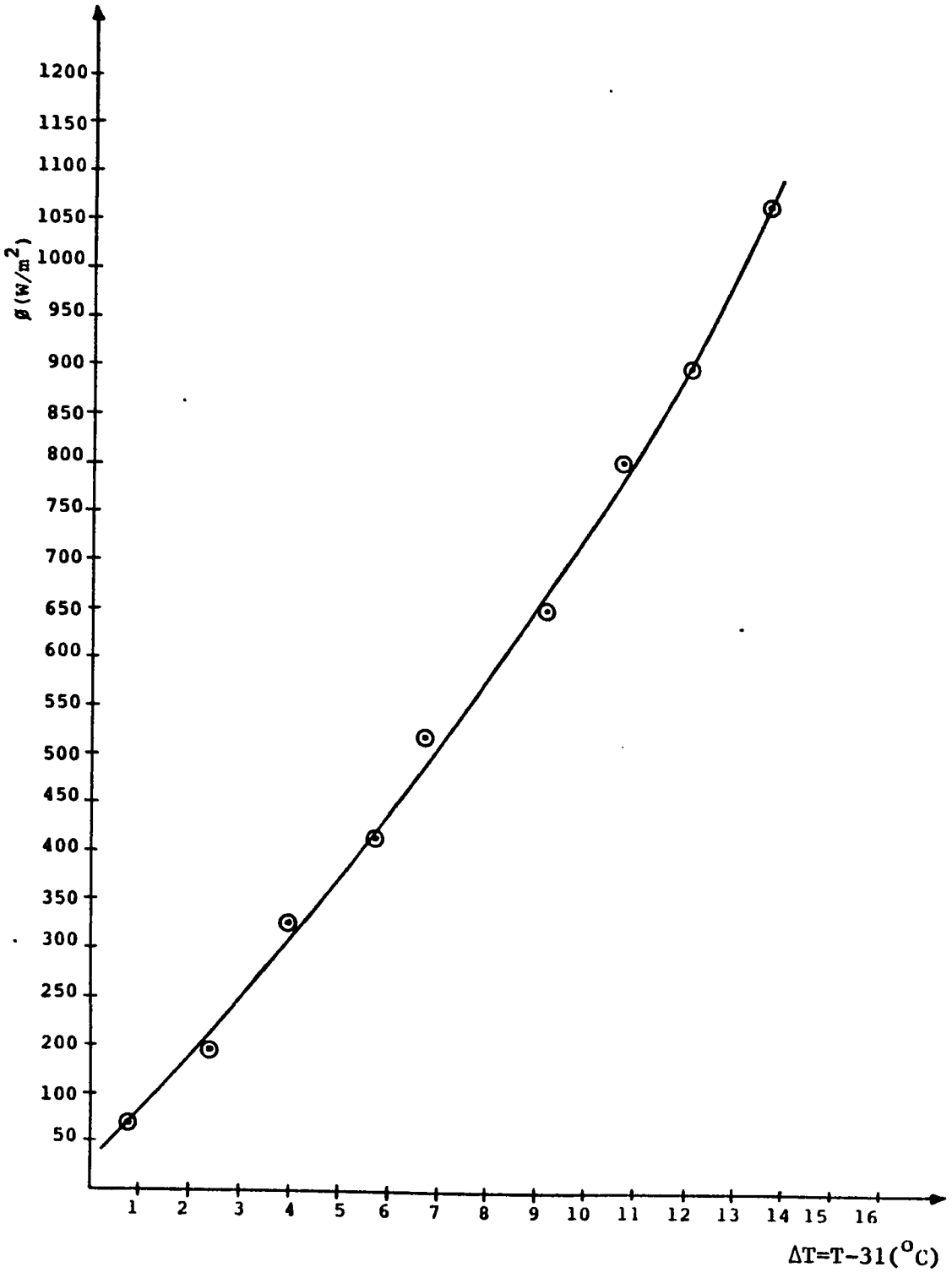

Figure 43. Insolation against temperature change of the transistor case, $\Delta T = T - 31^{o}C$, (Part a).

$$\phi = \frac{q_i}{s} = \sigma\varepsilon(T_{sky}^4 - T^4) \qquad (1\text{-}4)$$

This deviation is expected because the transistor case is not a perfect blackbody. Also the limited accuracy of the instruments used contribute to this deviation.

Nevertheless, the results obtained are satisfactory enough to demonstrate the possibility of obtaining a direct relationship between insolation and the collector current as will be shown below.

3.2.2 Calibration of the Solarimeter

The curves discussed previously are used here to relate the insolation and collector current in order to use the circuit designed as a solarimeter.

By eliminating the temperature from the graphs shown in Figs. 42 and 43, the graph of Fig. 44 is obtained. The coordinate of any point on this curve are taken at the same temperature. The temperature range chosen here is the same as the one introduced by solar radiation starting from the minimum value of 75 W/m^2 and ending at maximum value of 1015 W/m^2. The most approximate curve for the measured points is a straight line. Generally however, the insolation-current relationship is not necessarily linear. A linearizing circuit will be discussed in the case of non-linearity in order to obtain a conversion factor between insulation and current.

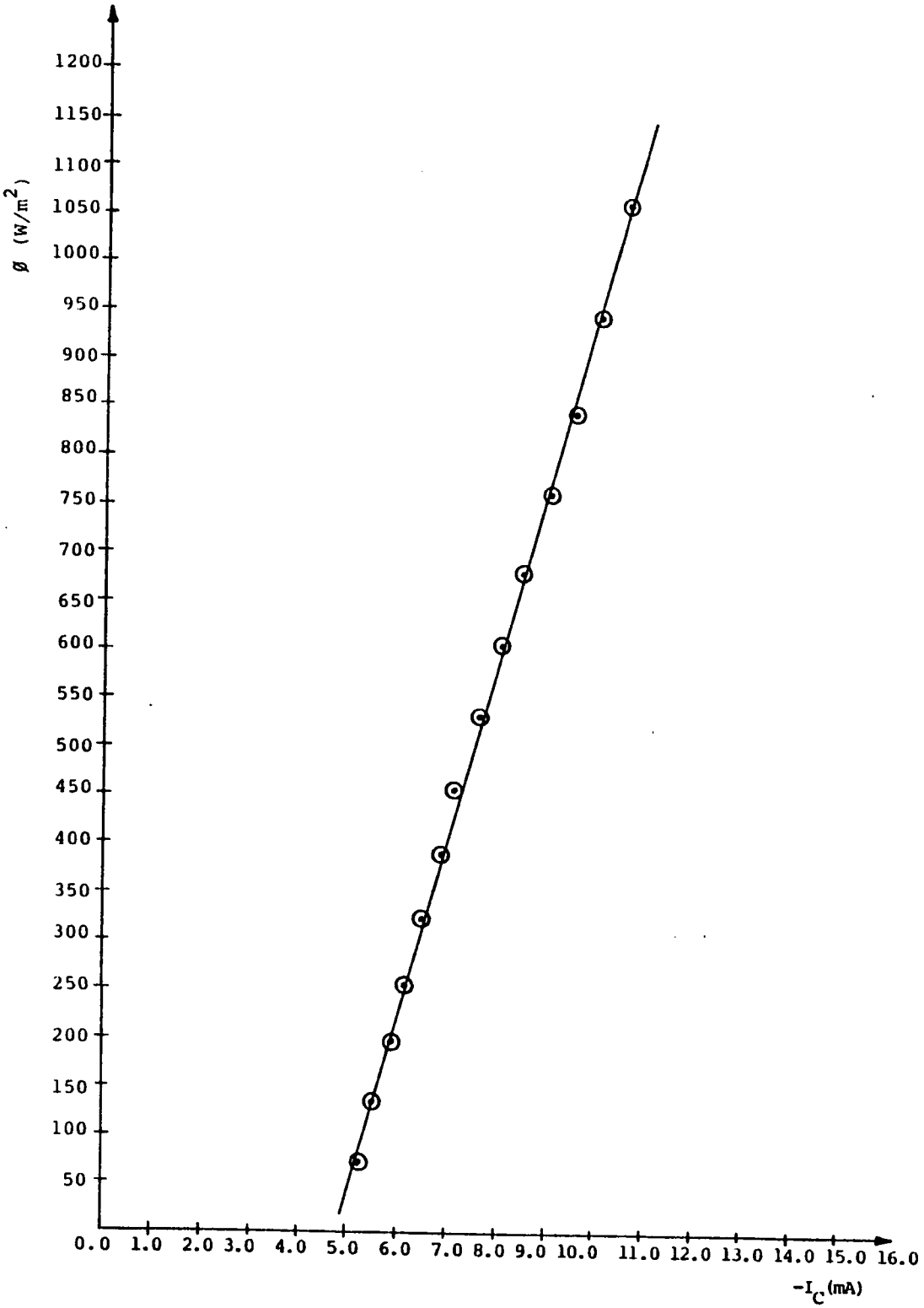

Figure 44. Insolation versus collector current.

The calibration is affected by ambient temperature, unless heat energy is transferred to the transistor by radiation only. Hence, there is a one-to-one correspondence between insolation and transistor temperature.

3.2.3 Transient Time

One of the problems encountered is the time interval taken for the collector current to reach steady state when the temperature of the transistor is changed. This transient time is due to the size and material of the transistor case and the capacitive effects in the transistor junctions.

From a mechanical point of view the transistor can be considered as a system (Fig. 45) subject to incident radiation ϕ_i causing a temperature rise $\Delta T = T_f - T_a$, where T_f is the steady state temperature and T_a is the initial (ambient) temperature.

The energy balance equation for this system is

$$q_i - q = MC_P \frac{dT}{dt} \qquad (3\text{-}25)$$

where t represents time, and

$$q_i = \phi_i s$$

with s = the surface area of the transistor case.

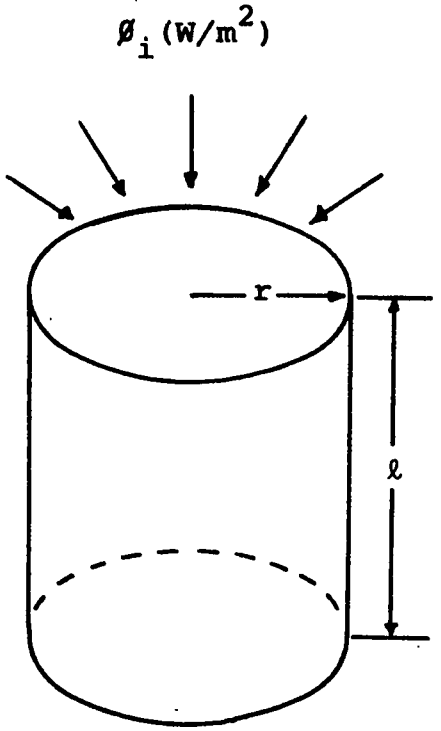

Figure 45. Transistor case and heat transfer.

$q = \theta_{jc}(T - T_a)$, from Newton rate equation

C_p = Specific heat in J/kg^oC

M = Mass of the transistor in kg

Substituting in Eqn. (3-25), and separating the variables,

$$\int_o^t dt = \frac{MC_P}{\theta_{jc}} \int_{T_a}^{T_f} \frac{dT}{\frac{\phi_i s}{\theta_{jc}} + T_a - T} \qquad (3\text{-}26)$$

The limits show that the transistor was at temperature T_a before it is exposed to solar radiation. Integrating Eqn. (3-26) gives

$$t = - \frac{MC_P}{\theta_{jc}} \ln \left(\frac{\phi_i s}{\theta_{jc}} + T_a - T\right)\Bigg|_{T_a}^{T_f}$$

$$t = - \frac{MC_P}{\theta_{jc}} \ln \frac{\frac{\phi_i s}{\theta_{jc}} + T_a - T_f}{\phi_i s/\theta_{jc}}$$

Solving for T_f to obtain

$$T_f = T_a + \frac{\phi_i s}{\theta_{jc}} (1 - e^{-t/\tau}) \qquad (3\text{-}27)$$

where $\tau = \frac{MC_p}{\theta_{jc}}$ = time constant

$$= \frac{\rho \nu C_p}{\theta_{jc}} \qquad (3\text{-}28)$$

where ρ is semiconductor density and ν is the transistor volume.

From Eqn. (3-27) it is inferred that the smaller the time constant, τ, the faster thermal equilibrium is reached.

From an electrical point of view, the transistor junctions exhibit a reactive effect responsible for increasing the time delay when the collector current increases.

There is a depletion-layer capacitance, C_{be}, of the emitter-base junction and a depletion layer capacitance, C_{bc}, of the collector-base junction. Furthermore, a diffusion capacitance, C_D, appears across the emitter-base junction. It accounts for the charge that must accompany the change in the minority-carrier gradient when the junction voltage is modified. Usually, C_{be} is negligible compared with C_D. C_{bc} and C_D are given by

$$C_{bc} = \frac{M}{\sqrt{|\Psi| + V_{CB}}} \quad \text{for reverse-biased junction,} \qquad (3\text{-}29)$$

$$C_D = \frac{W_B^2}{2D_p} \frac{qI_E}{kT} \qquad (3\text{-}30)$$

where

M = constant

$|\Psi|$ = barrier voltage

W_B = base width

D_P = holes diffusion constants

The equivalent model is given in Fig. 46.

The depletion layer, as given in Eqn. (3-29), depends on the reverse-biasing voltage V_{CB} and the diffusion capacitance, given in Eqn. (3-30), depends on the base width and the temperature. Therefore C_D can be minimized by reducing the base width.

3.2.4 Improving the Solarimeter

The transient time is a major problem in the solarimeter design. But it is not when the solarimeter is in service in non-cloudy days, because the change of insolation is slower than the solarimeter response. Thus, there is sufficient time for thermal equilibrium to take place on the transistor case.

The transient time can be reduced however. From Eqn. (3-28), it is seen that if the volume of the transister is reduced and its surface is coated with a

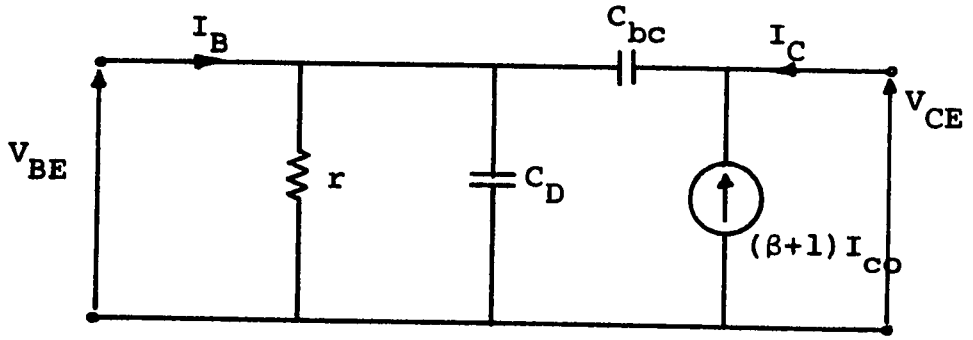

Figure 46. Complete temperature-dependent model of the transistor in the CE configuration.

thermally highly absorptive material, the time constant is decreased. Furthermore, if the base current of the transistor is kept constant, for all operating temperatures, the effect of the depletion-layer capacitance of the base collector junction is reduced. In addition, the effect of the diffusion capacitance given in Eqn. (3-30), can be minimized by making the base width small so that the thermally generated charge carriers will diffuse in a short time.

The radiation-sensing device should be protected from winds to eliminate heat losses caused by convection. Figure 47 shows the transistor located at the center of a spherical glass cover.

In order to completely eliminate the effect of convection and hence maximize heat transfer by radiation, the space between the cover and the transistor should be totally evacuated. Also, the transmittance coefficient of the glass material should be as large as possible.

3.2.5 Part (b)

Objective: To study the relation between the transient time and the number of glass covers which could be used for eliminating heat loss caused by convection.

3.2.5.1 Procedure

The schematic diagram in Fig. 48, shows the set-

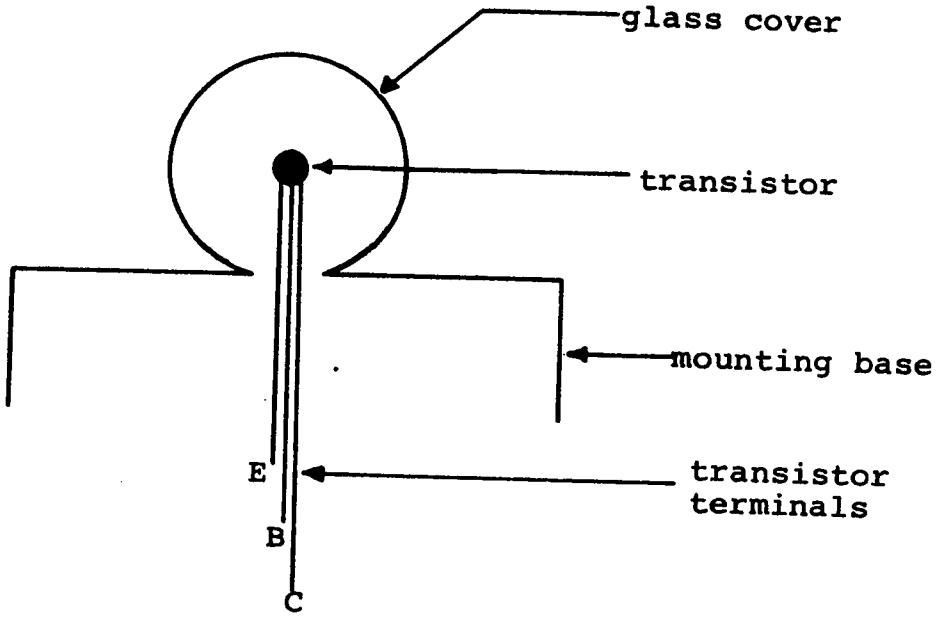

Figure 47. Protection of the transistor.

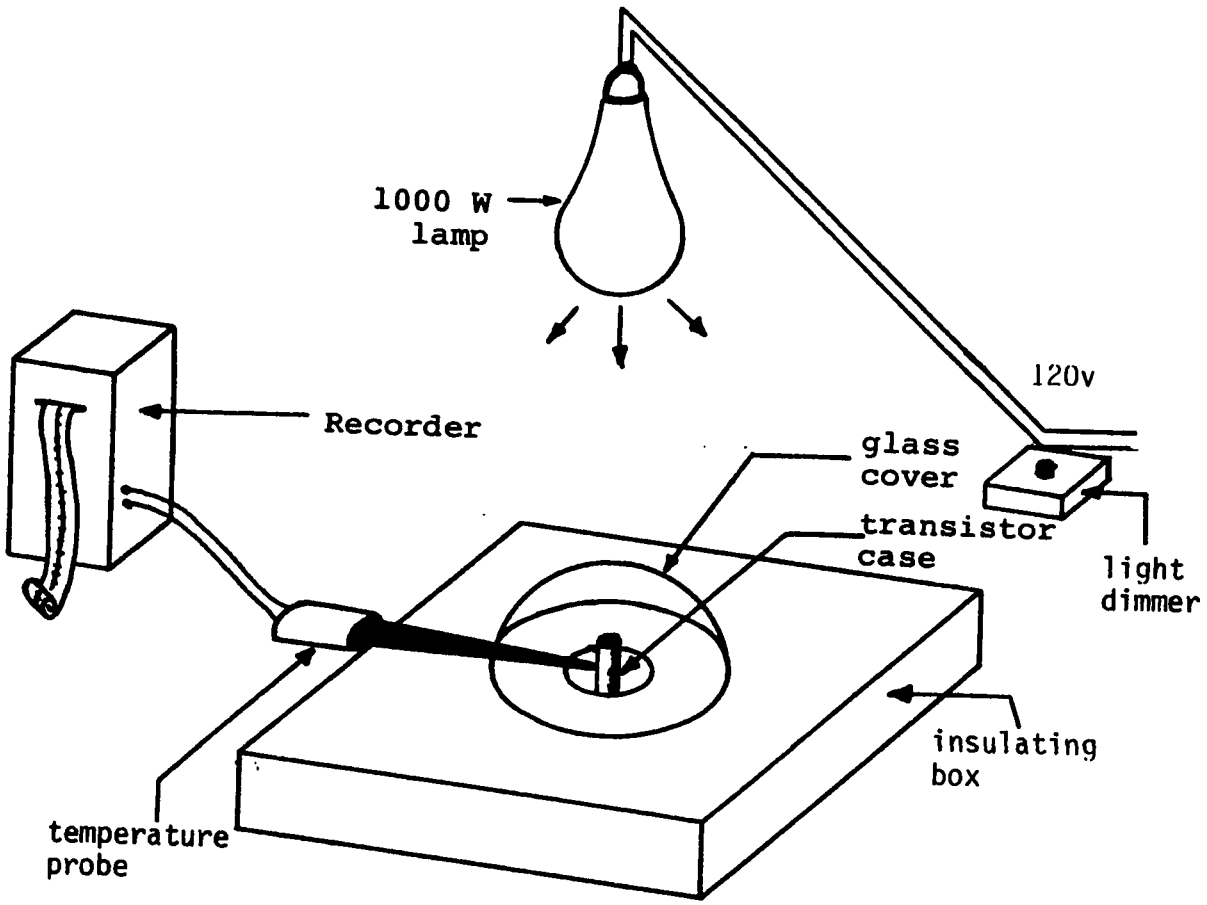

Figure 48. Schematic diagram for studying the effect of glass covers on transient time.

up of the experiment. First the case of the used AC132 germanium transistor is coated with a black paint in order to increase absorbitivity and hence reduce reflection. Then temperature increase is plotted against the transient time. The graphs taken are shown in Fig. 49. These graphs were plotted when the transistor was covered with one, two, and three glass covers.

3.2.6 Part (c)

Objective: to investigate the effect of the depletion-layer capacitance of the base-collector junction on the transient time of the current-temperature relation.

3.2.6.1 Procedure

The same circuit in Fig. 32 is used with the addition of a germanium diode connected in series with the base. The diode is reverse-biased to keep the base current constant. The data in Table III are obtained by following the steps in part (a) and then plotted in Fig. 50.

3.2.7 Conclusions

1. In part (a), the base-to-emitter voltage, V_{BE}, has increased by 15%, at 60^{o}C, of its value at room temperature and the base current was observed to be constant (I_B = ,018 mA) for all measurements. Does this agree with the input characteristics shown in Fig. 36? Considering the base loop equation given below

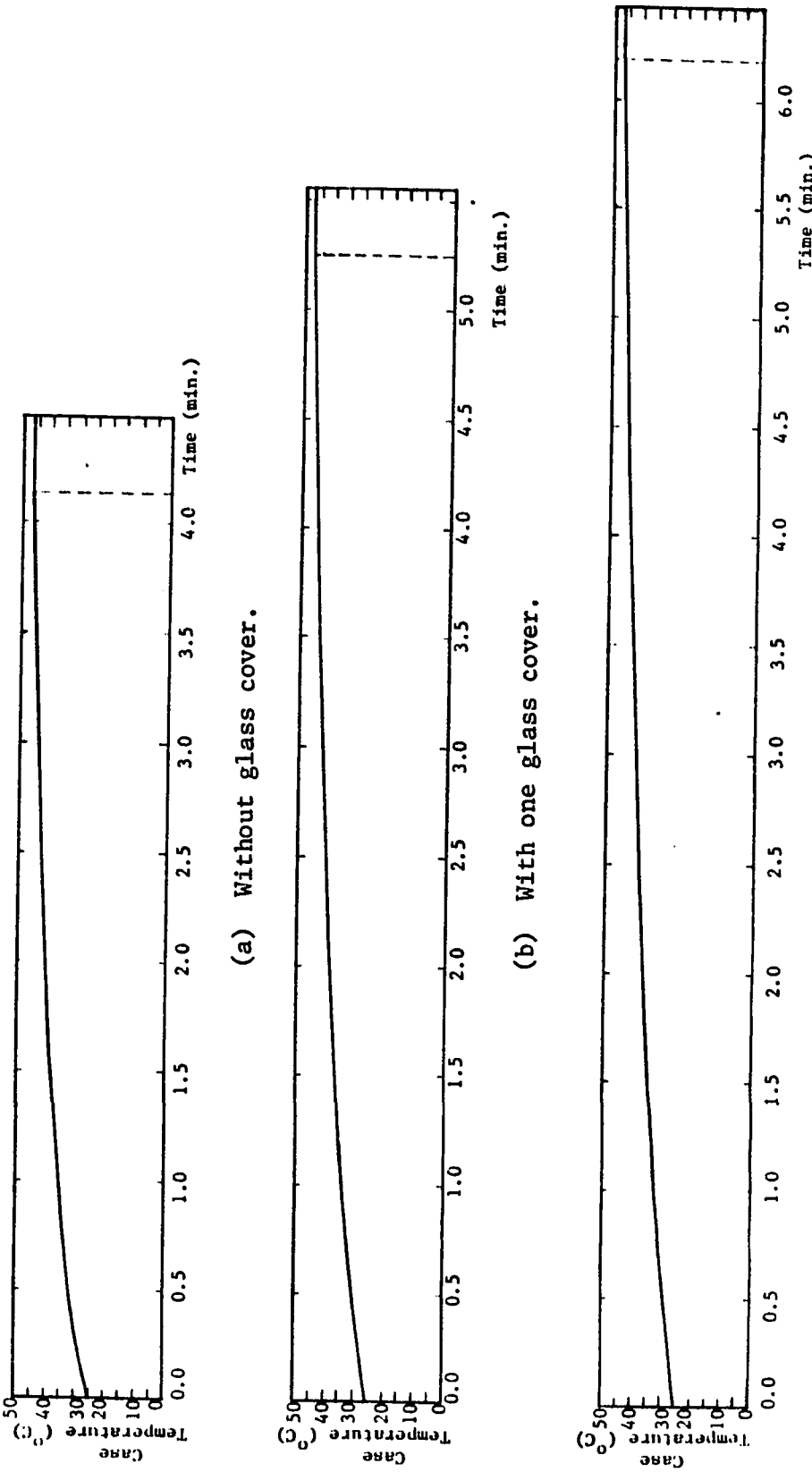

(a) Without glass cover.

(b) With one glass cover.

(c) With two glass covers.

Figure 49. Transient time for thermal equilibrium to take place on the transistor case for different numbers of glass covers.

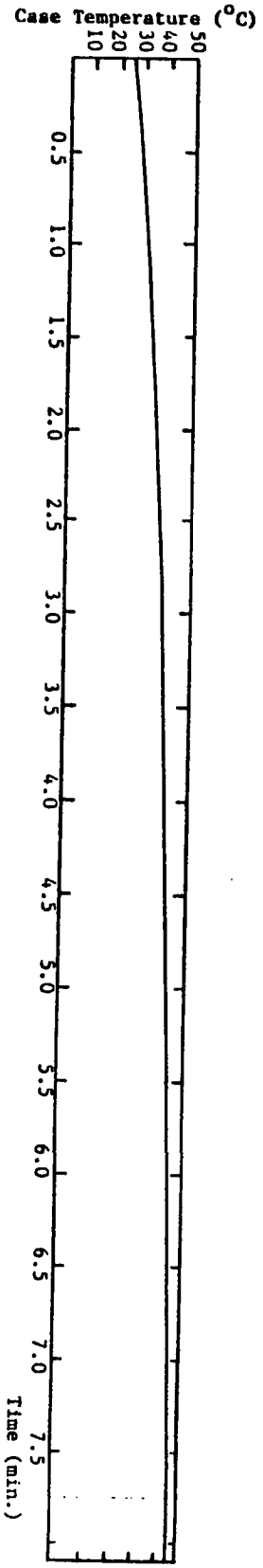

(d) With three glass covers.

TABLE III. These Readings were Taken at Room Temperature of 23°C, T is the Temperature of the Transistor Case and $\Delta T = T - 23$.

$\Delta T^{o}C$	I_C(mA)
0.0	-0.5
2.2	-0.65
5.5	-0.97
8.4	-1.3
11.1	-1.8
15.4	-3.0
17.1	-3.5
19.8	-4.6
22.2	-5.6
24.0	-6.83
27.0	-8.6
28.0	-9.2

An average transient time of 8 minutes is measured

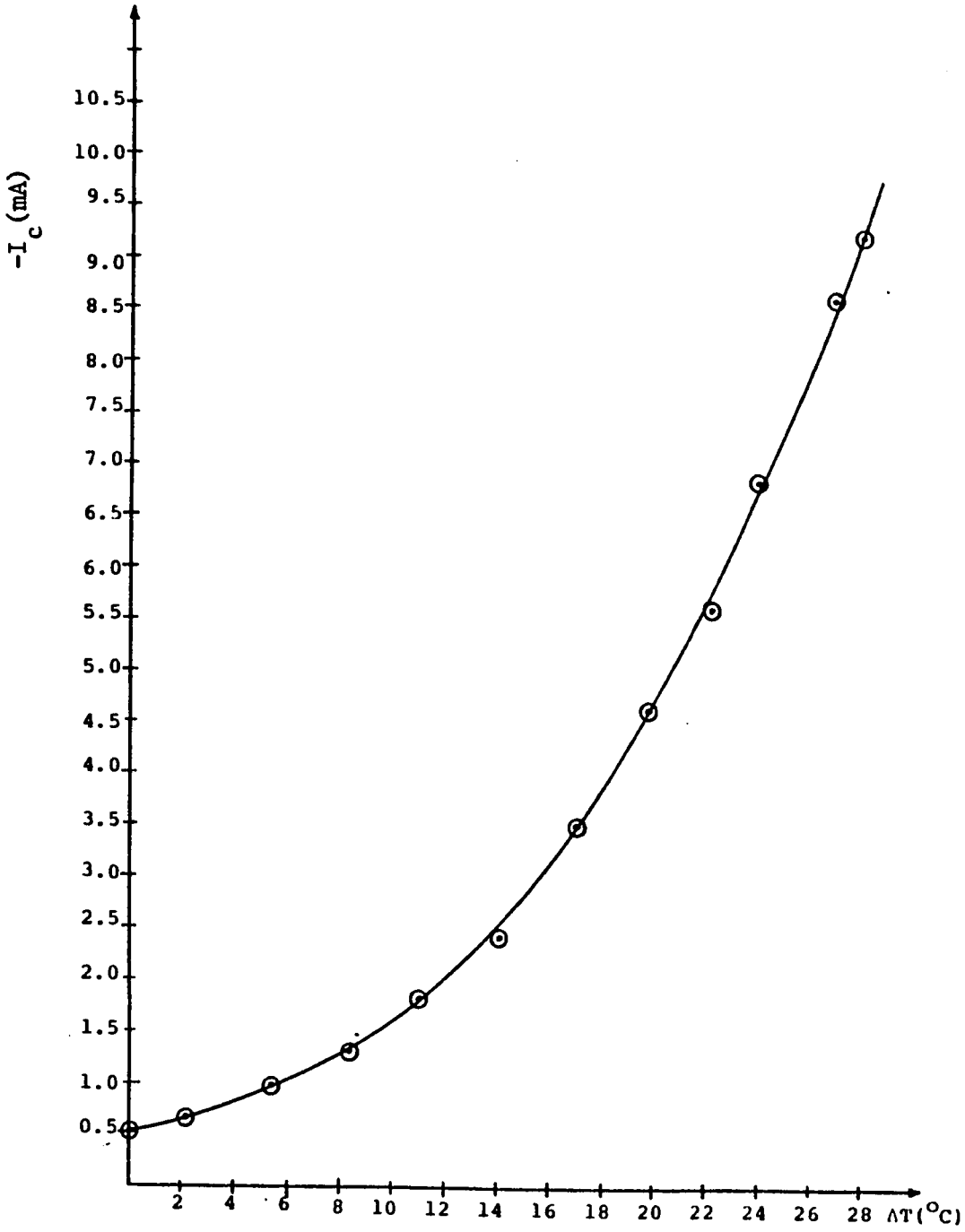

Figure 50. Collector current versus temperature change of the transistor case, $\Delta T = T - 25^{o}C$, (Part c).

$$I_B = \frac{V_{CC} - V_{BE}}{R_B}$$

Hence

$$\Delta I_B = - \frac{\Delta V_{BE}}{R_B} \qquad (3\text{-}31)$$

According to Eqn. (3-31), I_B is decreased by

$$\Delta I_B = 6 \times 10^{-8} \ \mu A$$

when the case temperature is $60^{o}C$, but this change is too small to be detected.

Also, the increase in V_{BE} with increasing temperature does not follow the input characteristics which show that V_{BE} is decreased at $60^{o}C$. But knowing that those characteristics were taken with an open-circuited collector, makes the situation here completely different. All the terminal voltages of the transistor are involved when the measurements are taken. The following equations are analysed.

$$V_{BE} = V_{CE} - V_{BC} \qquad (3\text{-}32)$$

$$V_{CE} = V_{CC} - I_C R_C \qquad (3\text{-}33)$$

$$V_{BC} = I_B R_C - I_C R_C \qquad (3\text{-}34)$$

when the temperature increases, all the three voltages change but with different quantities. In other words V_{BC} must have a larger change than V_{CE} in order to satisfy Eqn. (3-32). Taking the differential changes in Eqns. (3-33) and (3-34), then

$$\Delta V_{CE} = - R_C \Delta I_C \quad , \text{ and}$$

$$\Delta V_{BC} = R_B \Delta I_B - R_C \Delta I_C$$

Therefore, I_B must be decreased to contribute to the change of V_{BC} making it larger than that of V_{CE}. Physically, when all the terminals of the transistor are involved, there is a reverse collector saturation current, I_{CBO}, flowing in the opposite direction of the base current. Two factors cooperate to cause I_{CBO}. First, there exists a leakage current which flows, not through the base-collector junction, but around it and across the surfaces. Second, new carriers may be generated by collision in the base-collector junction transition region, leading to avalanche multiplication of current[10] and, if the permissible temperature is exceeded, eventual break down takes place. Yet this current is too small to detect, but it leads to a discernible increase in V_{BE}.

2. In part (a), when the transistor is not connected to the power supply, a transient time of about 8 minutes is

observed for thermal equilibrium to take place from 25°C to 60°C. On connecting the transistor, the same time is taken for the current to reach steady state over the same temperature range. But this does not mean that the capacitive effects do not contribute to make the transient time longer because, in this case, the transistor is heated by its power dissipation in addition to the incident radiative power. Because the transistor dissipation is very small compared to the radiative power, it can be said that the parasitic capacitances have negligible transient times.

3. When the transistor is coated with a black paint, the transient time is reduced as shown in Fig. 49a. Due to the fact that the transient time increases with increasing glass covers, as demonstrated in Fig. 49, there is no need for more than one glass cover to protect the transistor.

4. The addition of the reverse-biased diode, in series with the base, does not affect the shape of the current-temperature relation (Figs. 42 and 50). On the contrary, the diode keeps the base current constant and thus the depletion-layer capacitance of the base-collector junction is eliminated. An average transient time of 8 minutes is measured in both parts (a) and (c), for the same temperature intervals. Therefore, it can be

said that the depletion-layer capacitance of the base-collector junction does not have a significant contribution to the overall transient time and it can be neglected in the model shown in Fig. 46 for the used transistor.

5. The transient time is not only dependent on the initial and final temperatures, but it is also dependent on the intensity of the incident radiation: i.e., the higher the radiation intensity is the faster thermal equilibrium takes place. This explains why approximately constant transient time is observed even for elevated temperatures.

6. The maximum temperature caused by incident solar radiation is $45^{o}C$. This value is far below the maximum temperature specified for the transistor, by the manufacturer.

7. Since the ambient temperature changes from place to place and from time to time, it is necessary to establish a reference point, independent of the ambient temperature variations, on the insolation-temperature graph shown in Fig. 44. This can be achieved by connecting, in parallel, two transistors having the same characteristics, and the same biasing elements (Fig. 51). But each transistor must have different casing material in order to introduce a temperature difference between the two cases when exposed to solar radiation. In this case the radiation intensity will be related to the

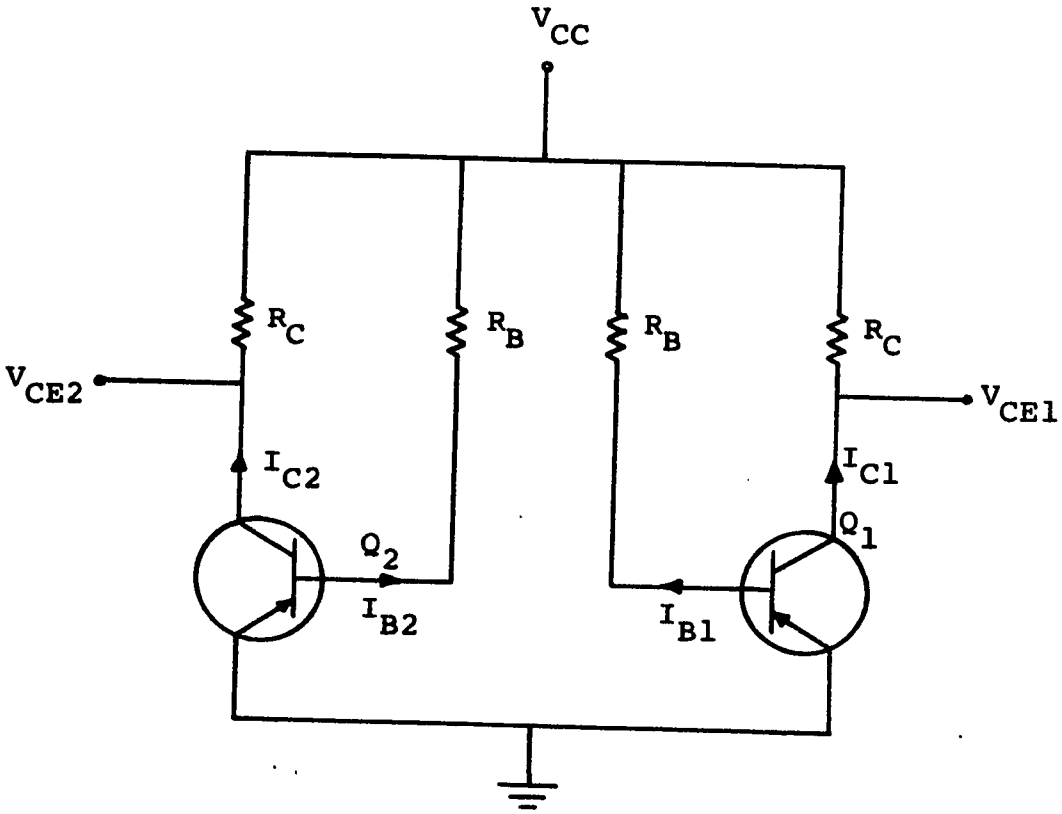

Figure 51. The solarimeter circuit with ambient temperature-compensating transistor.

difference between the two voltages, V_{CE2} and V_{CE1} shown in Fig. 51. Now, if both transistors are at the same temperature then

$$V_{CE1} = V_{CE2}, \text{ and}$$

$$\Delta V = V_{CE1} - V_{CE2} = 0$$

Assuming that transistor Q_2 has higher absorptivity than that of transistor Q_1, therefore on exposure to solar radiation, Q_2 will be at a temperature higher than that of Q_1. Thus V_{CE2} will be less than V_{CE1} and there will be a voltage difference of

$$\Delta V = V_{CE1} - V_{CE2} > 0$$

And this shows that the voltage difference, ΔV, increases with increasing the intensity of solar radiation.

5.2.8 Linearization

In case, the collector current is related to insolation in a nonlinear manner (Fig. 52), it can be linearized for calibrating the solarimeter.

The voltage across R_C will be used to indicate the amount of insolation instead of I_C. The voltage-insolation relationship is the same as the curve shown in Fig. 52 with I_C replaced by $V_i = R_C I_C$ (Fig. 53).

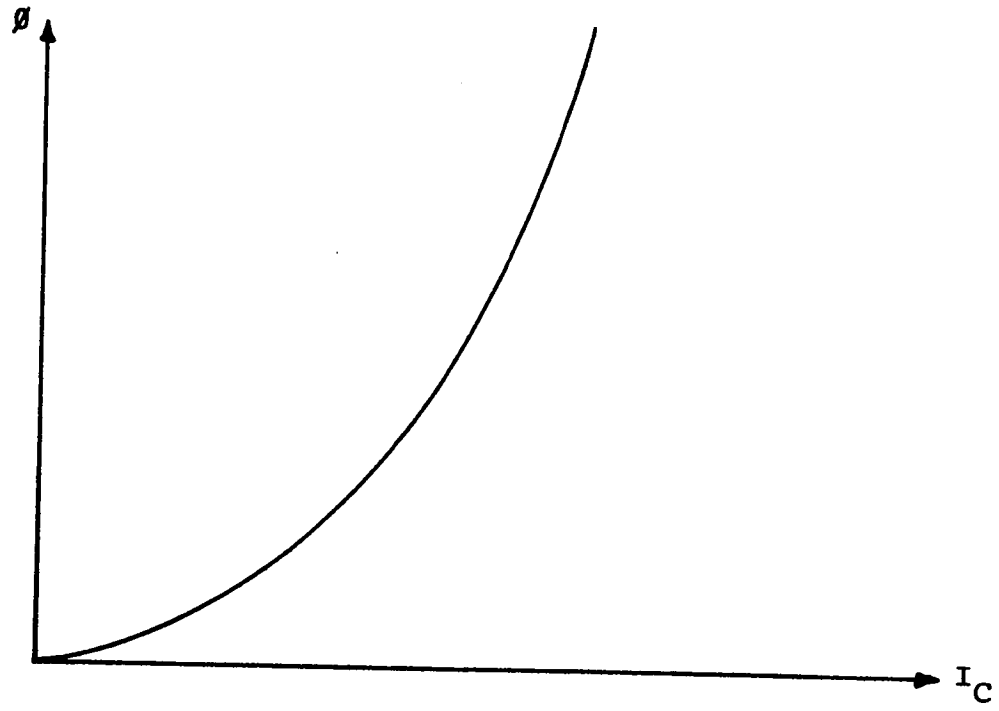

Figure 52. General relation between insolation and collector current.

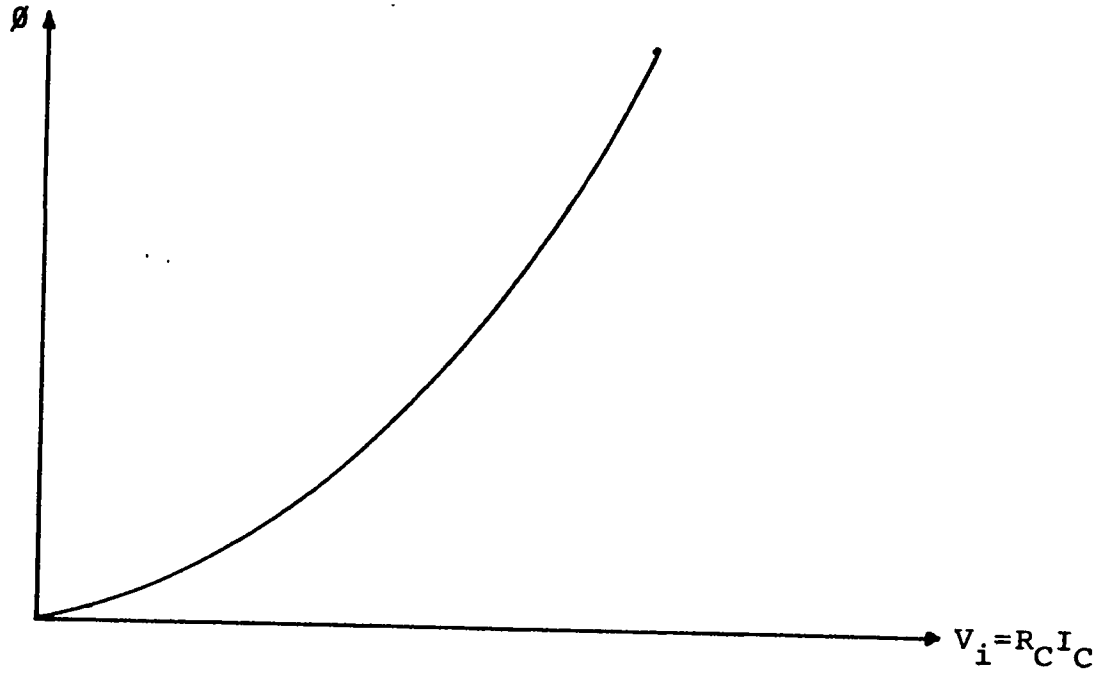

Figure 53. Insolation-voltage relation.

Figure 54 shows the complete circuit for the solarimeter, where the voltage across R_C is taken through a differential amplifier with gain of -1 so that I_C is limited to the transistor circuit.

In order to design the appropriate nonlinear compensating network (Fig. 54), an appropriate transfer characteristic is sought, then a technique is used to synthesize the transfer-chacacteristic.

The problem now is to determine the V_o-VS-V_i plot so that $v_o = b\emptyset$, where b is a constant. The desired relation between v_o and v_i is found graphically as shown in Fig. 55.

The transfer-function of V_o-VS-V_i may be synthesized by using the operational amplifier configuration, as shown in Fig. 55, this method leads to a monotonic driving-point function as long as the transfer-function is also monotonic.

The transfer-function synthesis is as follows. From the circuit in Fig. 56, the input current of the operational amplifier is zero ($i_i = 0$). Hence $i_1 = - i_f$, and

$$v_o = v \qquad (3\text{-}35a)$$

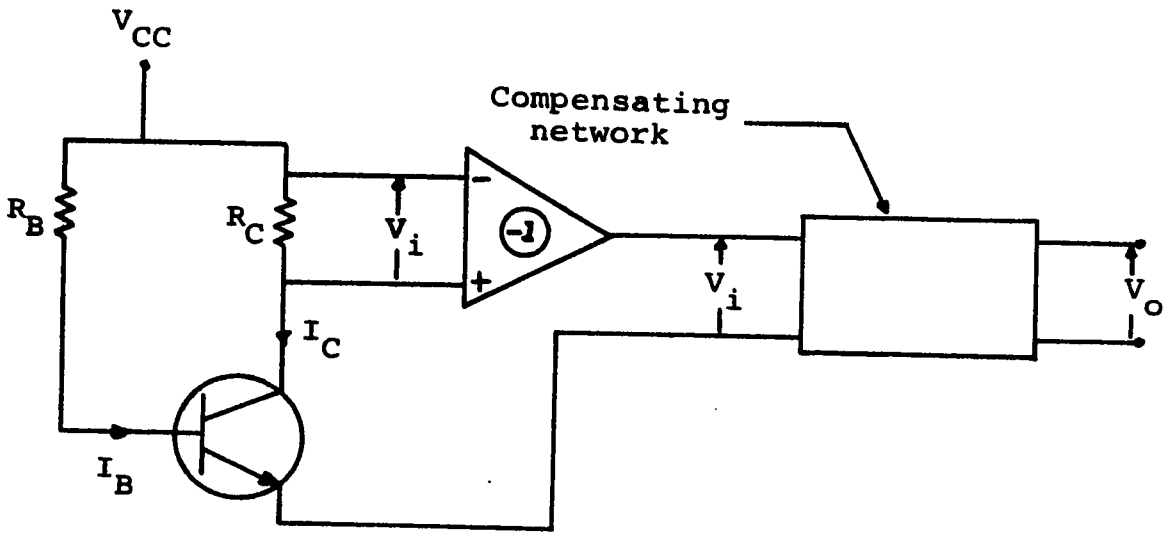

Figure 54. Solarimeter with a compensating network.

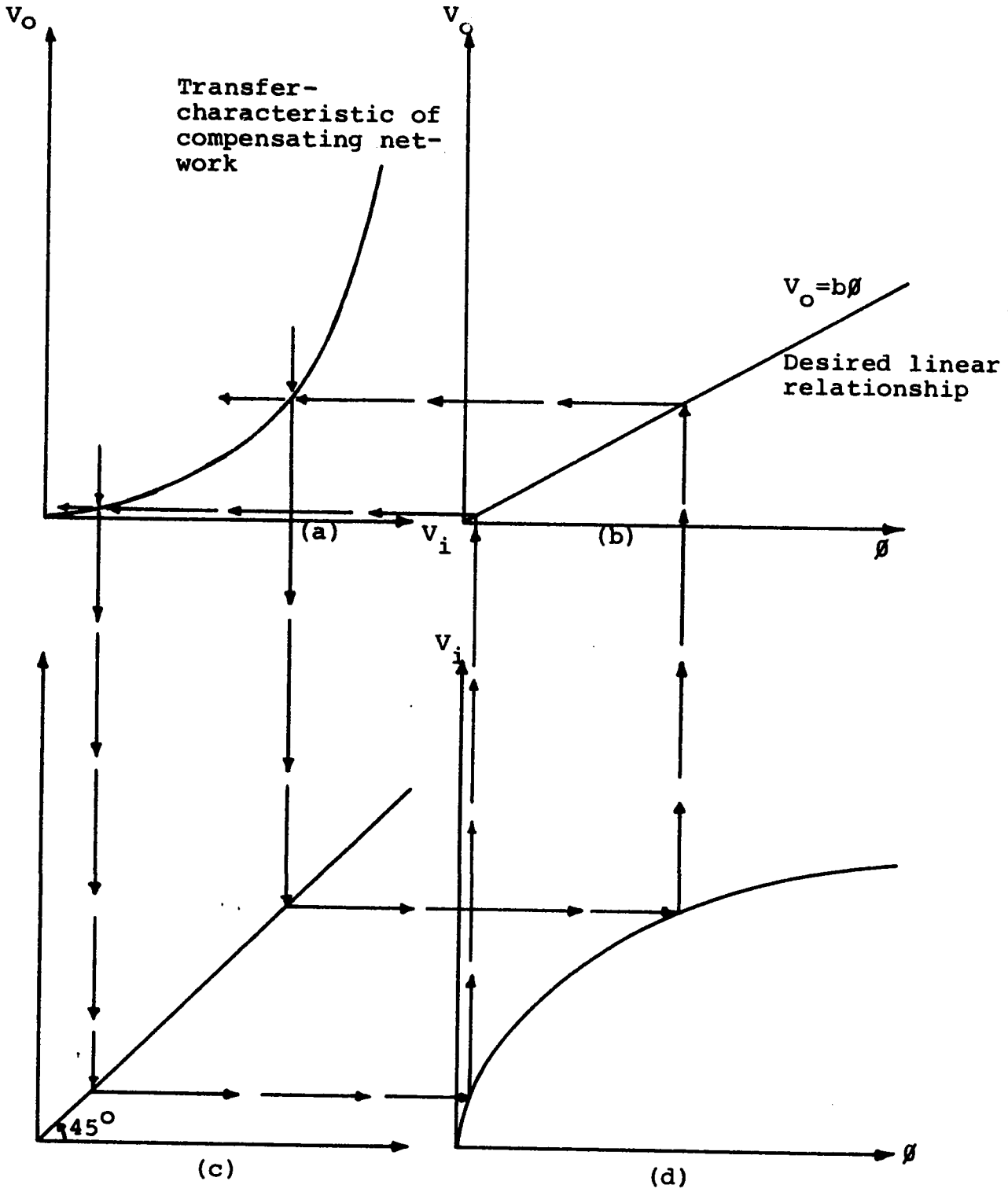

Figure 55. The graphical composition procedure for obtaining the transfer-characteristic of the compensating network.

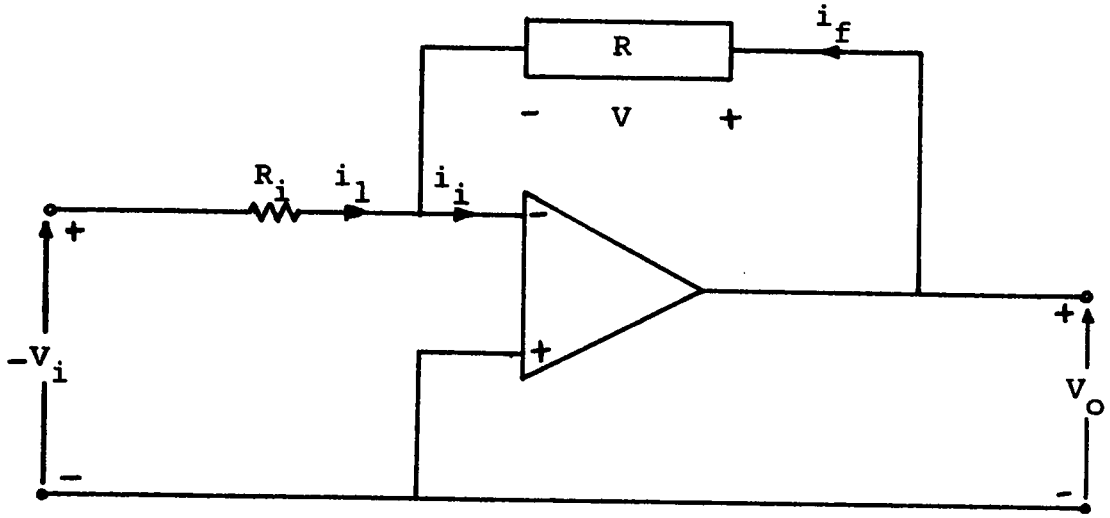

Figure 56. Compensating network.

$$v_i = -R_i i_1 \qquad (3\text{-}36b)$$

If the v-i characteristic of the nonlinear resistor R is $v = g(i)$, then from Eqns. (3-36)

$$v = g(-i_1) = g\left(\frac{v_i}{R_i}\right)$$

or
$$v_o = g\left(\frac{v_i}{R_i}\right) \qquad (3\text{-}37)$$

This equation implies that any transfer-function $v_o = f(v_i)$ can be realized by the circuit shown in Fig. 56, provided that the v-i characteristic of the nonlinear resistor R is chosen to be

$$v = f\ (-R_i i_1)$$

and that because

$$v_o = f(v_i) = g(i_f)$$

$$\therefore \quad g(i_f) = f(R_i i_f)$$

Furthermore, if R_i is replaced by a constant K_i, then this constant can be used to change the scale of the input voltage v_i.

Also, applying the technique of piecewise linear

analysis, a simple circuit can be designed to meet the transfer function of the compensating network. First the nonlinear characteristic is approximated by connecting straight-line segments as shown in Fig. 57. The line segments intersect at the points (V_{i1},V_{o1}), (V_{i2}, V_{o2}), ---, (V_{in}, V_{on}). Then a network, that realizes the piecewise linear curve, is constructed by utilizing diodes, resistors, and a constant voltage source. One possible diode-resistor network is shown in Fig. 58.

The design procedure, is to apply the break point analysis. At the ℓth break point the current through and the voltage across the ℓth diode simultaneously are zero, thus the design equations, in generalized form are[1]

$$R_{2\ell} = \frac{V_{o\ell} + V_{DC}}{V_{i\ell} - V_{o\ell}} R_{1\ell}, \qquad \ell = 1, 2, \text{---}, n \quad (3\text{-}38)$$

$$\frac{V_{o\ell+1}}{R_B} = \frac{V_{i\ell+1} - V_{o\ell+1}}{R_A} + \sum_{m=1}^{\ell} I_{Dm}, \quad \ell = 1,2,\text{---}, n \quad (3\text{-}39)$$

$$I_{D\ell} = \frac{V_{i\ell+1} - V_{o\ell+1} - V_{D\ell}}{R_{1\ell}} - \frac{V_{o\ell+1} + V_{D\ell} + V_{DC}}{R_{2\ell}}$$

$$\ell = 1, 2,\text{---},n \quad (3\text{-}40)$$

Also, from Eqn. (2-5)

$$I_{D\ell} = I_o(e^{qV_{D\ell}/kT} - 1),$$

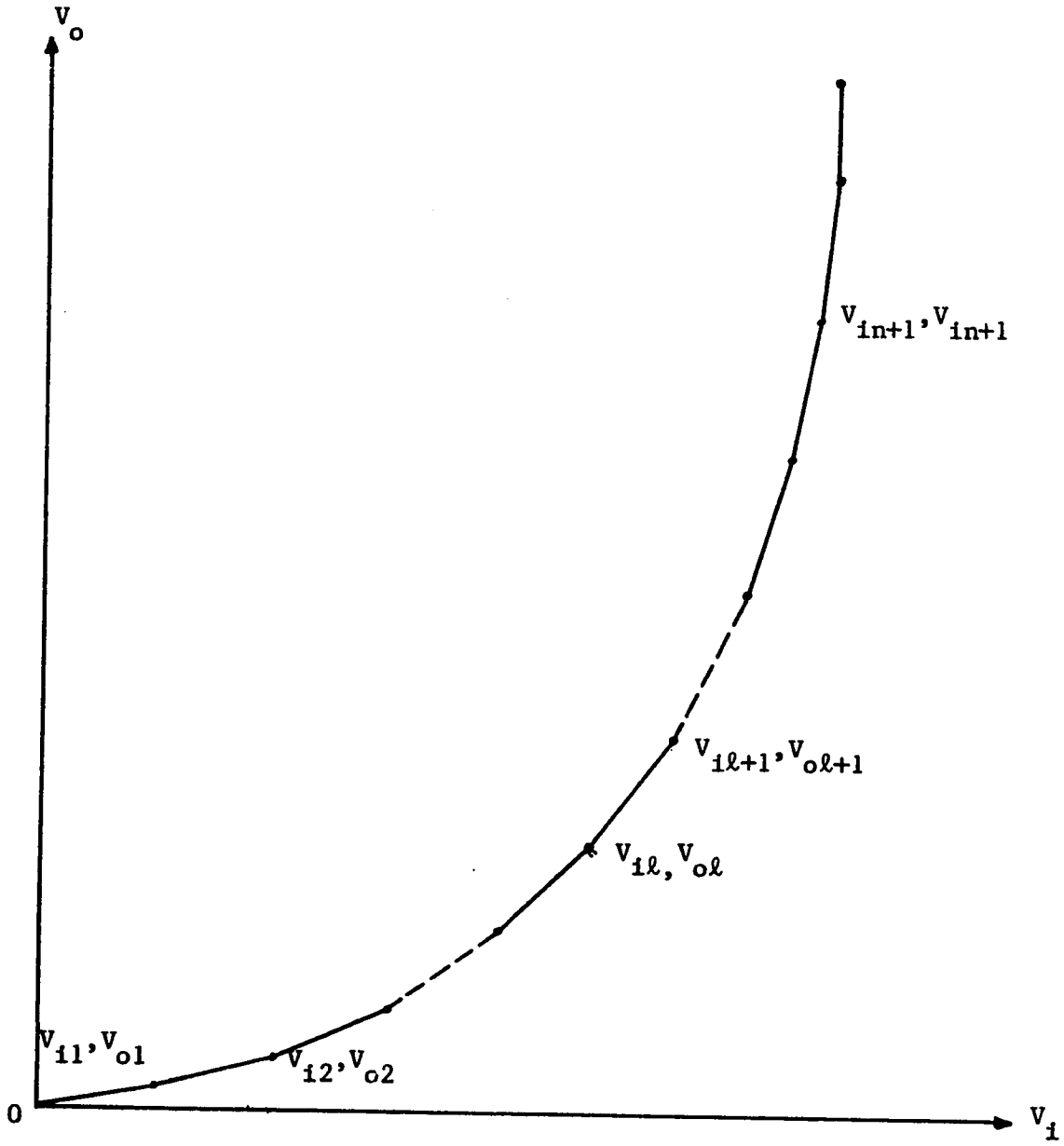

Figure 57. Lines piece-wise approximation.

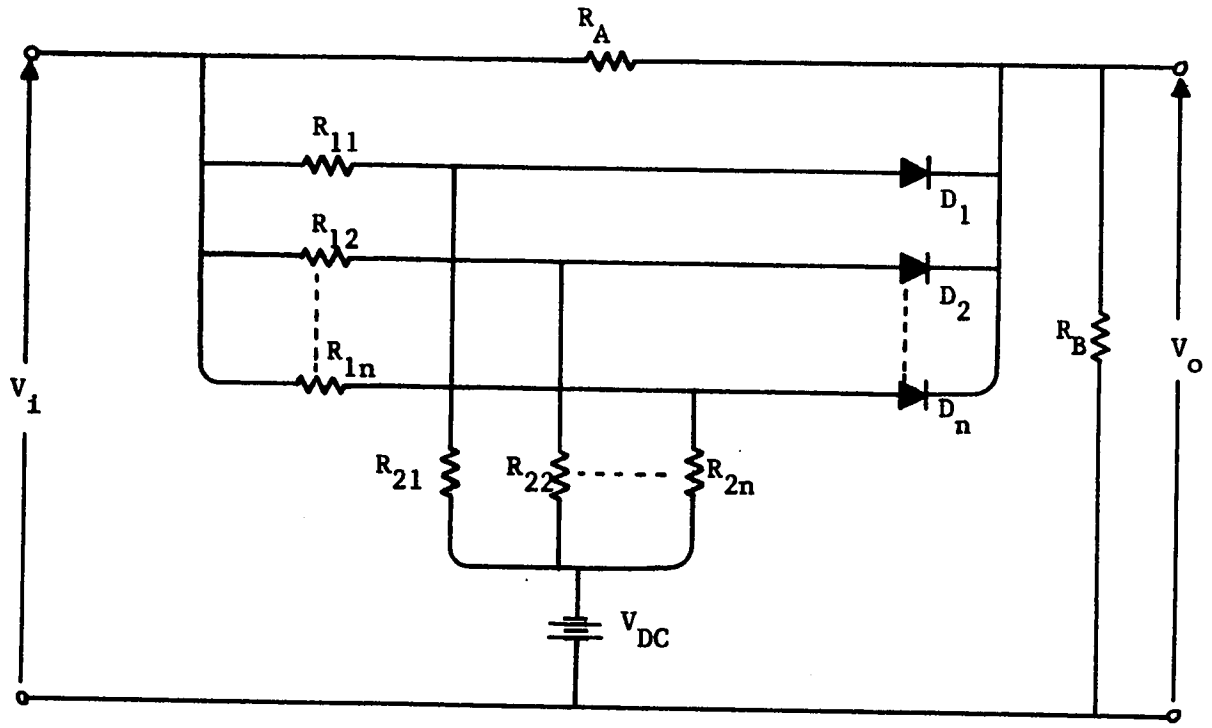

Figure 58. Diode-resistor network for realizing monotonically increasing concave characteristic of the type shown in Fig. 57.

where $I_{D\ell}$ and $V_{D\ell}$ are current and voltage of the ℓth diode.

For the ℓth diode, initial conditions in Eqn. (3-40) are from the $(\ell-1)$th calculation. Combining Eqn. (3-38) and Eqn. (3-40) for $R_{1\ell}$ in terms of known quantities gives

$$R_{1\ell}I_{D\ell} = V_{i\ell+1} - V_{o\ell+1} - V_{D\ell} - \frac{(V_{o\ell} + V_{D\ell} + V_{DC})(V_{i\ell} - V_{o\ell})}{(V_{o\ell} + V_{DC})} \qquad (3\text{-}41)$$

When all the diodes are reverse biased, then from Eqn. (3-39)

$$V_{o\ell+1} = \frac{R_B}{R_A + R_B} V_{i\ell+1} \qquad (3\text{-}42)$$

and this gives the freedom of choosing R_A & R_B such that the combination $R_B/(R_A + R_B)$ is equal to the slope of the first line segment.

It is obvious that, the transfer characteristic can be approximated as best as possible by increasing the number of break points. In this case a computer program can be written to give the appropriate values of $R_{1\ell}$ and $R_{2\ell}$.

3.2.9 Battery Recharge

Finally, a drop may occur in the biasing voltage

due to the aging of the battery. To overcome this problem the use of a rechargeable heavy duty battery is recommended. The solar-supplied circuit shown in Fig. 59 may be used to charge the biasing battery when there is a voltage drop.

Diode D1 is an important part of the charging system. It is possible, that the battery voltage would exceed the charging source voltage because of full charge on low insolation. Without the diode in the circuit, the battery would then discharge into the solar source. To avoid this under conditions of high battery voltage and low charge voltage, the diode is reverse biased, making the anode more negative than the cathode. With use of the Zener diode D2 the output can be regulated within the battery voltage. A requirement is that the regulated output voltage be less than the voltage of the solar supply. After the voltage of the solar supply drops below a chosen minimum voltage, the Zener diode goes out of regulation. This minimum value is used to determine the value of the series resistor, R_s. The basic equation is

$$V_{SMIN} = R_s (I_{BMAX} + I_{ZMIN}) + V_Z + V_D \qquad (3\text{-}43)$$

or

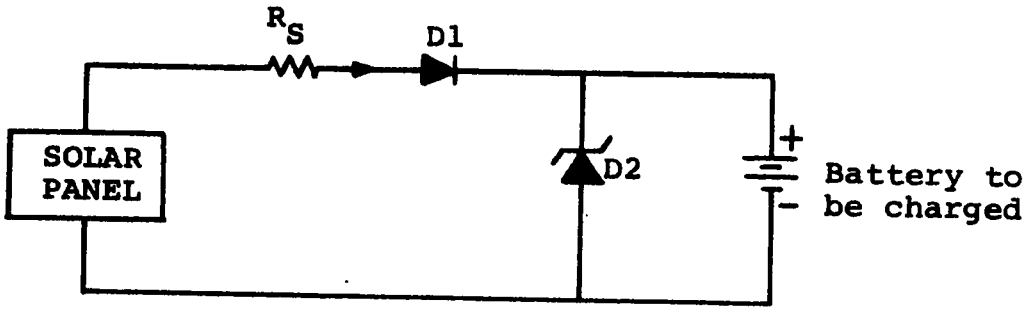

Figure 59. Charging circuit.

$$R_S = \frac{V_{SMIN} - V_Z - V_D}{I_{BMAX} + I_{ZMIN}} \qquad (3\text{-}44)$$

where

V_{SMIN} = minimum source voltage

V_Z = Zener breakdown voltage

I_{BMAX} = Maximum charging current

I_{ZMIN} = Minimum Zener current

V_D = Forward voltage drop of the diode D1

Moreover, a solar relay may be used to put the solarimeter "on" or "off" depending on the presence or absence of solar radiation. This will save power consumption from the battery.

3.3 SUMMARY

The demand for radiation-measuring instruments increased tremendously in order to collect regional long-term solar data. These data are analyzed for designing cost-effective solar systems. Usually, the measuring-devices convert radiation to some other form of energy and provide a measure of the energy flux produced by radiation. There are the pyrheliometers and the pyranometers used for measuring direct and total radiation. These devices were designed many years ago for obtaining data needed in meteorological analysis. Their operation was based on thermoelectrical or mechanical principles.

Thermoelectric instruments have been in widespread use for the measurements of direct or total radiation. Used, in general, without frequent calibration they yield data with an error of no less than $\pm$ 5%. The measured value vary somehow if the instruments are inclined.

Other solarimeters were designed on the basis of the photovoltaic principle. However, the solar cell has the disadvantage that its calibration is a function of the spectral distribution of solar radiation. Also, the calibration varies with the angle of incidence of the radiation.

In this thesis, the design of a cheap, and easy-to-build solarimeter is described. The operation of this solarimeter is based on the temperature effect in bipolar junction transistors. The transistor is chosen because of the remarkable change in its collector current when the case temperature is changed. Also, the geometry of the transistor case can be chosen in such a way that the same area of the case is exposed to radiation regardless of the position of the sun making the calibration independent of the angle of incidence.

Theoretical analysis has been made to choose the appropriate biasing elements. Resistors are selected so that a prescribed temperature range is covered and at the same time, damage of the transistor is prevented. The temperature range is determined by exposing the transistor to minimum and maximum insolation. Thermal runaway is avoided by taking into consideration the transistor dissipation and the power input provided by the incident solar radiation. Experimental data were reported. These data were used to obtain a direct linear relation between insolation and the transistor current.

Furthermore, theoretical analysis, supported with experimental conclusions, to deal with the transient time problem are reported. Two methods are included to linearize the relationship between radiation intensity and collector current.

Compared with the previously mentioned instruments, this solarimeter can be used for measuring either total or direct radiation. In the case of total radiation, the differential output of two exposed transistors is taken as a measure, and in the case of direct radiation one transistor is shielded and the output will indicate the amount of radiation. This, of course, will reduce the amount of error which is noticed when a long tube is used to limit the view angle of the sensor to the circumsolar sky. The error is due to the diffuse radiation permitted through the radiation-limiting tube.

Besides, the output difference of the transistors is taken at the same time with the same meter and this eliminates completely the effect of diffuse radiation when direct insolation is measured only.

REFERENCES

1. Abuelma'atti, M.T., "Diode Function Generator", Wireless World, (Vol. 87, No. 1550; November 1981).

2. Brown, W.L. and Perrine, D.E., "Don't Guess at Bias Circuit Design", Electronic Design, (May 9, 1968, pp. 80-86).

3. Duffie, J.A. and Beckman, W.A., Solar Energy Thermal Processes, (John Wiley & Sons, Inc., New York, 1974).

4. Early, J.M., Effects of Space-Change Layer Widening in Junction Transistors, (Proc. IRE, 40, 1401, 1952.).

5. Escoffery, C.A. and Luft, W., "Optical Characteristics of Silicon Solar Cells and of Coatings for Temperature Control", Solar Energy (Vol. 4, No. 4, Oct. 1960, pp. 1-10).

6. Ghausi, M.S., Electronic Circuits, (Litten Educational Publishing, Inc., 1971).

7. Harison, T.R. and Wannamaker, W.H., "Improved Radiation Pyrometer", Temperature, Its Measurements Control in Science and Industry, Fairchild et al, Eds., (International Textbook Press, Scranton, PA, 1941).

8. Instruments for Surface Observations, Handbook of Meteorological Instruments, Part I, (Her Magesty's Stationary Office, London 1958).

9. Maita, J.P. and Morin, F.J., Electrical Properties of Silicon Containing Arsenic and Boron, Phys. Rev., 96, 28 (1954); also Conducting and Range of Germanium, Phys. Rev., 94, 1525 (1954).

10. Millman, J. and Halkias C.C., Integrated Electronics, (McGraw-Hill Kogakusha, Ltd., Tokyo, 1972.

11. NASA SP-8005, National Aeronautics and Space Administration, Solar Electromagnetic Radiation (May 1971).

12. Streetman, B.G., Solid State Electronic Devices, (Prentice-Hall, Inc., Englewood Cliffs, N.J., 1972).

13. Swinbank, W.C., Long-Wave Radiation from Clear Skies, Quart. J. Roy. Meteorol. Soc., 53, 360, (April 1972).

14. Thekaekara, M.P., "Survey of Quantitative Data on the Solar Energy and its Spectral Distribution", Heliotechnique & Development, Vol. I, Kettani, M.A. and Soussou, E.J., Eds., (Development Analysis Associates, Inc., Massachusetts, 1976).

15. Varshi, Y.P., Temperature Dependence of the Energy in Semiconductors, Physica, 34, 149, (1967).

16. Whillier, A., Design Factors Influencing Solar Collectors, Low Temperature Engineering Applications of Solar Energy, (New York, ASHRAE, 1967).